2003

Self-healing in power systems: an approach using islanding and rate of frequency decline based load shedding

Haibo You
Iowa State University

Self-healing in power systems: An approach using islanding and rate of frequency decline based load shedding

by

Haibo You

A dissertation submitted to the graduate faculty

in partial fulfillment of the requirements for the degree of

DOCTOR OF PHILOSOPHY

Major: Electrical Engineering (Electric Power)

Program of Study Committee:
Vijay Vittal, Major Professor
Gerald B. Sheblé
James D. McCalley
Wolfgang Kliemann
Murti V. Salapaka

Iowa State University

Ames, Iowa

2003

Graduate College
Iowa State University

This is to certify that the doctoral dissertation of

Haibo You

has met the dissertation requirements of Iowa State University

Signature was redacted for privacy.

Major Professor

Signature was redacted for privacy.

For the Major Program

TABLE OF CONTENTS

LIST OF FIGURES

LIST OF TABLES

ACKNOWLEDGEMENTS

I would like to take this opportunity to express my thanks to those who helped me with various aspects of conducting research and the writing of this thesis.

First, I want to thank Dr. Vijay Vittal, for his tremendous guidance and support throughout this research work, my academic study, and writing of this dissertation.

I want to thank my committee members, Dr. James McCalley, Dr. Gerald Sheblé, Dr. Wolfgang Kliemann, and Dr. Murti Salapaka for their efforts and contributions to this work. Dr. McCalley also provided great help in setting up the initial contingency of the simulation case.

I would additionally like to thank Zhong Yang for his work on the designing the load shedding scheme, which leads to our first Transaction paper; and Xiaoming Wang, who has made indispensable tests following the feedback of the reviewers on our second Transaction paper. Thank also to all the EPRI/DoD project faculty members and students for the discussions during the weekly presentations, monthly, quarterly and annual reports. These discussions were very beneficial in the development of this dissertation. Thanks to all the students in the power group for every joyful moment we have had together. I would also like to express my gratitude to Iowa State University and the department of Electrical and Computer Engineering for providing first-class research facilities and library resources.

I would like to thank my wife Yan Yang, for her great love, understanding and support.

ABSTRACT

This dissertation provides a self-healing strategy to deal with catastrophic events such as simultaneous loss of several generating units or major transmission lines when power system vulnerability analysis indicates that the system is approaching an extreme emergency state. In our approach, the system is adaptively divided into smaller islands at a slightly reduced capacity with consideration of quick restoration. The basis for forming the islands is to minimize the generation load imbalance in each island, thereby facilitating the restoration process. Then a carefully designed load shedding scheme based on the rate of frequency decline is applied to limit the extent of the disruption and expedite the restoration process. A slow coherency based islanding theory is provided. Issues regarding the linear and nonlinear applicability of the theory are discussed in detail. Then switching actions performed by out of step relays need to be taken to form the island. The R-Rdot out of step relay which has been developed by Bonneville Power Administration (BPA) and used in industry for almost 20 years is deployed to initiate the tripping actions. The function of the relay can be enhanced with the help of phasor measurement technology and decision tree knowledge. An overall scheme including a new two-level load shedding scheme is proposed. The proposed scheme is tested on a 179-bus, 29-generator sample system and shows very good performance. The current grouping algorithm is modified considering a detailed generator model and induction motor load dynamics and illustrated on a three-machine equivalent system. Spectral analysis helps to verify the grouping results in two cases.

CHAPTER 1 INTRODUCTION

1.1 BACKGROUND

Power systems are being operated closer to the stability limit nowadays as deregulation introduces many more economic objectives for operation. As open access transactions increase, weak connections, unexpected events, hidden failures in protection system, human errors and other reasons may cause the system to lose balance and even lead to catastrophic failures. Iowa State University, together with University of Washington, Virginia Polytechnic Institute and State University, and Arizona State University has worked as a consortium to conduct research on power system network security issues. The project has been conducted under a grant from the Electric Power Research Institute (EPRI) and the U.S. Department of Defense (DoD). "Our vision is to create a wide-area intelligent, adaptive protection and control system that empowers the future power grids by providing critical and extensive information in real-time, assessing system vulnerability quickly, and performing timely self-healing and adaptive reconfiguration actions based on system-wide considerations." The system is referred to as Strategic Power Infrastructure Defense (SPID) system. In the conceptual design, the system should acquire the following abilities [1]:

- Ability to acquire and interpret extensive real-time information from diverse sources, ranging from instrumentation to satellites and Internet.
- Ability to quickly evaluate system vulnerability with respect to catastrophic events in a market environment involving competing, self-serving agents.
- Ability to adapt the protective device performance based on system-wide assessment.
- Ability to reconfigure the power network to minimize system vulnerability.
- Ability to develop system restoration plans to minimize the impact of disruption.

One of the tasks involves the development of self-healing schemes to reconfigure the power network to minimize the system vulnerability and facilitate the restoration process to minimize the impact of disruption. This should be done through identifying the control

hierarchies and protection mechanisms between the various agents and the various components of the power system. This dissertation addresses the topic of designing a self-healing strategy after large disturbances. When a power system is subjected to large disturbances such as simultaneous loss of several generating units or major transmission lines, and the vulnerability analysis indicates that the system is approaching a catastrophic failure, control actions need to be taken to limit the extent of the disturbance. The disturbance can be categorized into the following five types [1]:

- Transient angle instability emergency
- Transient voltage instability emergency
- Small disturbance voltage instability emergency
- Small disturbance oscillatory instability emergency
- Long term frequency instability emergency

In our approach, frequency instability emergency is dealt with first. In general, the method developed can be applied to the transient angle instability and small disturbance oscillatory instability emergency, too. As a summary of the control strategy to deal with the large disturbance, the system is separated in a controlled fashion into smaller islands at a slightly reduced capacity. The basis for forming the islands is to minimize the load-generation imbalance in each island, thereby facilitating the restoration process. Then by exploring a carefully designed load shedding scheme based on the rate of frequency decline, we limit the extent of the disruption, and are able to restore the system rapidly. We refer to this corrective control scheme as controlled islanding followed by load shedding based on the rate of frequency decline.

Subsumption architecture is employed in our load shedding scheme design as well as the overall control strategy design. Subsumption architecture [2], which is used in the field of controlled robots, is adopted here to identify the hierarchies of the various controls, protection, and communication systems between various agents in the deregulated electric utility environment. The architecture is based on the premise that storing models of the world is dangerous in dynamic and unpredictable environments because representations may be incorrect or outdated. It defines layers of Finite State Machines (FSMs) that are augmented with timers. Sensors feed information into FSMs at all levels. The FSMs of the lowest level are control actuators. The FSMs of the higher levels may inhibit (attenuate the signal of one

output wire) or suppress (attenuate the signal on all output wires) output values of the FSMs on the layers below them. In this way, a hierarchy of progressively refined behaviors may be established. Agents in the Subsumption architecture do not use symbol manipulation in a fixed manner to represent processing. They also have no global knowledge and are generally decentralized. The agents are non-programmable, single-purpose devices because of their lack of symbolism and global knowledge. However, they have the advantage of rapid response for dealing with dynamic and unpredictable events. The proposed scheme designed based on the Subsumption model is tested on a 179-bus 20-generator test system and shows very good performance.

1.2 LITURATURE REVIEW

Special protection schemes (SPS) have been designed and used in Canada, France and Romania to counteract the extreme contingencies. [3] They are different from each other in design philosophy and objective, which in turn affect the contingencies considered and the preventive and corrective measures. These experiences give us good lessons to learn from. Geography has played a decisive role in the development of the Hydro-Québec system, with most of the hydro generation located in the north and most of the load located in the south. Load shedding, reactance and capacitance switching and other simple measures consist of the defence plan. The philosophy they adopted is "... a general power failure must not be the consequence of a situation that could reasonably have been avoided. The objective is therefore to preserve the integrity of the electric system by using automatic measures that are simple, reliable and safe for the system... [4]." The Electricité de France (EDF) defence plan includes more actions to counteract voltage collapse, frequency collapse, cascade line tripping or loss of synchronism for such a complex system. It consists of a complete strategy against major contingencies instead of one specific scheme for one particular type of contingency. Fast and slow system degradation mechanisms are identified. The curative measure for fast system degradation or loss of synchronism consist of a load shedding plan on a frequency criteria and an islanding plan implemented with local relays called DRS (French acronym of "area islanding protections in case of loss of synchronism"), which are able to detect any loss of synchronism and isolate the disturbed network portion from the

healthy one. DRSs are local devices set at the ends of Extreme high voltage (EHV) lines that detect the voltage beats, which is a characteristic of a loss of synchronism. The arrangement of DRSs is based on the principle according to which the electric system can be structured into areas that generators of an area have a homogeneous dynamic behavior in case of a disturbance. The French defense system provides us a prototype to build upon. When a large disturbance happens, it is necessary to break up the interconnected system before the impact of the disturbance spreads all over the network so that the synchronous operation of the power network is likely to collapse. Controlled separation followed by load shedding is suggested in paper [5]. The network frequency is suggested as a reliable indicator of a system-wide emergency state, where the voltage is mostly of a local nature. Island area selection is based on several suggested principles in the case that it is difficult to choose the areas that are suitable for all system conditions. Normal form is used as nonlinear analysis to determine the selection of the grouping of generators in paper [6]. This method is dependent on the power system working condition and selected large disturbances. In paper [7], the authors provide a method to identify the inter-area groups in the following steps: collect machine speed data; perform spectrum estimation on machine speed data; identify the frequencies of possible modes of inter-area oscillations; perform clustering on the phases of machine spectrum data at inter-area frequencies. This method gets the information of the oscillatory modes by analyzing the generator speed data after the disturbance. They treat the oscillation as the energy exchange between groups of machines and formulate an emergency control by modulating the admittance of the thyristor-controlled series capacitor (TCSC) to reduce the energy exchange.

The following conclusions can be made after the literature review.

- Defense plan can be varied according to the characteristics of the power system networks.
- It is necessary to break the system into several islands before the large disturbance become severe all over the power system.
- Though many types of methods exist when forming the controlled islands, it is necessary to have a general method with a theoretical basis.
- Existing methods to deal with the islanding problem can be classified into two categories: when and where to form the islands. The first category defines an index to initiate the tripping action. The second category determines the generator grouping thereby determining the boundary of the

islands. These two categories address the two main problems in islanding issue: they are where and when to form the islands.

1.3 DISSERTATION ORGANIZATION

This dissertation is organized as follows. After a brief introduction in Chapter 1, Chapter 2 presents the theory of slow coherency in detail. Issues regarding the two-time-scale method, the grouping algorithm, the linear and nonlinear applicability of the method are addressed. A C++ program is developed to find the exact boundary of the islands and is addressed in detail in this chapter. Illustration and simulation of a modified grouping algorithm on a three-machine system is also included in this chapter. Chapter 3 presents the details of tripping actions and provides an illustration of the overall control strategy. Chapter 4 addresses the issue of the design of the load shedding scheme. Simulation results are given in Chapter 5. Finally, Chapter 6 summarizes the work that has been done, the contributions made, and proposes some possible future research directions.

CHAPTER 2 SLOW COHERENCY BASED ISLANDING

2.1 INTRODUCTION

In the controlled islanding self-healing approach, the determination of the islands for a given operating condition is the critical step. A reasonable approach to islanding can result in significant benefit to the corrective control actions that follow the islanding procedure. Usually the islanding problem can be reduced to a problem of properly identifying the generator groupings. Methods that are commonly used are methods based on experience, weak link identification, and simulations on specific range of contingencies [8]. These techniques do not have a concrete theoretical basis. There is also a method based on the application of the normal form that takes into account the nonlinear interaction [6]. The existing methods are all disturbance dependent. In determining the islands, the inherent structural characteristics of the system should be considered. In addition, the choice of these islands should not be disturbance dependent. These conditions are imposed in order to provide a self-healing scheme that is fairly general and easy to implement.

Slow coherency was originally used in the development of dynamic equivalents for transient stability studies [9]. Previously, several methods were used to identify coherent groups of generators. They include electrical distance method; time domain approach; frequency domain approaches utilizing Fourier transform and Laplace transform techniques. In these methods, two assumptions were made: the coherent groups of generators are independent of the size of the disturbance, so that linearized model can be used to determine the coherency; the coherent groups are independent of the amount of the detail in the generating unit models so that a classical generator model can be considered. The first assumption is based on the observation that the coherency behavior of a generator is not significantly changed as the clearing time of a specific fault is increased. Although the amount of the detail of the model can affect the swing curve a lot, it does not radically change the basic network characteristics such as interarea modes. This forms the basis of the

second assumption. These assumptions are also applied in slow coherency theory. But it has more important features that are especially applicable and suitable to the islanding problem.

In the rest of this chapter, an introduction of the basics of time scales in power system and the modal analysis is provided. Then the two-time-scale method is introduced. A grouping algorithm defining the procedure to group the generators is presented next. Issues regarding the linear and nonlinear applicability of the slow coherency theory are discussed next. Then the program, which is used for identifying the exact boundary between the islands considering certain criteria is discussed. A modified grouping algorithm and its application on a three-machine system are presented. Finally, a summary is given.

2.2 TIME SCALE AND MODAL ANALYSIS

We begin our introduction of the slow coherency method with some basics of time scale and modal analysis, which are important for the understanding of the grouping algorithm to be discussed.

2.2.1 Time Scale

To analyze the different stability problems, power system dynamics are usually modeled into the following four time scales [10]:

- Long term dynamics (several minutes and slower): Boiler dynamics, daily load cycles, etc.
- Mid-term dynamics (1-5 min): Load Tap Changers (LTC), Automatic Generation Control (AGC), thermostat controlled loads, generator over-excitation limiters, etc.
- Transient dynamics (seconds): Generators, Automatic Voltage Regulators (AVR), governors, induction motors, HVDC controllers, etc.
- Practically instantaneous (less than msec): Electromagnetic and network transients, various electronically controlled loads, etc.

The time scale together with the type of instability determines the emergency type as classified in section 1.1. These time scales can be further divided. Reference [10] shows by using a two-time-scale method, a multi-machine power system containing both frequency and voltage dynamics, which belong to the transient time scale in the above, can be accurately decomposed into two separate subsystems: A fast subsystem consisting of

electromechanical oscillation modes and a slow subsystem consisting of flux/voltage response modes. It is described that a singularity of the algebraic equations in a differential-algebraic representation of a system could be understood as instability of fast dynamics that are not modeled. Basically, different dynamical model requirements should be enforced according to the research objective.

Electromechanical dynamics, which can be represented by rotor angle and speed, are usually faster than voltage or flux dynamics such as E_q'. From Table 2.2.1.1 observe the time constants of the WSCC three machines equivalent system [11]. The time constants of rotor angles and speeds (the second column) are smaller or faster than the time constants of transient, sub-transient state variables and exciter state variables (the other columns). It is to be noted that the inertias of the three machines here are highly equivalent ones, where as in practice they are much less than these numbers. As a result, the time constants for the actual machines are much less than the data shown in the second column.

Table 2.2.1.1 Time constants of the three-machine equivalent system.

	δ, ω $(2H/\omega_s)$(s)	T_{d0}' (s)	T_{q0}'(s)	T_A(s)	T_E (s)	T_F (s)
Machine 1	0.788	8.96	0.310	0.2	0.314	0.35
Machine 2	0.213	6.00	0.535	0.2	0.314	0.35
Machine 3	0.100	5.89	0.600	0.2	0.314	0.35

Following a large disturbance, the objective of stabilizing the power system after the large disturbance is achieved by controlled islanding followed by load shedding based on rate of frequency decline. Properly controlled power system islanding shortly after the detection of a large disturbance is the first step. Out of step relays are deployed to detect the system emergency state and island the system with local and remote tripping actions. Hence, it is necessary to have the power system islanded based on a theory considering the dynamics of the transient time scale. Slow coherency meets this need by considering the power system electromechanical modes and grouping the generators with slow coherency. Further issues dealing with the modification of the existing grouping algorithm considering voltage stability and the fact that the interarea mode shape may be affected by fast control devices such as governors, exciters, etc will be discussed.

2.2.2 Modal Analysis

In power systems, each mode corresponds to an eigenvalue, which has its distinctive time dependent characteristic shape, or mode shape. The eigenvalues can be calculated after linearizing the system state space matrix around an operating point. The following phenomena regarding the modes and the stability are observed [12]:

- A real eigenvalue corresponds to a non-oscillatory mode. A negative real eigenvalue represents a decaying mode. The larger its magnitude is, the faster the decay will be. A positive real eigenvalue represents an aperiodic instability. The characteristics of the mode can be shown by the curve $e^{\lambda t}$.
- Complex eigenvalues occur in conjugate pairs. Each pair corresponds to an oscillatory mode. For an eigenvalue $\lambda = \sigma \pm j\omega$, the effect of the eigenvalues on the state variable, or the characteristic curve of the state variable with respect to this mode has the form of $(a + jb)e^{(\sigma - j\omega)t} + (a - jb)e^{(\sigma + j\omega)t}$, which can be simplified as $e^{\sigma t} sin(\omega t + \theta)$. The frequency of the oscillation in Hz is given by $f = \omega / 2\pi$. The time constant of amplitude decay is $1/|\sigma|$. In other words, the amplitude decays to 1/e or 37% of the initial amplitude in $1/|\sigma|$ seconds.
- The mode's effect can be seen by transformations made on the linearized dynamic equations. If the linearized equation is

$$\dot{X} = AX \tag{2.2.2.1}$$

With transformation

$$X = \Phi Z(t) = [\Phi_1 \quad \Phi_2 \quad \cdots \quad \Phi_n] \times [z_1(t) \quad z_2(t) \quad \cdots \quad z_n(t)]^T \tag{2.2.2.2}$$

Where Φ is the modal matrix of A, then

$$\dot{Z} = \Lambda Z = diag(\lambda_1, \lambda_2, \cdots, \lambda_n) Z \tag{2.2.2.3}$$

Equation (2.2.2.2) shows that the effect of each mode λ_i on the state variables is determined by the entries of the corresponding column of the modal matrix or eigenvector Φ_i. This concept is important for the understanding of the grouping algorithm of slow coherency theory. Slow coherency analysis shows that partitioning according to the r slowest modes will obtain the weakest connection between areas [13]. After the r slowest modes are selected, the corresponding columns of the modal matrix will determine the effect of the selected modes on the state variables. If two rows of the modal matrix have the same entries

corresponding to the r modes, the corresponding machines will be coherent with each other with respect to the selected modes. In the original slow coherency grouping algorithm, first-order linearized power system state space equations are considered, where only real negative eigenvalues exist. When there are pairs of complex eigenvalues, the situation will be more complex. Both the real part and the imaginary part of the eigenvalues need to be considered when the reference modes are being selected, because a small real part represents a slowly decaying time constant and a small imaginary part represents a slow oscillatory frequency. The existing grouping algorithm is modified and will be illustrated in section 2.8.

2.3 TWO-TIME-SCALE METHOD

The two-time-scale method is also called the singular perturbation method. It is a theory dealing with the dynamical equations of state variables with large differences in time constants. A brief introduction is provided below. More detailed information can be obtained in [14]. It is assumed that the state variables of an nth order system are divided into r "slow" states y and $(n\text{-}r)$ "fast" states z. The full scale model is written as

$$dy/dt = f(y,z,t), \qquad y(t_0) = y_0 \tag{2.3.1}$$

$$dz/dt = G(y,z,t), \qquad z(t_0) = z_0 \tag{2.3.2}$$

Define a new time variable $\tau = (t - t')/\varepsilon$, which is much larger than the original time scale. Also we rescale G as $g = \varepsilon G$ such that g and f are of the same order of magnitude. The model (2.3.1) and (2.3.2) are the explicit form. In the limit as $\varepsilon \to 0$, the model gives the slow model:

$$dy_s/dt = f(y_s,z_s,t), \qquad y_s(t_0) = y_0 \tag{2.3.3}$$

$$0 = g(y_s,z_s,t) \tag{2.3.4}$$

For the fast parts, y and z are as given below:

$$dy/d\tau = \varepsilon f(y,z,t'+\varepsilon\tau) \tag{2.3.5}$$

$$dz/d\tau = g(y,z,t'+\varepsilon\tau) \tag{2.3.6}$$

Let $\varepsilon \to 0$, which yields $dy/d\tau = 0$. Or y is constant in the fast time-scale. Then

$$dz_f/d\tau = g(y_0,z_s(t_0)+z_f(\tau),t_0), \qquad z_f(0) = z_0 - z_s(t_0) \tag{2.3.7}$$

So the overall values of y and z are expressed as:

$$y(t) = y_s(t) + O(\varepsilon) \tag{2.3.8}$$

$$z(t) = z_s(t) + z_f((t - t_0)/\varepsilon) + O(\varepsilon) \tag{2.3.9}$$

If f and g are twice differentiable functions of x, z and t, the above equations (2.3.8) and (2.3.9) are based on the following two assumptions:

- The equilibrium $z_f = 0$ is asymptotically stable and $z_f(0)$ belongs to its domain of attraction.
- The eigenvalues of $\partial g / \partial z$ evaluated along $y_s(t), z_s(t)$ for all t in the interval $[t_0, T]$ have real parts strictly smaller than a fixed negative number.

In particular, if the ε is sufficiently small, there exists $t_1 > t_0$ such that the following approximation holds for all t in $[t_1, T]$:

$$y(t) = y_s(t) + O(\varepsilon) \tag{2.3.10}$$

$$z(t) = z_s(t) + O(\varepsilon) \tag{2.3.11}$$

For linear systems, the time-scale properties of singularly perturbed systems are described by linear time-invariant systems shown as the following equations:

$$dy/dt = Ay + Bz, \quad y(t_0) = y_0 \tag{2.3.12}$$

$$\varepsilon dz/dt = Cy + Dz, \quad z(t_0) = z_0 \tag{2.3.13}$$

Observe that the r-vector of slow variables y and $(n\text{-}r)$ vector of fast variables z are coupled. Considering the slow part of the two variables, the slow model is given by:

$$dy_s(t)/dt = Ay_s(t) + Bz_s(t), \quad y_s(t_0) = y_0 \tag{2.3.14}$$

$$0 = Cy_s(t) + Dz_s(t) \tag{2.3.15}$$

When D^{-1} exist, then $z_s(t) = -D^{-1}Cy_s(t)$. The slow reduced model is:

$$dy_s(t)/dt = (A - BD^{-1}C)y_s(t), \quad y_s(t_0) = y_0 \tag{2.3.16}$$

The fast reduced model is:

$$dz_f(\tau)/d\tau = Cy_f(\tau) + Dz_f(\tau) = Dz_f(\tau), \quad z_f(0) = z_0 + D^{-1}Cy_0 \tag{2.3.17}$$

Transform the state variables of the original system using:

$$\eta = z - Ly \tag{2.3.18}$$

The slow mode will not appear in η. Substitute this transformation into (2.3.12) and (2.3.13), then

$$dy/dt = (A + BL)y + B\eta \tag{2.3.19}$$

$$\varepsilon d\eta/dt = [C + DL - \varepsilon L(A + BL)]y + (D - \varepsilon LB)\eta \tag{2.3.20}$$

For all L satisfying the algebraic Riccati equation (2.3.21),

$$C + DL - \varepsilon L(A + BL) = 0 \tag{2.3.21}$$

the subsystem (2.3.20) will decouple from the other system.

$$\varepsilon d\eta / dt = (D - \varepsilon LB)\eta \tag{2.3.22}$$

Furthermore, a transformation $\xi = y + H\eta$ will transform the system into $d\xi / dt = (A + BL)\xi$, where H satisfies the following linear equation

$$H(D - \varepsilon LB) - \varepsilon(A + BL)H + \varepsilon B = 0 \tag{2.3.23}$$

Then the exact fast and slow subsystems of the original systems are obtained.

If the system has r small eigenvalues and $(n\text{-}r)$ large eigenvalues, where,

$$\lambda_s = \lambda(A + BL) = \lambda(A - BD^{-1}C) \tag{2.3.24}$$

$$\lambda_f = \lambda(D - \varepsilon LB) / \varepsilon = (\lambda(D) + O(\varepsilon)) / \varepsilon \tag{2.3.25}$$

In addition, if $\mathrm{Re}\{\lambda(D)\} \le -\sigma_0 < 0$, where σ_0 is positive scalar independent of ε, then for all $t > t_0$,

$$y(t) = y_s(t) + O(\varepsilon) \tag{2.3.26}$$

$$z(t) = -D^{-1}Cy_s(t) + z_f((t - t_0) / \varepsilon) + O(\varepsilon) \tag{2.3.27}$$

This is true mostly for first-order systems. In general for second-order systems $\mathrm{Re}\{\lambda(D(o))\} = 0$, in this case, we have existence of ε^* and T such that for all ε in $[0, \varepsilon^*]$ and t in $[T, \infty]$,

$$y(t) = y_s(t) + O(\varepsilon) \tag{2.3.28}$$

$$z(t) = -D^{-1}Cy_s(t) + z_f(t) + O(\varepsilon) \tag{2.3.29}$$

For application of the singular perturbation method to power systems, a generator model of constant voltage V_i behind transient reactance is used and the network is reduced to the generator internal nodes. With this assumption, our grouping algorithm determines the groups of generators that are weakly coupled. The grouping has not considered the effect of loads. The grouping of generators also does not consider the geographical features or the exact boundary in terms of the boundary nodes yet. A little more work is needed to consider these effects, which is realized by a C++ program introduced later.

2.4 A GROUPING ALGORITHM

Slow coherency is an application of the singular perturbation method or two-time-scale method in power systems. A grouping algorithm is dedicated to obtaining groups of generators with slow coherency. The method assumes the state variables of an *n*th order system are divided into *r* slow states *y*, and (*n*-*r*) fast states *z*, in which the *r* slowest states represent *r* groups with the slow coherency. The user provides an estimate for the number of groups. However the automatic islanding program takes into account the mismatch between generation and load and availability of the tie lines to form islands and appropriately combines groups when islands cannot be formed.

2.4.1 Grouping Algorithm

Both the linearized and nonlinear power system models can be used to apply the two-time-scale method. In the linearized model, we start from the basic classical second order electromechanical model of an *n*-machine power system [11]:

$$\dot{\delta}_i = \Omega(\omega_i - 1) \tag{2.4.1.1}$$

$$2H_i\dot{\omega}_i = -D_i(\omega_i - 1) + (P_{mi} - P_{ei}) \qquad i = 1,2,...,n \tag{2.4.1.2}$$

Where, δ_i Rotor angle of machine i in radians,

ω_i Speed of machine i, in per unit (pu),

P_{mi} Mechanical input power of machine i, in pu,

P_{ei} Electrical output power of machine i, in pu,

H_i Inertia constant of machine i, in seconds,

D_i Damping constant of machine i, in pu,

Ω Base frequency, in radian per second.

If we neglect damping and line conductance and we linearize the system dynamic equation around an equilibrium point $(\delta^*,1)^T$, we obtain:

$$\ddot{X} = -(1/2)\Omega H^{-1}KX = AX \tag{2.4.1.3}$$

$$x_i = \Delta\delta_i = \delta_i - \delta^* \tag{2.4.1.4}$$

$$H = diag(H_1, H_2,..., H_n) \tag{2.4.1.5}$$

$$K = (k_{ij}) = (V_iV_jB_{ij}\cos(\delta_i - \delta_j)\big|_{\delta^*}) \quad j \neq i \tag{2.4.1.6}$$

Where,

V_i Voltage of bus i in pu,

B_{ij} Susceptance between bus i and bus j in pu.

In the above procedure, several reasonable assumptions are made:

- Mechanical input power P_{mi} is constant. The governor's effect is omitted here to concentrate on the network's characteristic.
- Damping is omitted, which doesn't change the mode shape very much.
- K is symmetric, the off-diagonal terms of the connection matrix K are nonnegative and conductance G_{ij} is omitted for simplification.
- System is stable with negative eigenvalues.

Under these assumptions, the square roots of the eigenvalues of matrix A represent the modes of the system. For a stable power system, the eigenvalues of A are 0 and several negative real numbers. The following derivations will be developed around the second order linearized state space matrix A [13].

The state x_i and x_j of a system $\ddot{X} = AX$ are slowly coherent if and only if they are coherent with respect to a set of r slowest modes σ_s of the system, or if $x_i(t) - x_j(t) = z_{ij}(t)$ where $z_{ij}(t)$ contains none of the r slow modes. Note in general $x_i(t)$, $x_j(t)$ will contain all the modes of the systems. Some modes will be more dominant than the others. Slow coherency is manifested when $z_{ij}(t)$ the difference between the two states does not contain any of the slow modes. When the system has r slow modes, we can say that the system is r decomposable. We use a 3-area 5-machine system as an illustration. x^1 contains the reference states or machines and x^2 contains all the other machines in the system. The matrix L_g is called a grouping matrix, which has only one 1 in each row with all the other elements being 0. It provides the grouping information. For each entry that contains a 1 in the matrix, the row number represents each machine state in x^2 and the column number corresponds to a reference state in x^1, which are grouped together. For example,

$$x^1 = (x_1, x_2, x_4)' \tag{2.4.1.7}$$

$$x^2 = (x_3, x_5)' \tag{2.4.1.8}$$

$$L_g = \begin{matrix} \\ x_3 \\ x_5 \end{matrix} \begin{matrix} \begin{matrix} x_1 & x_2 & x_4 \end{matrix} \\ \begin{bmatrix} 1 & 0 & 0 \\ 0 & 1 & 0 \end{bmatrix} \end{matrix} \tag{2.4.1.9}$$

This indicates there are three areas. These areas are composed of machines 1 and 3, machines 2 and 5, and machine 4. L_g is called a grouping matrix. Then

$$x^2(t) - L_g x^1(t) = z^2(t) \tag{2.4.1.10}$$

Where $z^2(t)$ contains none of the r slowest modes. Then we define the transformation:

$$\begin{bmatrix} x^1 \\ z^2 \end{bmatrix} = \begin{bmatrix} I & 0 \\ -L & I \end{bmatrix} \begin{bmatrix} x^1 \\ x^2 \end{bmatrix} \tag{2.4.1.11}$$

Substituting the transformation into (2.4.1.3), we get

$$\begin{bmatrix} \dot{x}^1 \\ \dot{z}^2 \end{bmatrix} = \begin{bmatrix} B_1 & A_{12} \\ R(L) & B_2 \end{bmatrix} \begin{bmatrix} x^1 \\ z^2 \end{bmatrix} \tag{2.4.1.12}$$

Where

$$B_1 = A_{11} + A_{12}L \tag{2.4.1.13}$$

$$B_2 = A_{22} - LA_{12} \tag{2.4.1.14}$$

$$R(L) = A_{22}L - LA_{11} - LA_{12}L + A_{21} \tag{2.4.1.15}$$

A_{11}, A_{12}, A_{21}, A_{22} are the sub-matrices of A conformal with x^1, x^2 such that the system (2.4.1.3) can be written as:

$$\begin{bmatrix} \dot{x}^1 \\ \dot{x}^2 \end{bmatrix} = \begin{bmatrix} A_{11} & A_{12} \\ A_{21} & A_{22} \end{bmatrix} \begin{bmatrix} x^1 \\ x^2 \end{bmatrix} \tag{2.4.1.16}$$

When $R(L) = 0$ and $|\lambda_j(B_1)| < |\lambda_i(B_2)|$, such an L is called dichotomy and denoted by L_d. Normally L_d is not a grouping matrix. In such case, we use a near r decomposable system. We compare different combinations of the selection of slow variable x^1 and get different solution of L_d. We use L_d with $\min\|L_d - L_g\|$ as the approximation and then let the largest number of each row be 1. Define

$$V = \begin{bmatrix} V_1 \\ V_2 \end{bmatrix} \tag{2.4.1.17}$$

Where V is the r columns of the eigensubspace of the matrix A. The rxr matrix V_1 is nonsingular, being a basis of the eigensubspace of the slow modes. Then

$$L_d = V_2 V_1^{-1} \tag{2.4.1.18}$$

It can be proven that L_d is the unique dichotomy solution of the Riccati equation. If two coherent machines are in x^1, then V_1 will be singular. In the near r decomposable system, V_1 will be near singular. Thus we aim to find r largest and most linearly independent rows of V. We use Gaussian elimination with complete pivoting to find the r most independent vectors

of V. Permutation is done in the elimination, and the first r steps provide the V_1. A grouping algorithm is provided in the following procedures:

- Choose the number of areas r.
- Compute a basis matrix V for a given ordering of the x variables containing slow modes.
- Apply Gaussian elimination with complete pivoting to V and obtain the set of reference machines. Each group will then have one and only one reference machine.
- Compute L_d for the set of reference machines chosen in step 3. Then determine the group that each generator belongs to from the matrix L_d by comparing the row of each generator with the row of the reference machine.

Given the reference machines, the above grouping algorithm provides a method to get the generator groupings with slow coherency. By selecting the r slowest modes, an objective can be achieved to have the weakest connections between the areas, which will be discussed in the next section. So it provides a complete procedure to determine the generators in each island.

2.4.2 Illustration

As an illustration of the algorithm, a three-machine equivalent system from [11] is selected as our sample system shown in Fig. 2.4.2.1. The system uses 100MVA and 100kV as active power and voltage bases.

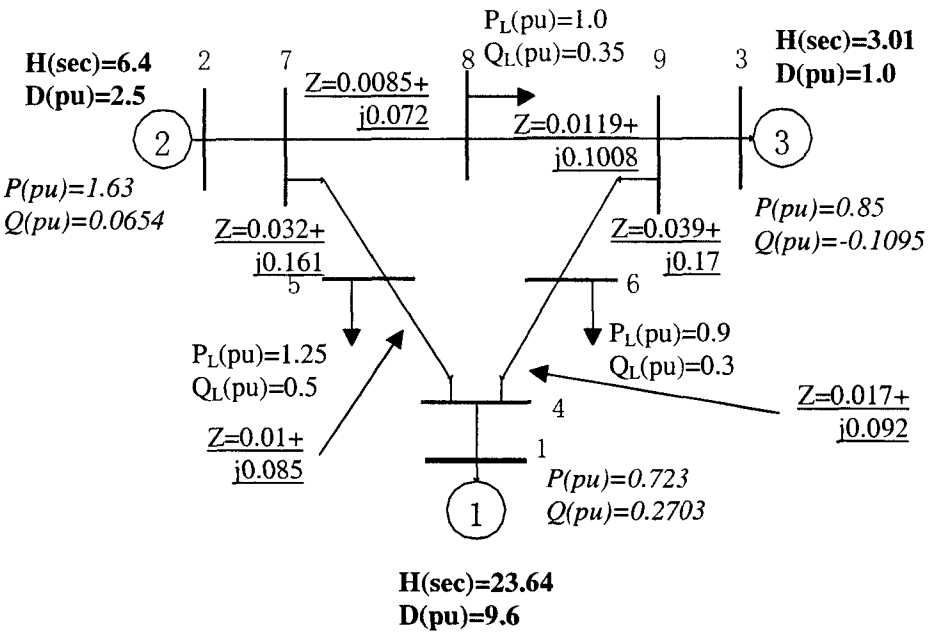

Fig. 2.4.2.1 The three-machine equivalent system

A power flow program is run to obtain the base case solution. The procedures of the slow coherency grouping algorithm as described in 2.4.1 are repeated. The system nonlinear equations are linearized around the base case with dynamic equations of all three generators represented by the classical electromechanical model. The damping constants are set to zero at first in order to obtain a second order electromechanical system state space representation as shown below:

$$\ddot{X} = AX \tag{2.4.1.19}$$

$$A = \begin{bmatrix} -24.18 & 13.53 & 10.65 \\ 44.36 & -77.58 & 33.23 \\ 78.33 & 73.93 & -152.2 \end{bmatrix} \tag{2.4.1.20}$$

The state variables X are $[\delta_1 \quad \delta_2 \quad \delta_3]^T$. With eigenvalues $D = [0.0078 \quad -75.5031 \quad -178.4647]$, the corresponding eigenvectors are:

$$E = \begin{bmatrix} -0.5772 & -0.3150 & -0.0398 \\ -0.5773 & 0.8234 & -0.2968 \\ -0.5775 & 0.4720 & 0.9541 \end{bmatrix} \tag{2.4.1.21}$$

Select two slow modes 0.0078 and -75.5031, their corresponding eigensubspace is:

$$V = \begin{bmatrix} -0.5772 & -0.3150 \\ -0.5773 & 0.8234 \\ -0.5775 & 0.4720 \end{bmatrix} \tag{2.4.1.22}$$

It can be observed that machine 2 and 3 will form one group since they have similar entries. When the results of Gaussian elimination are evaluated, the first row and the second row are selected as the most independent rows of eigenvectors. If the independent rows are chosen by Gaussian elimination:

$$V_1 = \begin{bmatrix} -0.5773 & 0.8234 \\ -0.5772 & -0.3150 \end{bmatrix} \tag{2.4.1.23}$$

Thus

$$V \cdot V_1^{-1} = \begin{bmatrix} -0.0000 & 1.0000 \\ 1.0000 & 0.0000 \\ 0.6914 & 0.3089 \end{bmatrix} \tag{2.4.1.24}$$

Machine 1 and 2 are selected as reference machines. Obviously 0.6914 is closer to 1 than 0.3089, which means machine 3 is coherent with machine 2 with respect to the selected slow modes.

2.5 LINEAR METHOD

Slow coherency solves the problem of identifying theoretically the weakest connection in a complex power system network. The two-time-scale weak connection form best states the oscillation feature of the large-scale power system: the fast oscillation within the group and the slow oscillation between the groups via weak tie lines. Since fast dynamics are weakly connected, it is reasonable to select these weak connections as places to form the islands during the short period after the disturbance. The short period is comparable with the fast time scale. Plus, as stated before, coherency is unrelated with the disturbance size and generator model detail. Coherent groups can be obtained considering the modes of the oscillation of the linearized state space equations.

Previous work shows groups of generators with slow coherency may be determined using Gaussian elimination on the eigensubspace matrix after selection of r slowest modes σ_a. In this section, we will show by linear analysis that with selection of the r slowest modes, the aggregated system will have the weakest connection between groups of generators [13].

2.5.1 Aggregability Condition

As stated in section 2.1, slow coherency was originally used in the development of dynamic equivalents for transient stability studies. Grouping and aggregation are two important steps in forming equivalents. In order to aggregate, aggregability condition should be satisfied. Under the assumptions described in section 2.4.1, the system described by the dynamic equation (2.4.1.3) can be written as:

$$\ddot{X} = M^{-1}KX \tag{2.5.1.1}$$

Where,

$$X = [x_1, x_2, ..., x_n]^T \tag{2.5.1.2}$$

$$M = diag(\, m_1, m_2, ..., m_n \,) \tag{2.5.1.3}$$

$$k_{ij} = k_{ji} \tag{2.5.1.4}$$

$$k_{ii} = -\sum_{j=1, j\neq i}^{n} k_{ij} \tag{2.5.1.5}$$

The matrix K is symmetric based on the assumptions in section 2.4.1. If a dynamic network is partitioned into r areas such that every state x_i is assigned to one and only one set or area, the states can be reordered sequentially according to areas.

$$X_{seq} = [x^1, x^2, \cdots, x^r]^T \tag{2.5.1.6}$$

Where, each x^i is a collection of the states in the area i. Assume each area α has n_α states in a set J_α. Define

$$U = diag(u_1, u_2, \ldots, u_r) \tag{2.5.1.7}$$

Where

$$u_\alpha = [1,1,\ldots,1]^T \tag{2.5.1.8}$$

is a n_α vector. Accordingly,

$$M_a = diag(m_{a1}, m_{a2}, \ldots, m_{ar}) \tag{2.5.1.9}$$

Where

$$m_{a\alpha} = \sum_{i}^{i \in J_\alpha} m_i \tag{2.5.1.10}$$

Here "a" stands for aggregated. The symbol $m_{a\alpha}$ is an aggregated inertia of all the machines in the area α. If a state x_i belongs to area α, then the dynamic equation for x_i can be written as:

$$m_i \ddot{x}_i = \sum_{j,j\neq i}^{j \in J_\alpha} k_{ij}(x_j - x_i) + \sum_{\beta=1,\beta\neq\alpha}^{r} \left(\sum_{j,j\neq i}^{j \in J_\beta} k_{ij}(x_j - x_i) \right) = K_i^I X + K_i^E X \tag{2.5.1.11}$$

Each connection k_{ij}, $i \neq j$ can be categorized into K_i^I or K_i^E according to whether j belongs to the same area as i. Also k_{ii} is divided into two parts, which are composed of the internal connections of i in area α and external connections of i to the other areas. If the states are ordered sequentially, and u_α is expanded with zeros filling the blank positions to make it the same length as a vector in U, then

$$K_i^I u_\alpha = 0 \tag{2.5.1.12}$$

If equation (2.5.1.11) and (2.5.1.12) are written in full matrix form, then

$$M\ddot{X} = KX = K^I X + K^E X \tag{2.5.1.13}$$

$$K^I U = 0 \tag{2.5.1.14}$$

Where, K^I is a r-block matrix. Furthermore,

$$M_a = diag(m_{a1}, m_{a2}, \ldots, m_{ar}) = U^T M U \tag{2.5.1.15}$$

Define

$$K_a = U^T K U \tag{2.5.1.16}$$

From equations (2.5.1.13) and (2.5.1.14),

$$K_a = U^T K U = U^T K^E U \tag{2.5.1.17}$$

The state variable aggregation in area α is:

$$y_{a\alpha} = (\sum_{i}^{i\in J_\alpha} m_i x_i) / (\sum_{i}^{i\in J_\alpha} m_i) \tag{2.5.1.18}$$

For the system,

$$Y = C_a X = M_a^{-1} U^T M X \tag{2.5.1.19}$$

Where,

$$C_a = M_a^{-1} U^T M \tag{2.5.1.20}$$

$$\ddot{Y} = C_a \ddot{X} = C_a M^{-1} K X = A_a Y = A_a C_a X \tag{2.5.1.21}$$

In order to aggregate, the following equation must exist:

$$A_a C_a = C_a M^{-1} K \tag{2.5.1.22}$$

Here we introduce the aggregability condition:

A second order dynamic network defined in (2.5.1.1) is aggregable with respect to the transformed system by the transformation defined in (2.5.1.19), if and only if the external connections satisfy the following aggregability condition:

$$M^{-1} K^E U = U M_a^{-1} K_a \tag{2.5.1.23}$$

Proof:

Substitute (2.5.1.20) into (2.5.1.22),

$$A_a M_a^{-1} U^T M = M_a^{-1} U^T M M^{-1} K = M_a^{-1} U^T K \tag{2.5.1.24}$$

Post-multiply by U,

$$A_a M_a^{-1} U^T M U = A_a = M_a^{-1} U^T K U \tag{2.5.1.25}$$

From equation (2.5.1.13) and (2.5.1.14),

$$A_a = M_a^{-1} U^T K U = M_a^{-1} U^T K^E U = M_a^{-1} K_a \quad \blacksquare \tag{2.5.1.26}$$

The aggregated system will be

$$\ddot{Y} = A_a Y \tag{2.5.1.27}$$

2.5.2 Weakest Connection

From the analysis in section 2.5.1, it can be seen that a grouping can be accepted for aggregation as long as the aggregability condition is satisfied. A matrix U in equation

(2.5.1.7) will represent one grouping since each state represents one machine. However, the grouping method in section 2.4 provided many possible groupings and aggregations with different selections of reference modes. In order to show with selection of the r slowest modes, the aggregation system will have the weakest connection between groups of generators, a scalar quantity is taken as a measure of the strength of connections between the areas.

$$s = \sum_{\alpha=1}^{r} (\sum_{\beta=1,\beta\neq\alpha}^{r} k_{\alpha\beta}^{\alpha} / m_{a\alpha}) \qquad (2.5.2.1)$$

It can be seen that the quantity s is monotonically increasing as any off-diagonal entries of the external connection matrix K^E increases. Plus, the quantity is related with the aggregated inertia in the area.

Suppose the aggregability condition is satisfied with respect to the r slowest modes $\sigma_a=\sigma_1$ and also with respect to another set of r reference modes σ_2. Then the strength of connections s_1 between σ_1-coherent areas is weaker than the strength of connections s_2 between σ_2-coherent areas, or $s_1<s_2$.

Proof:

Since K_a is a network matrix, $k_{\alpha\beta}^{a}$ is the α_{th} row and β_{th} column element of K_a. As in (2.5.1.5), we have

$$k_{\alpha\alpha}^{a} = - \sum_{\beta=1,\beta\neq\alpha}^{r} k_{\alpha\beta}^{a} \qquad (2.5.2.2)$$

Therefore, for a network matrix K_a with connection quantity s, we have,

$$s = -\sum_{\alpha=1}^{r} k_{\alpha\alpha}^{a} / m_{a\alpha} = -trace(A_a) \qquad (2.5.2.3)$$

Where $trace(A_a)$ denotes the sum of the diagonal entries of $A_a = M_a^{-1} K_a$ and is equal to the sum of the eigenvalues in σ_a, that is,

$$trace(A_a) = \sum_{\alpha=1}^{r} \lambda_\alpha \qquad (2.5.2.4)$$

Since σ_1 are r slowest modes, we have $s_1<s_2$. Or the strength of connections s_1 between σ_1-coherent areas is weaker than the strength of connections s_2 between σ_2- coherent areas. ■

In the following an illustration example is given on a RC-circuit shown in Figure 2.5.2.1.

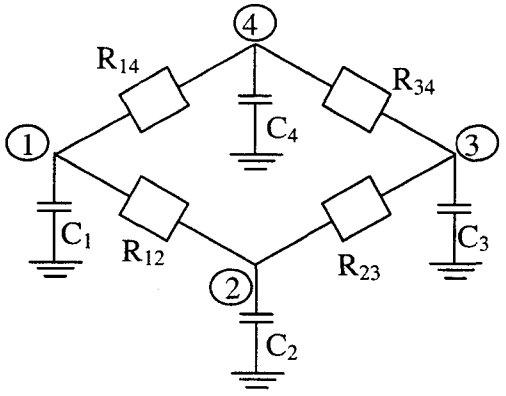

Fig. 2.5.2.1. RC-circuit illustration

The parameters of the circuit are:

$C_1 = C_2 = C_3 = C_4 = 1$, $1/R_{12} = 1/R_{34} = p$, $1/R_{23} = 1/R_{14} = q$.

Thus the dynamics can be written as:

$$\dot{X} = AX$$

$$= \begin{bmatrix} -(p+q) & p & 0 & q \\ p & -(p+q) & q & 0 \\ 0 & q & -(p+q) & p \\ q & 0 & p & -(p+q) \end{bmatrix} X \qquad (2.5.2.5)$$

The calculated eigenvalues of the A matrix are:

$$\sigma(A) = \{0, -2q, -2p, -2(p+q)\} \qquad (2.5.2.6)$$

The four corresponding eigenvectors are:

$$W(A) = \left\{ \begin{bmatrix} 1 \\ 1 \\ 1 \\ 1 \end{bmatrix}, \begin{bmatrix} 1 \\ 1 \\ -1 \\ -1 \end{bmatrix}, \begin{bmatrix} 1 \\ -1 \\ -1 \\ 1 \end{bmatrix}, \begin{bmatrix} 1 \\ -1 \\ 1 \\ -1 \end{bmatrix} \right\} \qquad (2.5.2.7)$$

For this system, with different selection of coherent modes, applying the grouping algorithm in section 2.4, we will get different groups of generators with respect to the modes. The connection quantity s of each grouping is calculated and listed in the following Table 2.5.2.1.

Table 2.5.2.1 Grouping and connections comparison of the RC-circuit

σ_a	**Coherent Groups**	$\sum_{\alpha=1}^{r=2}\lambda_\alpha$	**Connection Quantity** s
$\{0,-2q\}=\sigma_1$	$\{x_1,x_2\}$ $\{x_3,x_4\}$	$-2q$	$2q$
$\{0,-2p\}=\sigma_2$	$\{x_1,x_4\}$ $\{x_2,x_3\}$	$-2p$	$2p$
$\{0,-2(p+q)\}=\sigma_3$	$\{x_1,x_3\}$ $\{x_2,x_4\}$	$-2(p+q)$	$2(p+q)$

This table clearly distinguishes between the selected modes and the external connection quantity. In column 3 and 4, the sum of the eigenvalues is equal to the connection quantity in absolute value. Selecting the slowest modes means the aggregated system will have the weakest external connection or smallest connection quantity.

2.5.3 Singular Perturbation Forms

As shown in the section 2.3, a linear time-invariant system represented by equations (2.3.12) and (2.3.13) can be transformed using transformations (2.3.18) and $\xi = y + H\eta$. Then the system equation will contain new state variables η and ξ, which are separated from the original system and form fast and slow subsystems respectively. The transformed system equations (2.3.19) and (2.3.20) or (2.3.22) are called explicit separated form, which is one of the singular perturbation forms. However, power system electromechanical model takes the weak connection form. By making a transformation on the weak connection form, the explicit separated form may be obtained. Consider a system:

$$\varepsilon\frac{dX}{dt}=\frac{dX}{d\tau}=A(\varepsilon)X=(A_0+\varepsilon A_1(\varepsilon))X \qquad (2.5.3.1)$$

where t and τ are the slow and fast time variables as discussed in section 2.3, respectively. A_0 satisfies:

$$dim(N(A_0))=v\geq 1 \qquad (2.5.3.2)$$

$$dim(R(A_0))=\rho\geq 1 \qquad (2.5.3.3)$$

$$\rho+v=n \qquad (2.5.3.4)$$

Suppose the rows of $\upsilon \times n$ matrix P span the left null space of A_0, that is

$$PA_0 = 0 \tag{2.5.3.5}$$

Suppose the rows of a $\rho \times n$ matrix Q span the row space of A_0, that is

$$\forall X, X \in S, S = \{ X : A_0 X = 0 \}$$

The following equation exists:

$$QX = 0 \tag{2.5.3.6}$$

Then introduce a transformation matrix

$$T = \begin{bmatrix} P \\ Q \end{bmatrix} \tag{2.5.3.7}$$

Let

$$\begin{bmatrix} Y \\ Z \end{bmatrix} = TX = \begin{bmatrix} P \\ Q \end{bmatrix} X \tag{2.5.3.8}$$

where the rows of P, Q form bases for the left null and row spaces of A_0. For matrix T,

$$T^{-1} = \begin{bmatrix} V & W \end{bmatrix} \tag{2.5.3.9}$$

where the columns of V and W form bases for $N(A_0)$ and $R(A_0)$ respectively. They correspond to equations (2.5.3.5) and (2.5.3.10)

$$A_0 V = 0 \tag{2.5.3.10}$$

Apply (2.5.3.10) to the following equations:

$$T((A_0/\varepsilon) + A_1(\varepsilon))T^{-1}$$

$$= \frac{1}{\varepsilon}\begin{bmatrix} PA_0V & PA_0W \\ QA_0V & QA_0W \end{bmatrix} + \begin{bmatrix} PA_1(\varepsilon)V & PA_1(\varepsilon)W \\ QA_1(\varepsilon)V & QA_1(\varepsilon)W \end{bmatrix}$$

$$= \begin{bmatrix} PA_1(\varepsilon)V & PA_1(\varepsilon)W \\ QA_1(\varepsilon)V & QA_0W/\varepsilon + QA_1(\varepsilon)W \end{bmatrix} \tag{2.5.3.11}$$

That is,

$$\dot{Y} = A_s(\varepsilon)Y + A_{sf}(\varepsilon)Z \tag{2.5.3.12}$$

$$\varepsilon\dot{Z} = \varepsilon A_{fs}(\varepsilon)Y + A_f(\varepsilon)Z \tag{2.5.3.13}$$

where,

$$A_s(\varepsilon) = PA_1(\varepsilon)V \tag{2.5.3.14}$$

$$A_{sf}(\varepsilon) = PA_1(\varepsilon)W \tag{2.5.3.15}$$

$$A_{fs}(\varepsilon) = QA_1(\varepsilon)V \tag{2.5.3.16}$$

$$A_f(\varepsilon) = QA_0W + \varepsilon QA_1(\varepsilon)W \tag{2.5.3.17}$$

This system is now in the explicit separated form that can be compared with equation (2.3.19) and (2.3.22).

Furthermore, as $\varepsilon \to 0$, $A_f(\varepsilon) \to QA_0W$. We know the rows of W are the bases of $R(A_0)$. Since $R(A_0)$ is the eigenspace of the non-zero eigenvalues of A_0, there exists a $\rho \times \rho$ nonsingular matrix G whose eigenvalues are the non-zero eigenvalues of A_0 such that

$$A_0W = WG \tag{2.5.3.18}$$

So

$$A_f(0) = QA_0W = QWG = G \tag{2.5.3.19}$$

where $A_f(0)$ is nonsingular.

For a linear time invariant system (two subsystems for example), the weak connection form is shown in the following equations:

$$\varepsilon\begin{bmatrix} dX_1/dt \\ dX_2/dt \end{bmatrix} = \begin{bmatrix} dX_1/d\tau \\ dX_2/d\tau \end{bmatrix} = \begin{bmatrix} A_{11} + \varepsilon A_{11}' & \varepsilon A_{12} \\ \varepsilon A_{21} & A_{22} + \varepsilon A_{22}' \end{bmatrix}\begin{bmatrix} X_1 \\ X_2 \end{bmatrix} \tag{2.5.3.20}$$

where X_1 and X_2 are n_1 and n_2 vectors. Also,

$$dim\, R(A_{11}) + dim\, N(A_{11}) = n_1 \tag{2.5.3.21}$$

$$dim\, R(A_{22}) + dim\, N(A_{22}) = n_2 \tag{2.5.3.22}$$

Let P_i and Q_i span the left null and row spaces of A_{ii}, respectively, and V_i and W_i span the right null and range spaces, respectively, i=1,2. Writing

$$\begin{bmatrix} A_{11} + \varepsilon A_{11}' & \varepsilon A_{12} \\ \varepsilon A_{21} & A_{22} + \varepsilon A_{22}' \end{bmatrix} = \begin{bmatrix} A_{11} & 0 \\ 0 & A_{22} \end{bmatrix} + \varepsilon\begin{bmatrix} A_{11}' & A_{12} \\ A_{21} & A_{22}' \end{bmatrix} \tag{2.5.3.23}$$

Use transformations

$$\begin{bmatrix} Y_1 \\ Y_2 \end{bmatrix} = \begin{bmatrix} P_1X_1 \\ P_2X_2 \end{bmatrix} \tag{2.5.3.24}$$

$$\begin{bmatrix} Z_1 \\ Z_2 \end{bmatrix} = \begin{bmatrix} Q_1X_1 \\ Q_2X_2 \end{bmatrix} \tag{2.5.3.25}$$

Apply this transformation on equation (2.5.3.20) and get the following the slow model and fast model respectively:

$$\begin{bmatrix} \dot{Y}_{1s} \\ \dot{Y}_{2s} \end{bmatrix} = \begin{bmatrix} P_1A_{11}'V_1 & P_1A_{12}V_2 \\ P_2A_{21}V_1 & P_2A_{22}'V_2 \end{bmatrix}\begin{bmatrix} Y_{1s} \\ Y_{2s} \end{bmatrix} \tag{2.5.3.26}$$

$$\varepsilon\begin{bmatrix} \dot{Z}_{1f} \\ \dot{Z}_{2f} \end{bmatrix} = \begin{bmatrix} Q_1A_{11}W_1 + \varepsilon Q_1A_{11}'W_1 & \varepsilon Q_1A_{12}W_2 \\ \varepsilon Q_2A_{21}W_1 & Q_2A_{22}W_2 + \varepsilon Q_2A_{22}'W_2 \end{bmatrix}\begin{bmatrix} Z_{1f} \\ Z_{2f} \end{bmatrix} \tag{2.5.3.27}$$

The two equations (2.5.3.26) and (2.5.3.27) are in the explicit form of two-time-scale model as shown in (2.3.1) and (2.3.2). This system contains two subsystems. It can be extended without loss of generality to cases with more than two subsystems. It shows some important features of the weak connection form.

- Equation (2.5.3.23) shows each subsystem has weak connections with the other subsystem. But each subsystem has its own fast and slow states variables. Subsystem 1 contains the slow variable Y_1 and fast variable Z_1. Subsystem 2 contains the slow variable Y_2 and fast variable Z_2.
- Equation (2.5.3.27) shows fast variables in each subsystem have weak connections with fast variables in other subsystems so that the connection can be omitted. Or the fast variables are local.
- Equation (2.5.3.26) shows slow variables of each subsystem have strong connections to the other subsystems, which should be modeled together.

In all, for each subsystem, there are fast local models with weak connections to the other local fast models and slow models forming a slow "core", which describes the aggregate dynamics, with strong connection to the other subsystems.

The weak connection form best states the reason of islanding based on slow coherency. That is, when the disturbance occurs, it is required to separate in the transient time scale the fast dynamics through islanding, which could propagate the disturbance very quickly on the weak connections. While in the transient time scale, the slow dynamics will mostly remain constant or change slowly on the tie lines between the areas. In other words, once fast dynamics are detected on the tie lines, it means fast dynamics are being propagated through these weak connections.

2.6 NONLINEAR METHOD

Dynamic networks are usually nonlinear networks. The slow coherency theory is applicable to the nonlinear dynamic systems. Nonlinear two-time-scale dynamic system has two important properties: Conservation property and Equilibrium property. Wide separation of eigenvalues is a characteristic of the linear two-time-scale networks, while Conservation property and Equilibrium property exist in both linear and nonlinear models. They represent two auxiliary systems that respectively define a fast dynamic manifold and a slow

equilibrium manifold. For power system dynamics with a nonlinear weak connection form, it is proven in [13] that slow coherency can be shown with two linear transformations, which are derived from the dynamic manifold and equilibrium manifold. The power system dynamic models can be decomposed into nonlinear aggregate and local models with linear transformations. Actually slow coherency is a physical evidence of weak connection, which is a network characteristic. Hence, linearized generator electromechanical model is enough for determining the areas. In many large-scale practical systems, there always exist groups of strongly interacting units with weak connections between groups. But even very weak connections will become strong connection with significant interactions after short period of time. When a large disturbance happens, it is imperative to disconnect the weak connections before the slow interaction becomes significant, or before the fast dynamics propagate. In the following two subsections, a brief introduction is made on two generalized nonlinear two-time-scale dynamic models: explicit and non-explicit model. The procedure to transform the power system dynamic model as a non-explicit model into a local and aggregated model with linear transformations will be demonstrated.

2.6.1 Explicit and Non-explicit Model

An explicit nonlinear two-time-scale dynamic model takes the form shown below:

$$dY/d\tau = \varepsilon f(Y,Z,\varepsilon) \tag{2.6.1.1}$$

$$dZ/d\tau = g(Y,Z,\varepsilon) \tag{2.6.1.2}$$

where τ is the fast time variable as discussed in section 2.3. There are r slow states Y and n-r fast states Z in the equation (2.6.1.1) and (2.6.1.2). Set ε to be 0, the auxiliary system can be obtained in the following:

$$dY/d\tau = 0 \tag{2.6.1.3}$$

$$dZ/d\tau = g(Y,Z,0) \tag{2.6.1.4}$$

Two important properties are contained in the system: Conservation property and Equilibrium property. Conservation property:

An r-dimensional function of the state

$$Y = \psi(Y,Z) \tag{2.6.1.5}$$

remains at its initial value

$$Y(0) = \psi(Y(0),Z(0)) \tag{2.6.1.6}$$

That is, the state is conserved during the motion. Furthermore, the auxiliary system defines a fast dynamic manifold with conservation property defined by

$$F=\{Y,Z:Y=Y(0),dZ/d\tau=g(Y,Z,0)\} \tag{2.6.1.7}$$

Equilibrium property:

The auxiliary system defined by equation (2.6.1.3) and (2.6.1.4) possesses a set of continuous equilibrium points defined by an n-r dimensional function:

$$\varphi(Y,Z)=g(Y,Z,0)=0 \tag{2.6.1.8}$$

These are the quasi-steady states to which the fast transients of the original system will converge if they are asymptotically stable. It defines an equilibrium manifold:

$$S=\{Y,Z:g(Y,Z,0)=0\} \tag{2.6.1.9}$$

Usually a real system doesn't have an explicit two-time-scale form. Consider the following n-dimensional system function:

$$\varepsilon dX/dt=dX/d\tau=h(X,\varepsilon) \tag{2.6.1.10}$$

with the following auxiliary system:

$$dX/d\tau=h(X,0) \tag{2.6.1.11}$$

The auxiliary system has a v-dimensional continuously equilibrium manifold defined with ρ-dimensional continuously differentiable functions $\varphi(X)$ with $\rho=n-v$ and $rank(\partial\varphi/\partial x)=\rho$. The equilibrium manifold is:

$$S=\{X:\varphi(X)=h(X,0)=0\} \tag{2.6.1.12}$$

The auxiliary system has a ρ-dimensional dynamic manifold defined with v-dimensional continuously differentiable function $\psi(X)$. The dynamic manifold is:

$$F_{X(0)}=\{X:\psi(X)-\psi(X(0))=0\} \tag{2.6.1.13}$$

The dynamic manifold is an invariant manifold, which means a trajectory originating in F will remains in F. It is a representation of the conservation property. Moreover,

$$rank\begin{bmatrix}\partial\varphi/\partial X\\ \partial\psi/\partial X\end{bmatrix}=n \tag{2.6.1.14}$$

Then the following transformation,

$$Y=\psi(X) \tag{2.6.1.15}$$

$$Z=\varphi(X) \tag{2.6.1.16}$$

will transform the auxiliary system (2.6.1.11) into the explicit separated form.

Proof:

The τ-derivative with respect to the state Y in the equation (2.6.1.15) is:

$$dY/d\tau = d\psi/d\tau = (\partial\psi/\partial X)(dX/d\tau) = (\partial\psi/\partial X)h(X,0) = 0 \qquad (2.6.1.17)$$

The t-derivative with respect to the state Y is:

$$dY/dt = (1/\varepsilon)(\partial\psi/\partial X)h(X,\varepsilon) = (\partial\psi/\partial X)(\partial h/\partial\varepsilon) \qquad (2.6.1.18)$$

That implies Y is a slow variable vector. Suppose the inverse transformation of (2.6.1.15) and (2.6.1.16) is $X = \gamma(Y,Z)$ and take the t-derivative with respect to the state Z in the equation (2.6.1.16):

$$\varepsilon(dZ/dt) = (\partial\varphi/\partial X)h(X,\varepsilon) = (\partial\varphi/\partial X)h(\gamma(Y,Z),\varepsilon) = g(Y,Z,\varepsilon) \qquad (2.6.1.19)$$

Then $\partial g/\partial Z$ is nonsingular at $\varepsilon = 0$ because the transformation is nonsingular. Finally, from the definition of the equilibrium manifold S, X is in S if and only if $X = \gamma(Y,0)$ or $Z = \varphi(X) = 0$. So

$$h(\gamma(Y,0),0) = 0 \qquad (2.6.1.20)$$

Or

$$g(Y,0,0) = 0 \qquad (2.6.1.21)$$

This implies $Z_s(t) = 0$. Y and Z are respectively slow and fast state vectors. ■

2.6.2 Power System Nonlinear Model

Power system network two-time-scale dynamics take the form of weak connection form. Instead of using the linearized equations shown in (2.4.1.1) and (2.4.1.2), the second order nonlinear power system model can be written as the following equations by neglecting the off-diagonal conductance and the generator damping.

$$m_i\ddot{\delta}_i = P_{mi} - P_{ei} \qquad (2.6.2.1)$$

where,

$$P_{ei} = \sum_{j=1, j\neq i}^{n} V_i V_j B_{ij} \sin(\delta_i - \delta_j) + V_i^2 G_{ii} \qquad (2.6.2.2)$$

G_{ii} Self-admittance of bus i in pu,

B_{ij} Susceptance between bus i and bus j in pu.

Suppose the system is partitioned into r areas according to the grouping algorithm in section 2.4. It has been proven with the linear power system model that the connections between the areas are the weakest. The bus i belongs to area α, which contain a set of buses denoted by J_α. Then the system susceptance matrix B can be decomposed into

$$B = B^I + \varepsilon B^E \tag{2.6.2.3}$$

where B^I is the internal susceptance matrix for connections within an area and B^E is the weak external susceptance matrix for connections between the areas. Then

$$P_{ei} = \sum_{j=1, j\neq i}^{j\in J_\alpha} V_i V_j B_{ij}^I \sin(\delta_i - \delta_j) + V_i^2 G_{ii} + \varepsilon \sum_{\beta=1,\beta\neq\alpha}^{r} \sum_{j}^{j\in J_\beta} V_i V_j B_{ij}^E \sin(\delta_i - \delta_j)$$

$$= P_{ei}^I + V_i^2 G_{ii} + \varepsilon \sum_{\beta=1,\beta\neq\alpha}^{r} P_{ei}^E \tag{2.6.2.4}$$

Here we use εP_{ei}^E to refer to the weak connections between the area i and the other areas. Then, the power system electromechanical model can be written as:

$$m_i \ddot{\delta}_i = -P_{ei}^I - \varepsilon \sum_{\beta=1,\beta\neq\alpha}^{r} P_{ei}^E + (P_{mi} - V_i^2 G_{ii}) \tag{2.6.2.5}$$

Let

$$x_i = \delta_i \tag{2.6.2.6}$$

$$P_{ei}^I = \sum_{j, j\neq i}^{j\in J_\alpha} f_{ij}(x_i - x_j) \tag{2.6.2.7}$$

Where,

$$f_{ij}(x_i - x_j) = V_i V_j B_{ij}^I \sin(\delta_i - \delta_j) \tag{2.6.2.8}$$

$$P_{ei}^E = \sum_{j}^{j\in J_\beta} g_{ij}(x_i - x_j) \tag{2.6.2.9}$$

$$g_{ij}(x_i - x_j) = V_i V_j B_{ij}^E \sin(\delta_i - \delta_j) \tag{2.6.2.10}$$

Consider the following second order weakly connected dynamic system:

$$m_i d^2 x_i / d\tau^2 = \sum_{j, j\neq i}^{j\in J_\alpha} - f_{ij}(x_i - x_j) + \varepsilon \sum_{\beta=1,\beta\neq\alpha}^{r} \left(\sum_{j}^{j\in J_\beta} - g_{ij}(x_i - x_j) \right) + p_i(\varepsilon) \tag{2.6.2.11}$$

Where,

$$p_i(\varepsilon) = P_{mi} + V_i^2 G_{ii} \tag{2.6.2.12}$$

If the weak connection terms are neglected, we can get r weakly connected system:

$$m_i d^2 x_i / d\tau^2 = \sum_{j, j\neq i}^{j\in J_\alpha} - f_{ij}(x_i - x_j) + p_i(0) \tag{2.6.2.13}$$

$$p_i(0) = P_{mi} + V_i^2 G_{ii}^I \tag{2.6.2.14}$$

Suppose each of the isolated r dynamic systems has its own equilibrium states. Then $\sum_{i}^{i\in J_\alpha}(p_i(\varepsilon)-p_i(0))$ is the flow from area α to the other area. If the weak connection terms are neglected at the equilibrium point, then:

$$\sum_{i}^{i\in J_\alpha} p_i(0)=0, \alpha=1,2,...,r \tag{2.6.2.15}$$

Let x_i^e represent the state x_i in equilibrium. If the first state x_p^α of each area α is selected as the reference state, we can define the following $n_\alpha-1$ difference variables for each area α:

$$s_j = x_j^e - x_p^{e\alpha}, j\in J_\alpha, j\neq k_\alpha+\alpha \tag{2.6.2.16}$$

Where,

$$k_\alpha=\sum_{m=1}^{\alpha-1}(n_m-1), k_1=0 \tag{2.6.2.17}$$

Here, k_α is the number of difference variables defined in the previous α areas, and $k_\alpha+\alpha$ is the first state variable's number in the area α, which is already selected as the reference state for the area. Then the system has an equilibrium manifold S defined by

$$\varphi_k(X)=x_j-x_p^\alpha-s_j=0 \tag{2.6.2.18}$$

$$k=k_\alpha+1,...,k_\alpha+n_\alpha-1. \qquad \alpha=1,2,...,r \tag{2.6.2.19}$$

Thus the system has a dynamic manifold F for a given initial condition $X(0)$:

$$\psi_\alpha(X)-\psi_\alpha(X(0))=0 \qquad \alpha=1,2,...,r \tag{2.6.2.20}$$

where ψ_α is the center of inertia variable for the area α represented as following:

$$\psi_\alpha(X)=\sum_{j}^{j\in J_\alpha}(m_j x_j)/\sum_{j}^{j\in J_\alpha} m_j \tag{2.6.2.21}$$

Furthermore, the following transformations will transform the original states into slow and fast variables:

$$y_\alpha=\psi_\alpha(X), \alpha=1,2,...,r \tag{2.6.2.22}$$

$$z_k=\varphi_k(X), k=1,2,...n-r \tag{2.6.2.23}$$

Proof:

If all the elements of X satisfy the following equations, then X is equilibrium of the original system (2.6.2.11).

$$x_i-x_j=x_i^e-x_j^e, i,j\in J_\alpha, \alpha=1,2,...,r \tag{2.6.2.24}$$

Thus $\varphi_k(X)$ defined in (2.6.2.18) will constitute an equilibrium manifold, since

$$x_i-x_j=(x_i-x_p^\alpha)-(x_j-x_p^\alpha)=s_i-s_j=x_i^e-x_j^e \tag{2.6.2.25}$$

Substitute into the following equations and apply equation (2.6.2.15):

$$\sum_{i}^{i\in J_\alpha}(\sum_{j,j\neq i}^{j\in J_\alpha}(-f_{ij}(x_i-x_j))+p_i(0))$$

$$=\sum_{i}^{i\in J_\alpha}(\sum_{j,j\neq i}^{j\in J_\alpha}(-f_{ij}(x_i-x_j)))+\sum_{i}^{i\in J_\alpha}p_i(0)$$

$$=\sum_{i}^{i\in J_\alpha}(\sum_{j,j\neq i}^{j\in J_\alpha}(-f_{ij}(x_i^e-x_j^e)))+\sum_{i}^{i\in J_\alpha}p_i(0)$$

$$=0 \qquad (2.6.2.26)$$

Or

$$\sum_{i}^{i\in J_\alpha}m_i d^2x_i/d\tau^2=0 \qquad (2.6.2.27)$$

Integrating and scaling by $M_\alpha=\sum_{j}^{j\in J_\alpha}m_j$, we can get the dynamical manifold F as defined in (2.6.2.21). ■

With the above knowledge, slow coherency can be redefined in the nonlinear context:

States x_i and x_j are said to be slow coherent with each other if *X(0)* in *S* implies $x_i(t)-x_j(t)$ is constant. Or states x_i and x_j are said to be slow coherent with each other if *X(0)* in *S* implies

$$x_i(t)-x_j(t)=constant+\varepsilon\gamma(t) \qquad (2.6.2.28)$$

Under this definition, the transformed system with (2.6.2.22) and (2.6.2.23) has r near slow-coherent areas.

For instance, if $i,j\in J_\alpha$, then

$$x_i(t)-x_j(t)=(x_i-x_p^\alpha)-(x_j-x_p^\alpha)=z_i-z_j+s_i-s_j \qquad (2.6.2.29)$$

In (2.6.2.29), s_i-s_j is constant. In the slow time scale, when *X(0)* is in *S*,

$$z_S(t)=0(\varepsilon)=\varepsilon\gamma(t) \qquad (2.6.2.30)$$

So equation (2.6.2.28) is proven.

2.7 AN AUTOMATIC ISLANDING PROGRAM

2.7.1 Introduction

Having decided the coherent generators in each island, certain criteria need to be developed for the determination of the physical boundary of each island. The following criteria are followed:

- Generation load balance consideration.

The generation load imbalance needs to be minimized in each island. This is done by accounting for the total generation in each proposed island and the total load at all the load buses within this island. The reduction of imbalance reduces the amount of the load needed to perform under-frequency load shedding once the islands are formed. It also makes it easier for each island to be capable of matching the generation and load within the prescribed frequency limit and is beneficial during restoration.

- Topological requirements.

In order to form the islands and specifically isolate one island from the other, all the lines connecting the islands, two or three or even more, need to be determined and disconnected. This would require the analysis of the branch data to determine the lines that would need to be disconnected in order to form islands. In most cases, tie lines or EHV lines will act as the monitored lines in practice. However, relatively lower voltage lines, such as 230kV lines, can also be monitored as candidates for local and remote tripping.

- Restoration considerations.

Each island has to have the black start capability that is sufficient for critical equipment. Usually a large capacity hydro machine is needed for black start. Each island also has to have the proper voltage control capability to maintain a suitable voltage profile. Each island must be capable of being monitored by the control center for security checks and coordination. Synchronizing devices should be available near the boundary of the islands for re-closing the circuit and restoration function [15].

2.7.2 Data Structure

A C++ program has been developed based on the criteria provided in section 2.7.1 to identify from the grouping information the exact locations in the network where the islands can be formed. The program considers the boundary topology conditions and provides an exhaustive search-based list of all the possible cut sets with the generation load imbalance information. It is important to have a good data structure to store the power system topology network and necessary information for the islanding problem, since easy manipulation of the data structure will ease the procedure to identify the possible cut sets. So the program begins with the characterization of the network structure or connectivity using an adjacent link table data structure [16]. The structure is modified to apply in this case. With this structure, the original topological system is at first reduced to a sub-network, which contains all the possible branches that could form the islands. Then the search for the possible cut sets can be conveniently performed on the reduced power system topology network. The modified adjacent link table structure is shown in the following figure.

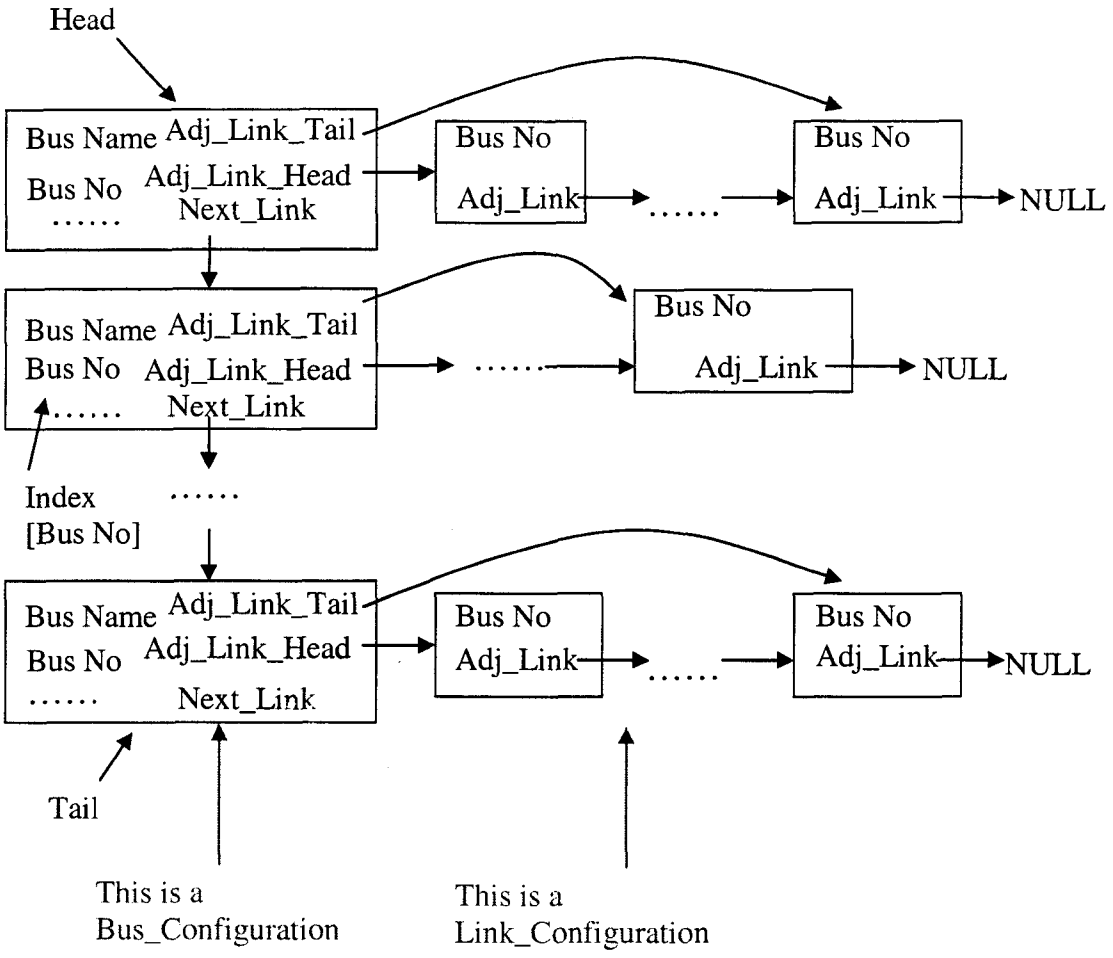

Fig. 2.7.2.1 Modified adjacent link table data structure

The network topology data are basically stored in two types of basic data structures: Bus_Configuration and Link_Configuration. Bus_Configuration contains information related with the bus: bus number, bus name, bus type (generator, load or connection bus), voltage level, etc. For generators, the data of active power and reactive power will also be stored. This will facilitate the calculation of generation load imbalance. Link_Configuration contains information related to the transmission lines or bus connections. It only contains the bus number which is connected and a pointer to the next Link_Configuration structure which is also connected with the head bus. All the buses can be retrieved using the bus number in the array Index [16]. Then each bus will have a chain of the data structure Link_Configuration, which contains all the buses the head bus is connected to. So with the above data structures,

the information of power system network topology and necessary information for the islanding problem can be easily saved, retrieved and manipulated with convenience.

2.7.3 Reduction Procedure and Cut Sets Identification

Having identified the groups of coherent generators, the tie lines or the cut sets between the coherent groups are identified. With the adjacent link table data structure provided above, the network information can be stored and manipulated. The interface buses between the coherent groups are then determined. Approximately, the interface buses are defined as the small network between the islands to be formed. The concept of the interface network can be illustrated with the Fig. 2.7.3.1. In the figure, the exact boundary between two groups of generators, which are represented with two areas in the figure, needs to be identified. The small network between the two areas are called interface network and the generators in the interface network are called interface generators.

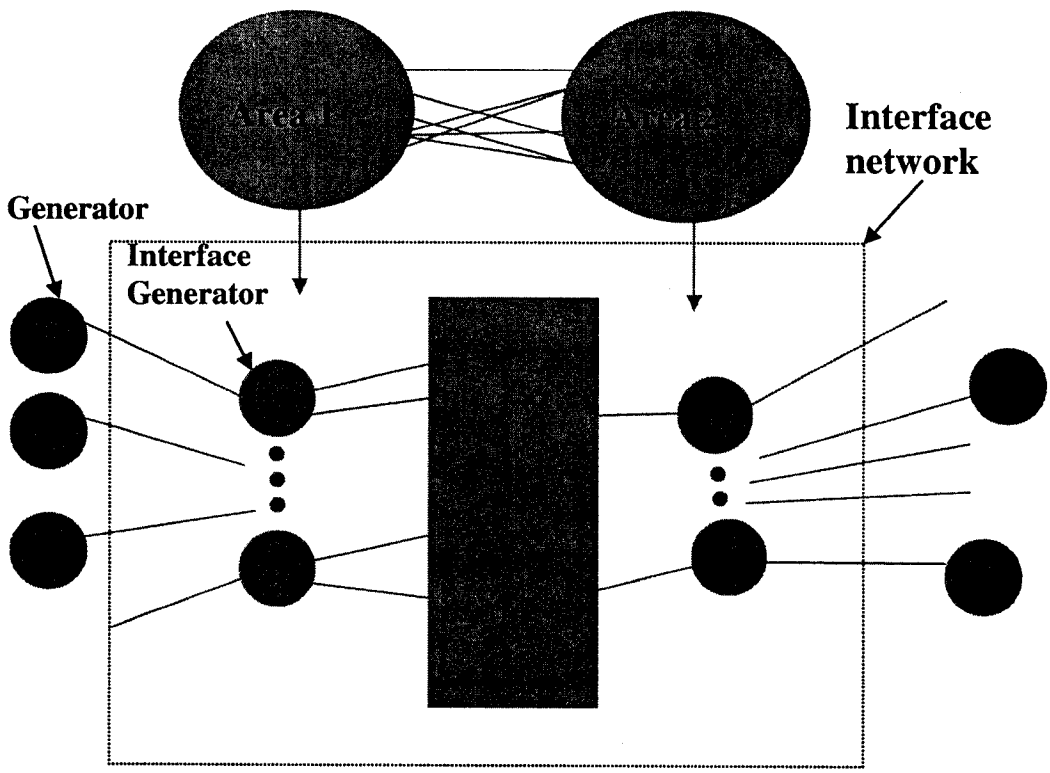

Fig. 2.7.3.1 Illustration of interface network

In determining the interface buses, the program concentrates only on the buses associated with the coherent groups under consideration or the groups to be islanded, since the tie lines or cut sets must come from the interface buses. Before forming these interface buses, some reductions on the original network should be done. The part of the network for all the groups except for the coherent groups under consideration is reduced. Several steps are taken in reducing the network. They include:

- Reduce all the generator buses to their terminal buses.

The procedure is needed just to reduce the total number of nodes in the system. Since the generator's information may be stored in the terminal buses, it is applicable.

- Remove the unnecessary generators that are not included in the groups under consideration.

They can be removed because we only search for the cut sets in one place between two or even more coherent generator groups.

- Search and remove the isolated buses.

Isolated buses or islands are usually formed after above two steps. Since these buses or islands are not in the concerned area, they may be removed from the system.

After these steps, a smaller network is formed. The search for the interface buses is based on the smaller network. The program will start from one of the buses or the center node from the user input in the interface between the groups, which is to be determined. The user needs to make a rough estimate of where the tie lines should be cut to form the islands and should select one of the buses as the center bus. At least 3 layers (3 adjacent nodes) and at most 8 layers, depending on the physical distance of the node from the center node by the user's estimation, of the system network around the center node are searched as the interface sub-network. A brute force search is then conducted on the interface network to determine the cut sets where the islands formed. Two assumptions regarding the cut sets are made during the search, which hold for most power system topological networks:

- All the cut sets, or combination of lines to be tripped, come from the lines of the interface network.
- A cut set is limited to 4 lines since not too many tie lines are expected to be tripped during islanding.

The sequence of the search for interface network is illustrated in the following Fig. 2.7.3.2 with the program run on a test system. The above procedures are illustrated in the flow chart shown in Fig. 2.7.3.3 with each step's function name in the program listed, too.

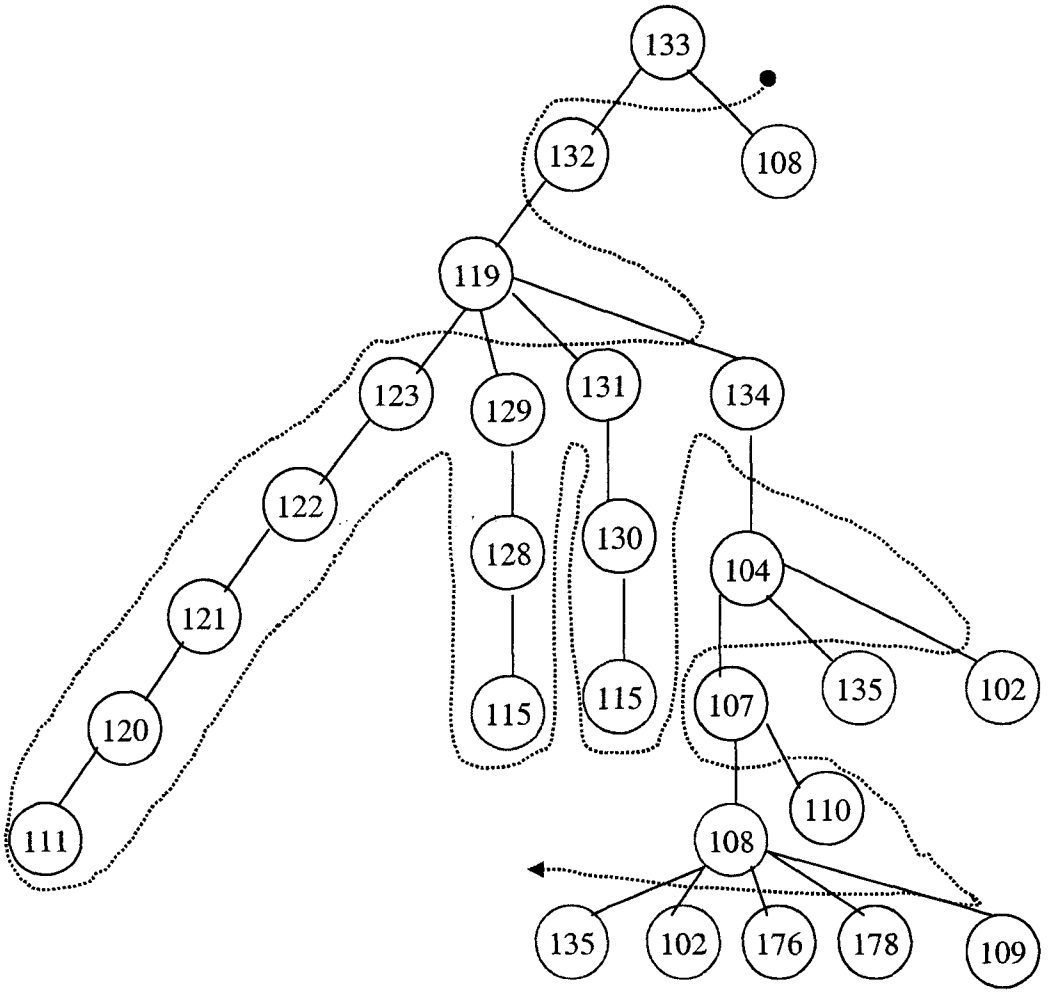

Fig. 2.7.3.2 Illustration of interface network search sequence.

Fig. 2.7.3.2 shows part of a power network, which is an interface network for this case. Circles and lines represent buses and lines in the power networks, respectively. The arrow shows the sequence in which the interface network is formed. The search for the interface network starts from the user specified center bus with bus number 133. Basically the search starts from the head node of bus 133 in the adjacent link table data structure and goes down the adjacent chains till the NULL pointer. On each Link_Configuration node met on the

chain, the procedure is repeated from the head node of the Link_Configuration node. At most 8 layers and at least 3 layers of the nodes from the center node of bus 133 are searched. Sometimes the node has been searched before. For example, bus 108,115,135 and 102 are these types of nodes. Then in the second meeting, the node will be ignored to avoid repetitive calculation. Finally, all the buses in the interface network are found through the recursion.

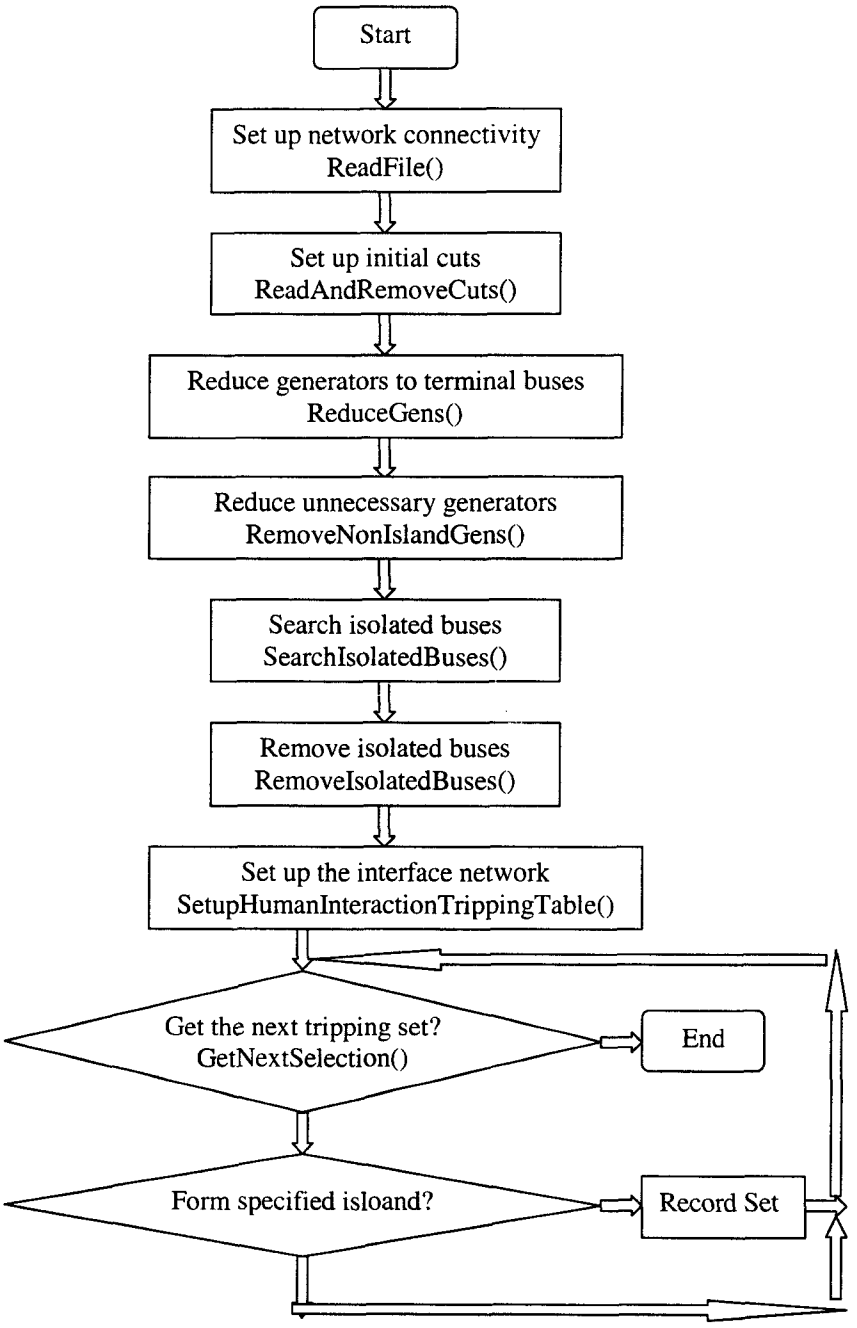

Fig. 2.7.3.3 Flow chart of automatic islanding program

By running the program, the exact optimum tripping lines are located once we have the coherent groups' information. The generation and load information stored in the data structure helps us determine the generation load imbalance in each island that is formed.

Based on this information, the optimal cut sets considering the criteria of the topological requirement and the minimum generation load imbalance requirement are obtained.

2.8 MODIFIED GROUPING ALGORITHM

2.8.1 Introduction

The slow coherency identification algorithm or the grouping algorithm has been introduced in section 2.4. The algorithm is illustrated on a three-machine equivalent system shown in Fig. 2.4.2.1. The algorithm is implemented on a second-order electromechanical model ignoring the effect of the damping and the model of the voltage regulator, governor, PSS and various controllers. The three machines are divided into two groups according to the eigenvector matrix from equation (2.4.1.24). This is done by first identifying the slow inter-area modes and the fast intra-area modes. The generators are then grouped based on their coherency information with respect to a selected spectrum of slow inter-area modes. This information is stored in the slow eigensubspace.

As pointed out in section 2.2, different dynamical model requirements should be enforced according to the research objective. Transient dynamics based on detailed modeling need to be taken into account in order to have a more precise grouping result. As pointed out in [10], transient dynamics have different time scales. Electromechanical dynamics, which can be represented by rotor angle and speed, are faster than voltage or flux dynamics such as E_q'. But recent results have shown that interarea mode shapes can be changed by the governor, exciter and by the effect of other controllers. Some controllers such as PSS, are designed to change the mode shape of the interarea modes. Load characteristics, in particular, have a major effect on the stability of interarea modes. The manner in which excitation systems affect interarea oscillations depends on the types and locations of the exciters, and on the characteristics of loads [17]. Though the controller's effect may not be as fast as the effect from the physical connections – electromechanical modes, they are not negligible. It is necessary to use the detailed generator model in order to make a precise coherency analysis. Furthermore, a mode of oscillation in one part of the system may interact with a mode of oscillation in a remote part due to mode coupling. This occurs when the frequencies of the two modes are nearly equal [18]. Choosing the correct electromechanical modes as reference

modes is important before applying the grouping algorithm. On the other hand, voltage stability becomes an important issue. Short-term dynamics such as the dynamics of induction motors need to be considered in modeling. This is especially important when the time constant of the induction motor is comparable to the time constant of the synchronous machine. The original grouping algorithm benefits from using the second order classical generator model to perform the analysis. Two problems will exist if the induction motor load model is included in the system state space representation or if the detailed generator model is used:

- Each eigenvector matrix or eigensubspace row does not represent one generator any more especially when the first order system state matrix A is introduced.
- It is not clear how to identify the slowest modes in the detailed model since eigenvalues are complex values.

2.8.2 Illustration of The Modified Grouping Algorithm

In this section, the current grouping algorithm is modified with a detailed generator model considering load dynamics [19]. The three machine equivalent system in Fig. 2.4.2.1 is again used as the sample system for illustration.

At first, the grouping algorithm is applied to the first order state space representation to compare the results. The model including the damping is shown as below:

$$\dot{X} = AX \tag{2.8.2.1}$$

Where

$$A = \begin{bmatrix} 0 & 0 & 0 & 1 & 0 & 0 \\ 0 & 0 & 0 & 0 & 1 & 0 \\ 0 & 0 & 0 & 0 & 0 & 1 \\ -24.18 & 13.53 & 10.65 & -0.20 & 0 & 0 \\ 44.36 & -77.58 & 33.23 & 0 & -0.19 & 0 \\ 78.33 & 73.93 & -152.00 & 0 & 0 & -0.17 \end{bmatrix} \tag{2.8.2.2}$$

$$X = [\delta_1 \quad \delta_2 \quad \delta_3 \quad \omega_1 \quad \omega_2 \quad \omega_3]^T \tag{2.8.2.3}$$

With eigenvalues:

$$D = [-0.09 \pm 13.36j \quad -0.10 \pm 8.69j \quad 0.03 \,\&\, -0.23]^T \tag{2.8.2.4}$$

These three pairs of eigenvalues correspond to states of three machines. The modes -0.23 and -0.10+8.69j are selected as reference modes. The three rotor angle rows in the eigensubspace matrix are selected to represent the three machines. Then

$$V = \begin{array}{c} \\ \delta_1 \\ \delta_2 \\ \delta_3 \end{array} \begin{array}{c} \lambda = -0.10 + 8.69j \quad \lambda = -0.23 \\ \begin{bmatrix} 0.0350 + 0.0084j & 0.5624 \\ -0.0916 - 0.0218j & 0.5625 \\ -0.05025 - 0.0126j & 0.5626 \end{bmatrix} \end{array} \tag{2.8.2.5}$$

By Gaussian elimination:

$$V_1 = \begin{bmatrix} -0.0525 - 0.0126j & 0.5626 \\ 0.0350 + 0.0084j & -0.5624 \end{bmatrix} \tag{2.8.2.6}$$

Thus,

$$V \cdot V_1^{-1} = L_d = \begin{bmatrix} 0.000 & 1.000 \\ 1.446 - 0.002j & -0.447 + 0.002j \\ 1.000 & 0.000 \end{bmatrix} \tag{2.8.2.7}$$

Machine 1 and 3 are selected as reference machines. In (2.8.2.7), 1.4464-0.0020j is closer to 1 than –0.4468+0.0020j, which means machine 2 is coherent with machine 3. If the rows of generators corresponding to the rotor speed or the other mode are selected, the same result will be obtained.

The above analysis gives an illustration of the grouping algorithm based on slow coherency. From this analysis, the following observations that are beneficial for more complex system models can be made:

- For a first order system, different from a second order system, each machine will be represented by two state variables. The grouping information can be obtained by examining only one of the variables, either rotor angle or speed.
- For a first order system, different from a second order system, each mode will appear in pairs. The grouping information can be obtained by examining the effect of any one of the modal pairs, or corresponding columns of the eigensubspace matrix.

Table 2.8.2.1 shows the time constants and oscillatory frequency. λ_3 is surely the slowest mode. It has a similar effect on the three rotor angles, which can be seen from the eigenvector entries of the mode in equation (2.8.2.5). The other two modes are faster oscillatory modes and λ_1 is slower. So basically λ_3 and λ_1 are two interarea modes. Fast oscillation exists between machine 2 and machine 3.

Table 2.8.2.1 Time constant and oscillatory frequency of three-machine system in classical model with damping

Eigenvalues	Time constant (second)	Frequency (Hz)
λ_1=-0.0957+8.688j	10.45	1.38
λ_2=-0.0858+13.3588j	11.65	2.1261
λ_3=-0.2315	4.32	0

Following the above analysis, the linearized system state matrix with the detailed generator model is analyzed. All the generators' data are obtained from [11]. The grouping algorithm is applied. An 11 by 11 linearized state space A matrix and 11 eigenvalues are calculated. They are shown in Table 2.8.2.2.

$\lambda_{1,2}$ and $\lambda_{3,4}$ are modes existing in the original classical modal. They are related to machine 2 and 3. By investigating the corresponding entries in the eigensubspace matrix or participation factors, it is observed that λ_7 and $\lambda_{8,9}$ are modes induced by machine 1. Since each selected mode represents one and only one machine, only one mode is selected from the three eigenvalues.

$\lambda_{1,2}$ and $\lambda_{3,4}$ have much larger norm magnitude than $\lambda_{5,6}$ and $\lambda_{10,11}$ since the former eigenvalues are representing electromechanical modes. $\lambda_{5,6}$ have very small time constants. The effect of these modes will decay quickly. $\lambda_{10,11}$ are very slow modes and remain the same values. $\lambda_{5,6}$ and $\lambda_{10,11}$ are non-oscillatory modes. In terms of the effect of the modes in the transient time scale (10 seconds), the oscillatory modes $\lambda_{1,2}$ and $\lambda_{3,4}$ will dominate the mode shapes. $\lambda_{3,4}$ have slower oscillatory frequency and larger effect on the state variables, which can be seen from their entries in the eigensubspace matrix. Overall, the two modes selected are λ_3 and λ_7. The rows corresponding to the three machines' angles are selected to represent the machines.

Table 2.8.2.2 Time constant and oscillatory frequency of three-machine system with detail model

Eigenvalues	Time constant (s)	Frequency (Hz)
$\lambda_{1,2}$= -0.71±12.76j	1.41	2.03
$\lambda_{3,4}$= -0.16±8.30j	6.25	1.32
λ_5= -5.14	0.19	0
λ_6= -3.56	0.28	0
λ_7 = 0.07	14.29	0
$\lambda_{8,9}$ =-0.14±0.01j	7.14	0.0016
λ_{10}= -0.03	33.33	0
λ_{11}= -0.17	5.88	0

Thus,

$$V = \begin{array}{c} \\ \delta_1 \\ \delta_2 \\ \delta_3 \end{array} \begin{array}{c} \lambda_3 = -0.16 + 8.30j \quad \lambda_7 = 0.07 \\ \begin{bmatrix} -0.2953 - 0.0389j & -0.0420 \\ 0.8090 + 0.0761j & -0.0420 \\ 0.4816 + 0.0669j & -0.0420 \end{bmatrix} \end{array} \tag{2.8.2.8}$$

By Gaussian elimination

$$V_1 = \begin{bmatrix} 0.8090 + 0.0761j & -0.0420 \\ -0.2953 - 0.0389j & -0.0420 \end{bmatrix} \tag{2.8.2.9}$$

Thus

$$V \cdot V_1^{-1} = \begin{bmatrix} 0.0000 & 1.0000 \\ 1.0000 & 0.0000 \\ 0.7061 + 0.0223j & 0.2947 - 0.0223j \end{bmatrix} \tag{2.8.2.10}$$

Machine 1 and 2 are selected as reference machines. In (2.8.2.10), 0.7061+0.0223j is closer to 1 than 0.2947-0.0223j, which means machine 3 is coherent with machine 2. Based on the above analysis the following observations can be made:

- Each generator can only have at most one mode selected into the reference slowest modes.
- Magnitudes of decaying time constants and oscillatory frequencies are factors to be considered when selecting reference modes. Electromechanical modes are representation of the physical connections and machines' inertias. Control modes are usually faster in oscillatory frequencies

and slower in time constants. It is necessary to choose the correct slowest electromechanical modes as the reference modes.

As an application of the previous work, an induction motor is included in the system and the machine grouping is determined. But the generations and loads are all reduced to 1/10 of the original system but with the same power factor so that the capacity of the induction motor is comparable to the generation and its effect on the shape of the modes are important. In this situation, the motor has 4.5 MW real power output and 3.4 Mvar reactive power output. The initial slip is 0.0025. The induction motor load constitutes 50% of the original constant *PQ* load on bus 6. The dynamic equations can be obtained in [20]. The parameters in IEEE format [21] are shown in the Table 2.8.2.3.

Table 2.8.2.3 Induction motor data in IEEE format

NLF	MID	ITYPE	IPFA	ISAT	ILTYPE		
6	1	2	50	0	3		
X_m	X_s	R_s	DBF	R_r			
3.6208	0.0409	0.0071	6.589	0.0062			
X_{so}	X_{ro}	C_{so}	C_{ro}	V1	V2	G1	G2
0.0409	0.0267	3.0	3.0	0.00	0.00	0.00	0.00
H	BASPR	BASVR	FR				
4.615	9.488	1.0	60				

With the classical generator model and third-order induction motor model, the system has 9 states variables. They are:

$$X = [\omega_1 \quad \delta_1 \quad \omega_2 \quad \delta_2 \quad \omega_3 \quad \delta_3 \quad v_d' \quad v_q' \quad s] \tag{2.8.2.11}$$

The eigenvalues are shown in the Table 2.8.2.4.

Table 2.8.2.4 Time constant and oscillatory frequency of three-machine system in classical model with induction motor

Eigenvalues	Time constant (s)	Frequency (Hz)
$\lambda_{1,2}$= -0.0884±13.3624j	11.31	2.13
$\lambda_{3,4}$= -0.0989±9.3244j	10.11	1.48
$\lambda_{5,6}$= -0.7024±2.0256j	1.42	0.32
λ_7 = 4349	2.30	0
λ_8= -0.0000	9999	0
λ_9= -0.0002	5000	0

Compared to the previous classical generator model, two voltage state variables and one speed state variable are introduced by the induction motor. λ_7 can be selected as a slow inter-area mode. $\lambda_{5,6}$ are two modes introduced by the motor. Compared with $\lambda_{1,2}$ and $\lambda_{3,4}$, they have smaller time constants and slower oscillation frequency. The modes' effect on the state variables dies out in less than 2 seconds. Though the frequency is slower, it dies out faster. Furthermore, if λ_5 and λ_7 are selected, the grouping algorithm obtains a result of three machines in one group and the motor in one group. However, there is a need to determine which generator the motor should be grouped with. So λ_3 and λ_7 are chosen. Since the effect of the modes on the same variable needs to be compared, only the speed rows are observed. As a result, the following sub-eigenspace matrix is obtained.

$$V = \begin{matrix} \\ \omega_1 \\ \omega_2 \\ \omega_3 \\ s \end{matrix} \begin{matrix} \lambda_3 = -0.099 + 9.324j & \lambda_7 = 0.4349 \end{matrix} \begin{bmatrix} -0.2779 - 0.0163j & 0.2180 \\ 0.8413 + 0.0513j & 0.2174 \\ 0.4476 + 0.0276j & 0.2197 \\ 0.0010 + 0.0001j & -0.3171 \end{bmatrix} \quad (2.8.2.12)$$

The sign of the last row should be changed since slip change is the negative of the speed change.

$$V = \begin{bmatrix} -0.2770 - 0.0163j & 0.2180 \\ 0.8413 + 0.0513j & 0.2174 \\ 0.4476 + 0.0276j & 0.2197 \\ -0.0010 - 0.0001j & 0.3171 \end{bmatrix} \quad (2.8.2.13)$$

By Gaussian elimination, the rows corresponding to the machine 2 and the motor are mostly independent with each other. Hence,

$$V_1 = \begin{bmatrix} 0.8413 + 0.0513j & 0.2174 \\ -0.0010 - 0.0001j & 0.3171 \end{bmatrix} \tag{2.8.2.14}$$

$$V \cdot V_1^{-1} = \begin{bmatrix} -0.3282 + 0.0007j & 0.9123 - 0.0005j \\ 1.0000 - 0.0000j & 0.0000 - 0.0000j \\ 0.5324 + 0.0003j & 0.3276 - 0.0002j \\ 0.0000 & 1.0000 \end{bmatrix} \tag{2.8.2.15}$$

The grouping algorithm shows machine 1 should be grouped with the induction motor and the other two generators should be grouped together. The electrical distance between them can also reveal this inference. The resistance between load 6 and machine 3 is 0.039 pu, where the resistance between load 6 and machine 1 is only 0.017 pu. The following observation can be made:

- When representing load dynamics in the power system model, in selecting the slow reference modes, both magnitude of the decaying constant and the oscillatory frequency need to be considered. Special care needs to be taken to select the correct slowest electromechanical modes.
- The generator mode instead of the load mode should be selected as the reference slowest mode.

2.8.3 Simulations On A Three-Machine Power System

In order to confirm the last grouping result of the three-machine system on classical model with induction motor, especially to check whether bus 6 should be grouped with the generator 1 or the generator 3, nonlinear simulations are run on the system shown in Fig.2.4.2.1. One small disturbance and one large disturbance have been simulated.

At first, a small disturbance consisting of 1MWof load increase at bus 8 is considered. The simulation is run for 15 seconds and voltage angle responses of the buses 1, 3 and 6 are observed. The voltage angle responses using machine 1's internal angle as reference angle are drawn. They are shown in the following Fig. 2.8.3.1.

In order to observe the curves clearly, the data is reduced to an interval of 3.5 seconds. Delta1, Delta3 and Delta6 correspond to the bus 1, bus 3 and bus 6' voltage angles. Delta1 and Delta6 have the same increasing and decreasing trend. But this is not so clear from the time domain since all of them have different oscillation magnitudes. So a spectral analysis is

conducted to further analyze the frequency components of the three responses. The MATLAB signal-processing tool is used to conduct the spectral analysis. The result is shown in Fig. 2.8.3.2 below.

For all three curves, two important peaks can be detected around 1.5 Hz and 2 Hz. They correspond to the two interarea modes. It is obvious from the figure that bus 1 and bus 6 have similar frequency spectrum except for different response magnitudes, which is due to their electrical distances from the fault location. This proves the point that bus 6 should be grouped with generator 1 instead of generator 3.

The second case is a three-phase to ground fault applied at bus 7, which is a large disturbance. Generator 2 will lose stability shortly after the fault. The other generators will experience large oscillations and reach a new equilibrium point. Fig. 2.8.3.3 and Fig. 2.8.3.4 give the time domain curves and frequency spectrum of the bus 1, 3 and 6's respectively. The time domain curves show the three angles have different magnitudes of oscillation. Delta1 and Delta6 have similar trends. Fig. 2.8.3.4 shows very clearly that Delta1 and Delta6 have a very similar frequency spectrum.

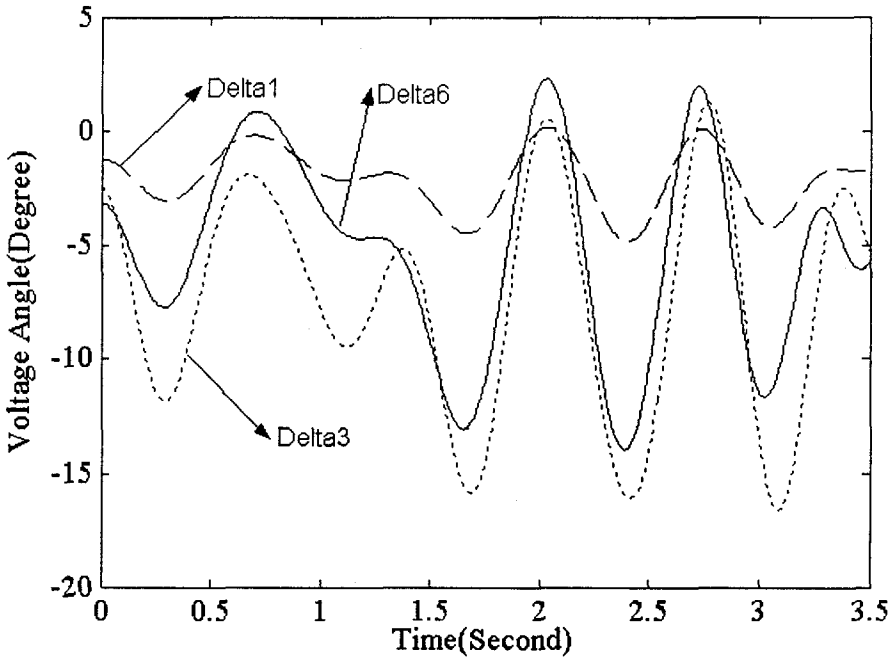

Fig. 2.8.3.1 Time domain curves of three buses' voltage angle responses of case 1- small disturbance case.

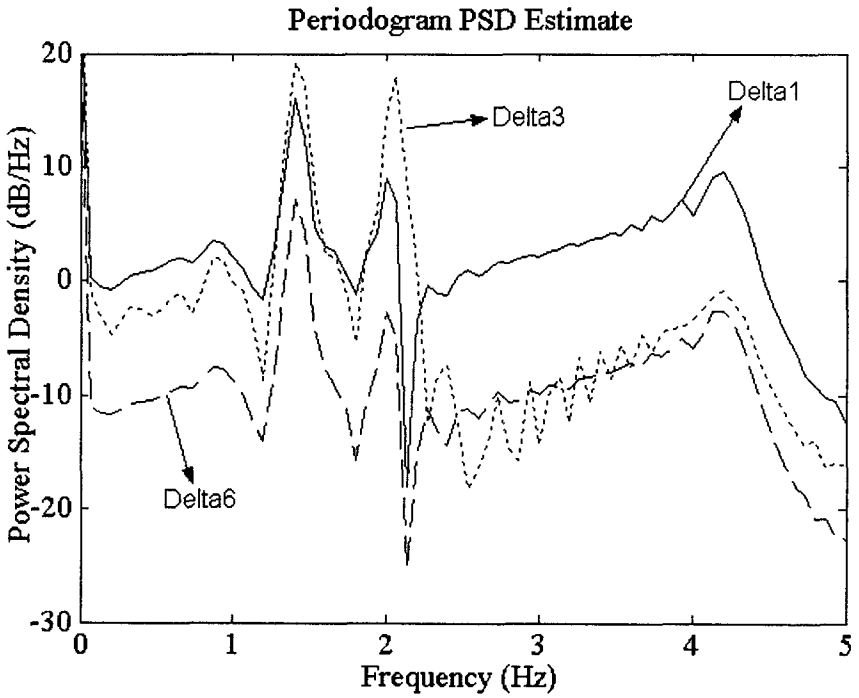

Fig. 2.8.3.2 Frequency spectrum of three buses' voltage angle responses of case 1-small disturbance case.

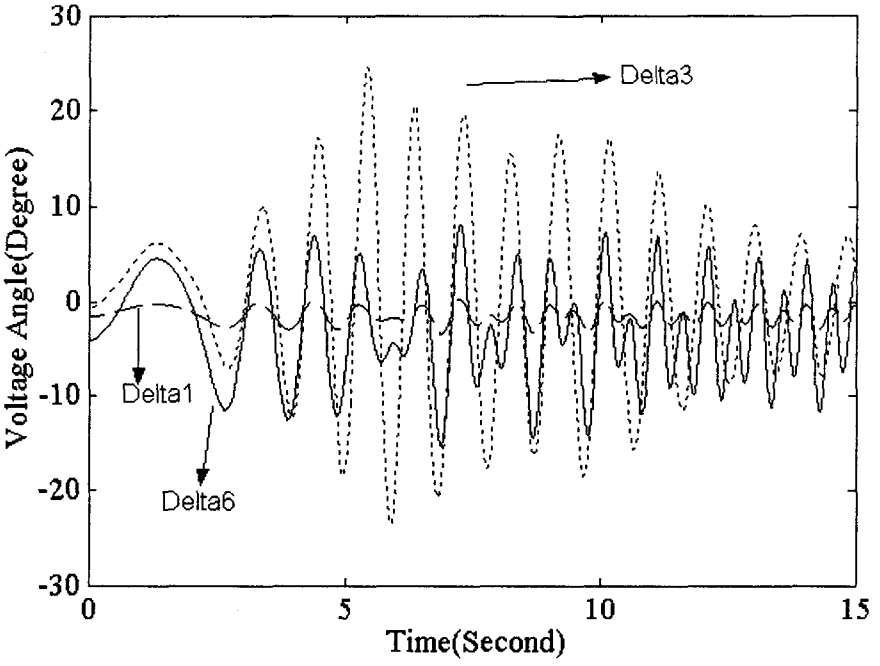

Fig. 2.8.3.3 Time domain curves of three buses' voltage angle responses of case 2- large disturbance case.

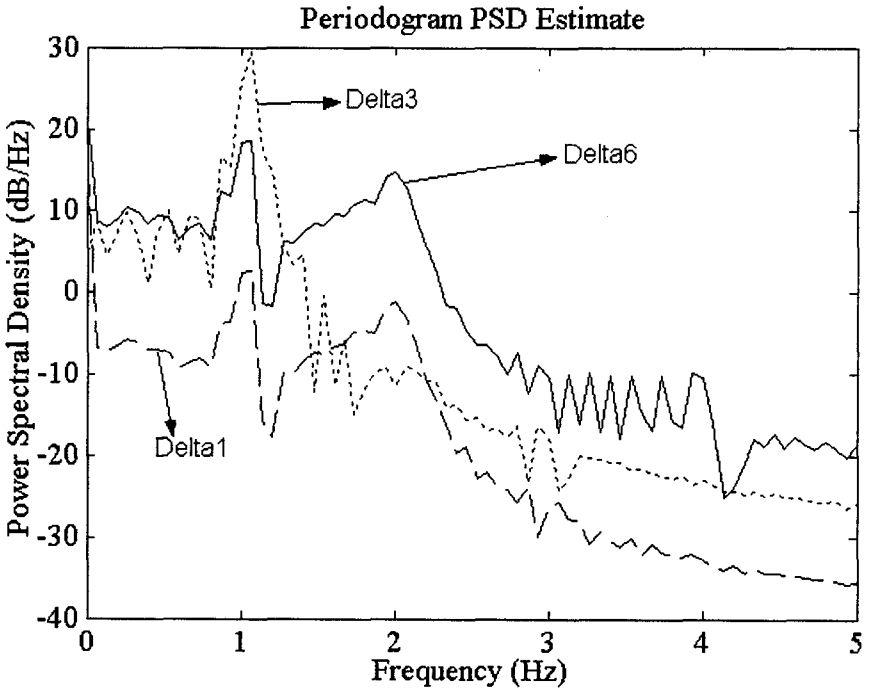

Fig. 2.8.3.4 Frequency spectrum of three buses' voltage angle responses of case 2-large disturbance case.

This section presents a modified generator slow coherency identification algorithm with illustration on a three-machine system. New steps are added into the original algorithm in order to consider more complex models such as second order system equations, generator detailed model and load dynamics. The modified algorithm will also be helpful to improve the system voltage stability due to the reason that the grouping method considers the short-term load dynamics.

2.9 SUMMARY

As a summary of chapter 2, the slow coherency based grouping method has the following explicit advantages or reasonable assumptions:

- Slow coherency is not significantly affected by initial condition and disturbance.

Slow coherency between the groups of the generators is a manifestation of the structural characteristics of the power system. Based on the simulation results provided later, we do observe the change in operating condition will affect the grouping of generators. But the variance of the power system initial condition will not change the attribute of the weakest connections in the power system topology very much. At the same time, the location, the size and the type of disturbance will not affect the topology of the network significantly. Since slow coherency is basically coherent with respect to the slow modes, it also preserves the features of the coherency-based grouping

- The two-time-scale weak connection form inherently describes the oscillation feature of large-scale power systems: the fast oscillation within a group of machines and the slow oscillation between the groups via weak tie lines.

The above phenomenon is explained as the effect of the interarea modes and local modes in the small signal disturbance analysis of power networks. The-two-time-scale theory provides explanation of the phenomenon in closed-form equations, which are very useful in the islanding problem. Even though the fast dynamics are weakly connected, they become strong oscillations if the disturbance is permitted to spread over the weak connection for longer time. Timely controlled separation with corrective control measures can prevent the degrading or even collapse of the overall system.

- It is applicable to both linear analysis and nonlinear analysis. Linear and nonlinear analyses have been shown in sections 2.5 and 2.6 and will be verified through nonlinear simulation result later.

The slow coherency theory is implemented in the Dynamic Reduction Program (DYNRED) in the Power System Analysis Package (PSAPAC) [8]. Groups of generators with slow coherency can be obtained by running the program. Then by running the automatic islanding program, the optimum cut sets will be obtained so that the problem of where to island is solved. In the next chapter, the switching action to island, or the problem of when to island will be discussed.

CHAPTER 3 TRIPPING ACTION

3.1 R-RDOT OUT OF STEP RELAY

We have shown in the previous chapter the procedure to determine where to form the islands. In this section we address the issue of when to form the islands following the disturbance. The detection of out of step condition conventionally requires initiating tripping at or before the voltage at the electrical center swings to the minimum value [12]. The out of step relay is deployed usually to assume this responsibility. In satisfying this condition, the out of step relay with R-Rdot phase plane controller developed by BPA shows much better performance than the conventional out of step relay, which is actually the impedance relay. Besides the impedance, the new relay uses the information of the rate of change of the impedance or resistance and gets better results in practice. The new out of step relay was developed by BPA in 1982 and was field-tested in 1983 for one and a half years before being commissioned [22]. The relay has been used for two decades or so. The relay was installed at the Malin substation on the Pacific 500kV AC Inter-tie line. The initiated controlled separation will separate the WSCC system into Northern and Southern parts. This scheme is based on an application of the equal area criteria using two equivalent machines. This concept mostly deals with first swing transient stability problem. The relay should operate at the fastest speed for catastrophic events. The relay can be set for early tripping for non-recoverable swings and avoid tripping for recoverable swings. Different switching lines make sure different corrective control actions are taken based on the level of the seriousness of the disturbance. The switching lines are shown as in the following Fig. 3.1.1 [23]. When a fault trajectory enters into the range defined by the switching lines, the tripping action will take place.

Typically, out of step impedance relays are installed on tie lines. In forming the islands for self-healing, some of the lines that would have to be disconnected are not necessarily tie lines. Hence, some care and thought needs to be given in order to choose the appropriate

means to form the islands. Out of step relaying typically occurs with a certain amount of time delay following the disturbance. For the purpose of self-healing, this time delay may be unacceptable. Hence, remote tripping would have to be implemented in order to reduce the impact of large disturbances and form the islands before the system performance degrades.

We have conducted simulations on the WSCC 179-buses system to test whether the relay will work in the slow coherency case. The result shows promising potential for the relay to work correctly in this case with proper settings. See the simulation part in section 5.3 and 5.6. for details.

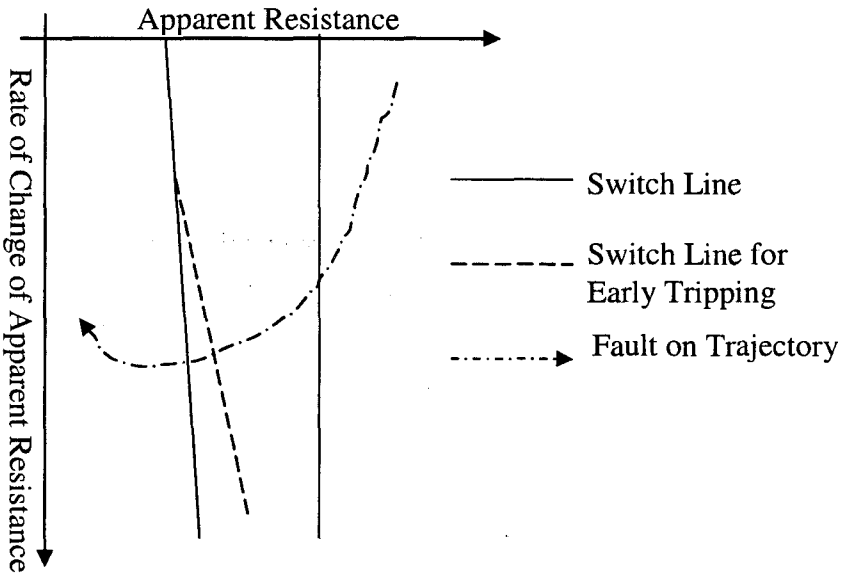

Fig. 3.1.1. Illustration of R-Rdot out of step relay switching lines.

3.2 ISLANDING SCHEME

One of the conspicuous features of the R-Rdot out of step relay is its sole requirement of local measurement for tripping action. Voltage and current measurement on the ends of the tie line need to be measured and the resistance can be calculated. Then the trajectory of the resistance can be plotted to be compared with the switching lines. The settings of the switching lines are based on various offline contingency simulations. Since we are looking for a decentralized solution to the catastrophic power events with corrective control, the

features of R-Rdot out of step relay become appreciable for the lowest level. However, many misoperations occurred without any catastrophic events happening during the field testing of R-Rdot out of step relays. Though there are no serious consequences of these misoperations, they are annoying. Furthermore, the relay needs adaptive training to reduce the unnecessary operations and false operations. Thus we support the out of step relay with Phasor Measurement Unit (PMU) and Decision Tree (DT) method and developed a three-layer islanding architecture. The three layers of islanding decision-making architecture are illustrated in the following Figure 3.2.1.

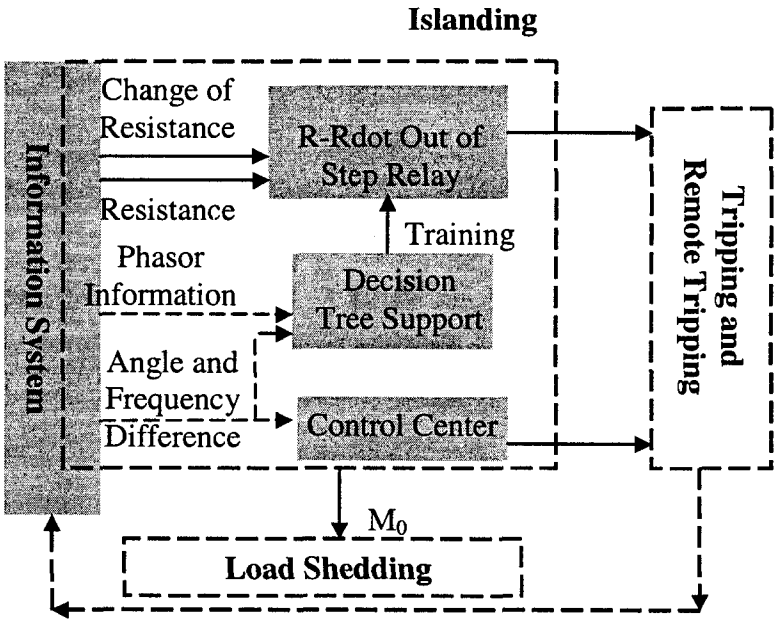

Fig. 3.2.1 Three-layer islanding scheme.

The out of step relay with a Phasor Measurement Unit (PMU) is developed by Virginia Tech [24]. This approach usually sets the out of step relay based on a two machine equivalent model. The equal area criterion [11] is used to predict stability. The system's pre-fault and post-fault power angle curves for different disturbance are stored in the PMU. Some online processing is also done to get a more precise value of system inertia or equivalent mechanical power. It requires Global Positioning System (GPS) technology, installation of Phasor Measurement Units and centralized decision-making. This capability is suitable for the highest level of the islanding scheme. The R-Rdot out of step relay has recently been

complemented with the Phasor Measurement technology and integrated with the Decision Tree method [25]. This feature will improve the function of R-Rdot of step relay and the relay with Decision Tree support can be employed as the middle level of the islanding scheme.

As a summary, with the help of the slow coherency program, we determine the coherent groups of generators that are not related with the disturbance. With the automatic islanding program, we determine the exact cut sets considering certain criteria. Then with the three layers of islanding decision-making process, we solve the problem of when to island. They are:

- The tripping decision from BPA's out of step relay with local measurement
- Response based R-Rdot out of step relay implemented with decision trees
- The centralized islanding decision with phasor measurement.

CHAPTER 4 LOAD SHEDDING

4.1 INTRODUCTION

Controlled islanding divides the power system into islands. Some of these islands are load rich; some are generation rich. In the load rich islands, in order to arrest the frequency decline and regain the balance between the generation and load, under-frequency load shedding is used. In the load deficient islands, in order to keep frequency from going up too high, generator tripping is used.

Generally, in a load rich island, the situation is more severe. The system frequency will decrease because of the generation shortage. If the frequency falls below a certain set point, e.g., 57.5 Hz, the generation protection system will begin operation and trip the generator, further reducing the generation on the island and making the system frequency decline even more. In the worst case, the entire island will blackout. In a load deficient island, either intentional or forced generator tripping will reduce the gap between the generation and the load. As a result, we put more effort to save the load rich island and develop a new two-layer load shedding scheme to perform the task. Load shedding is a corrective approach taken during severe conditions in power systems. It can help preserve the power system security during events that result in a serious energy imbalance and cause the frequency to decline. It is essential to minimize the risk of total system collapse and to protect generating equipment and transmission facilities against damage. Our load shedding scheme [26] is based on a Subsumption model.

Subsumption architecture [2], which is used in the field of controlled robots, is adopted here to identify the hierarchies of the various controls, protection, and communication systems between various agents in the deregulated electric utility environment. The architecture is based on the premise that storing models of the world is dangerous in dynamic and unpredictable environments because representations may be incorrect or outdated. It defines layers of Finite State Machines (FSMs) that are augmented with timers. Sensors feed

information into FSMs at all levels. The FSMs of the lowest level are control actuators. The FSMs of the higher levels may inhibit (attenuate the signal of one output wire) or suppress (attenuate the signal on all output wires) output values of the FSMs on the layers below them. In this way, a hierarchy of progressively refined behaviors may be established. Agents designed using the Subsumption architecture do not use symbol manipulation in a fixed manner to represent processing. They also have no global knowledge and are generally decentralized. The agents are non-programmable, single-purpose devices because of their lack of symbolism and global knowledge. However, they have the advantage of rapid response for dealing with dynamic and unpredictable events. A load shedding scheme based on the subsumption model is designed with consideration of certain criteria. The proposed scheme is tested on a 179-bus 29-generator test system and shows very good performance.

4.2 LOAD SHEDDING SCHEME

In the literature, there exist two kinds of load shedding schemes: load shedding based on frequency decline and load shedding based on rate of frequency decline [27][28]. The first approach [27] has mostly conservative settings because of the lack of information regarding the magnitude of the disturbance. Although this approach is effective in preventing inadvertent load shedding in response to small disturbances with relatively longer time delay and lower frequency threshold, it is not able to distinguish between the normal oscillations of the power system and the large disturbances on the power system. Thus, the approach is prone to shedding fewer loads. This is not beneficial to the quick recovery of the island and may lead to further cascading events. The second approach [28] avoids these shortcomings by utilizing the frequency decline rate as a measure of the load shortage. Thus it has a faster response time compared to the other scheme.

The idea of the load shedding based on the rate of change of frequency can be traced back to as early as in 1960s [29-30]. Issues of hardware implementations in the form of relays were discussed and resolved in the 70s and 80s. In [30], the leakage occurring in the fast Fourier transform (FFT) is advantageously used to detect the fluctuations in the fundamental frequency of a power system so that it can optimally estimate the mean frequency and its average rate of decline and determine the appropriate amounts of load to be

shed. The idea was then adopted in an isolated power system [31-32]. In the United Kingdom, the principal of the rate of change of frequency used for load shedding is referred to as ROCOF. In [33], an adaptive load shedding scheme that utilizes information including the system demand, spinning reserve, system kinetic energy, the amount of lower-priority load available for shedding elsewhere, and the locally measured rate of change of frequency is developed. A recent paper [34] has developed a much-improved adaptive load shedding scheme based on rate of change of frequency with capability of coordinating with under frequency governor control (UFGC). The paper first developed a load shedding scheme based on rate of frequency decline. The scheme is based on an reduced power system model of an equivalent machine connecting to an infinite bus. A phase plane boundary curve is drawn as the load shedding criteria. Then an adaptive feature is added on by identifying frequency drops subsequent to the initial frequency drop. Load shedding settings are thus able to be reset based on the difference between the last frequency local maximum and the last frequency local minimum. UFGS functions are able to be employed utilizing the Frequency-Rate of frequency decline phase plane boundary curve. The idea of the paper is adopted in our approach development by adding adaptive feature into the existing load shedding scheme. The detail can be obtained in the reference [35]

We develop a load shedding scheme based on the rate of frequency decline, which can identify the magnitude of the disturbance. At the same time, we incorporate the conventional load shedding scheme into our Subsumption model to form a new two-layer load shedding scheme as shown in Fig. 4.2.1.

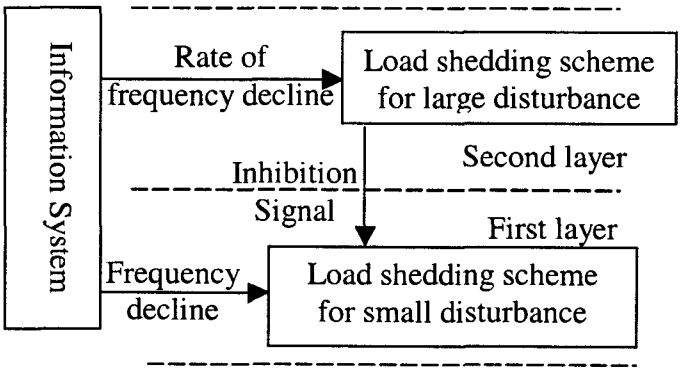

Fig. 4.2.1 The new two-layer load shedding scheme under Subsumption model.

Normally the relay will operate the conventional load shedding scheme. The conventional load shedding scheme has longer time delays and lower frequency thresholds, which can be used to prevent inadvertent load shedding in response to small disturbances. If the system disturbance is large and exceeds the signal threshold, the second layer will be activated and send an inhibition signal to the first layer and the load shedding scheme based on the rate of frequency decline will take effect. This layer of the load shedding will shed more loads quickly at the early steps to prevent the cascading events in the island. This can greatly enhance the system's ability to withstand large disturbances.

An obvious improvement of the new load shedding scheme is its capability of selecting different schemes according to the severity or the magnitude of the disturbance. A variable that measures the magnitude of the disturbance should be determined in order to make the Subsumption approach feasible. From an intuitive analysis [36], the rate of frequency decline at the beginning of the disturbance can accurately reflect the magnitude of the disturbance. From chapter 3 of [11], we have

$$\frac{df_i}{dt} = -\frac{60 \times P_{sik}}{2H_i}(P_{L\Delta}(0^+) / \sum_{i=1}^{n} P_{sik}) \qquad i = 1,2,\cdots,n \tag{4.2.1}$$

Define

$$\bar{f} = \sum_{i=1}^{n}(H_i f_i) / (\sum_{i=1}^{n} H_i) \tag{4.2.2}$$

In (4.2.1), we add all the equations to obtain

$$\frac{d\bar{f}}{dt} = \sum_{i=1}^{n}(H_i \cdot \frac{df_i}{dt}) / \sum_{i=1}^{n} H_i = -60 \times P_{L\Delta} / \sum_{i=1}^{n} 2H_i \tag{4.2.3}$$

Where

f_i The frequency of generator i in Hz.

$\frac{d\bar{f}}{dt}$ The average rate of frequency decline, in Hz/Second,

P_{sik} The synchronizing power coefficient between generator i and the disturbance node k, in pu. See chapter 3 of [11].

$P_{L\Delta}$ The magnitude of the disturbance, in pu,

H_i The inertia of generator i, in pu,

ω_i The rotor speed of each generator i, in pu,

Define

$$m_i = \frac{df_i}{dt} \tag{4.2.4}$$

$$m_0 = \frac{d\bar{f}}{dt} \tag{4.2.5}$$

Substituting (4.2.5) into (4.2.2), we have

$$m_0 = -60 \times P_{L\Delta} / \sum_{i=1}^{n} 2H_i \tag{4.2.6}$$

The equation can be alternatively written as

$$P_{L\Delta} = -m_0 \times \sum_{i=1}^{n} 2H_i / 60 \tag{4.2.7}$$

Since H_i is constant, the magnitude of the disturbance can be directly related to the average rate of system frequency decline. Hence, m_0 can be an indicator of the severity of the disturbance. The rate of frequency decline at the beginning of the disturbance can be used as the input signal of the second layer. Once the threshold of $P_{L\Delta}$ to activate the second layer is decided, the corresponding m_0 can be calculated. When the disturbance occurs, we measure m_i at each bus and compare it with m_0. If m_i is greater than m_0, the second layer is activated; otherwise the conventional load shedding scheme is used.

By using m_i at each bus to decide the amount of load that should be shed locally, the system oscillations after the disturbance can be reduced. We know that at the beginning of the disturbance, the impact of disturbance is shared immediately by the generators according to their synchronizing power coefficients with respect to the bus at which the disturbance occurs [11]. Thus, the machines electrically close to the point of impact will pick up the greater share of the load regardless of their size. On the other hand, standards [37] and guides [38] give a fairly strict regulation on tolerable frequency deviations. The range between 59.5 Hz and 60.5 Hz is the range of unrestricted time operating frequency limits. The ranges above 60.5 Hz and below 59.5 Hz are ranges of restricted time operating frequency limits. From [38], we know that the system frequency is not allowed to drop below 57 Hz. So for load shedding schemes, the detection of frequency below 59.5 Hz should trigger the corrective control ensuring that the system frequency will not drop below 57 Hz. Although the disturbance is ultimately shared according to the inertia of each machine, sometimes the frequency of some generators near the disturbance can drop below 57 Hz before reaching the final state. Using the value of frequency at each bus, the buses whose frequencies drop

quickly are likely to have more load shed locally; this can reduce the frequency deviation and system oscillations.

Considering the governor protection system limitation and regional operation criteria, we define $P_{L\Delta}$ as the minimum load deficit that can drive the system average frequency below 57 Hz. This frequency threshold is chosen because it is widely recognized that the system is not allowed to operate below 57 Hz. There are three main reasons why the system cannot operate below 57 Hz.

- Coordination with the Governor-turbine System. Under-frequency operating limitations imposed by manufacturers of turbine-generator units are primarily concerned with the avoidance of resonant frequencies and turbine blade fatigue. Since fatigue effects are cumulative, the limitation is defined in terms of total accumulated times of operation within specified frequency ranges. Turbine manufacturers provide limitations of various turbines to frequency variation. Based on this data it is very reasonable to choose 57 Hz as system operation limit [23].
- Coordination with the Plant Auxiliary System. Nuclear units having a pressurized water reactor steam supply use special under-frequency protection for their primary system reactor coolant pumps. For these units, this protection will trip the coolant pumps and shutdown the reactor at the fixed time of 0.25s and a pickup setting of 57.0 Hz [27].
- Coordination with Existing Operation Criteria. According to the North East Power Coordinating Council (NPCC) Standard, the generation rejection should be deployed immediately if system frequency drops below 57 Hz [28].

To find $P_{L\Delta}$, we use a reduced model for a reheat unit for frequency disturbance as shown in Fig. 4.2.2 [23].

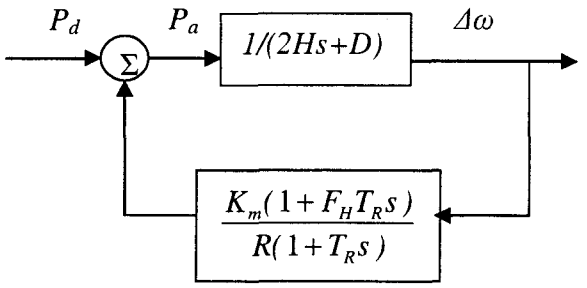

Fig. 4.2.2 The reduced model of reheat unit for frequency disturbance

Here, K_m is mechanical power gain factor. We use a typical value of 0.95.

H is inertia constant in seconds, typically 4.0 second.

F_H is high-pressure power fraction, typically 0.3.

D is damping factor, typically 1.0.

T_R is reheat time constant, seconds, typically 8.0 second.

R is fraction of the reheat turbine, typically 0.559.

P_d is disturbance power, in pu.

We use typical system data to compute the minimum load deficit that can drive the system to the minimum frequency of 57 Hz (representing the worst case scenario).

From Fig. 4.2.2, we have

$$\Delta\omega=\left(\frac{R\Omega_n^2}{DR+K_m}\right)\left(\frac{(1+T_Rs)P_d}{s^2+2\Omega_n^2\lambda s+\Omega_n^2}\right) \tag{4.2.8}$$

Where

$$\Omega_n^2=\frac{DR+K_m}{2HRT_R} \tag{4.2.9}$$

$$\lambda=\left(\frac{2HR+(DR+K_mF_H)T_R}{2(DR+K_m)}\right)\Omega_n \tag{4.2.10}$$

If P_d is a step function, we have

$$P_d(t)=P_{step}u(t) \tag{4.2.11}$$

Using this reduced model and normalizing, we obtain that the lowest system average frequency for this disturbance is 57 Hz when $P_d=P_{L\Delta}=0.3P_{sys}$. So we choose $0.3P_{sys}$ as the threshold value of $P_{L\Delta}$ for the new load shedding scheme. This value of $P_{L\Delta}$ is used in (4.2.6) to determine the limiting threshold for m_0.

The frequency threshold should be chosen carefully. First, it should not be too close to normal frequency in order to avoid tripping on severe but non-emergency frequency swings. On the other hand, it is more effective to shed load earlier.

The step size is an important variable in load shedding. Conventionally, the amount of load shed at each step is increased while the system frequency decreases. This choice is reasonable for those schemes that use the frequency as the criterion to shed load because before the system deteriorates, it is unreasonable to shed too much load if the disturbance is unknown. It has also been observed that for large disturbances, such schemes may be insufficient to arrest system frequency decline [29]. Our second layer of load shedding scheme, as stated before will only take action when the disturbances are large enough to cause the system frequency to drop below 57 Hz. So instead of increasing the step size while the system frequency is decreasing, we set the first step to be the largest step size. Since the first layer of the new load shedding scheme will mainly deal with small disturbances, we use the conventional philosophy. For the steps of load shedding, three facts are observed [29]:

- Frequency steps must be far enough apart to avoid overlap of shedding due to (intentional or inherent) time delay.
- The number of steps does not have very great impact on the effect of load shedding.
- Generally, the threshold of the last step of load shedding is chosen no less than 58.3Hz.

Time delay is very important for load shedding schemes to avoid over-lapping and unexpected action for small frequency oscillations. Generally, for the conventional load shedding scheme, the delay time for the first step is usually very long to avoid unexpected actions due to small frequency oscillations. For the following steps, the more the frequency declines, the quicker is the action. For the new scheme, to prevent sharp frequency declines following a large disturbance, we set the delay time for the first step of the second layer as 0 cycles.

Finally, the two layers of load shedding scheme are developed as shown in the Table 4.2.1. When the disturbance occurs, we measure m_i or the rate of frequency decline at each bus and compare it with m_0 calculated from $P_{L\Delta}$. If m_i is greater than m_0, the new load shedding scheme is deployed shown in the second row of the table. Twenty percent of the total load is shed with 0 cycle delay in the first step. The character C in the table means

cycle. Otherwise, the conventional load shedding scheme is used, which is shown in the second row.

Table 4.2.1 Step size and delay time of the two layers as percentage of the total load.

	59.5Hz	**59.3Hz**	**58.8Hz**	**58.6Hz**	**58.3Hz**
$\mathbf{m_0<m_i}$	20%(0*C*)		5%(6*C*)	4%(12*C*)	4%(18*C*)
$\mathbf{m_0>m_i}$		10%(28*C*)	15%(18*C*)		

In all, the new two-level load shedding scheme has the following explicit features:

- Suitable for Large and Small Disturbances.
- Suitable for Self-healing when combined with islanding in power system recovery.

Details of the development of the load shedding scheme can be obtained in [26] and [39]. Furthermore, with cooperation of colleagues in University of Washington, a new adaptive feature has been added into the original scheme and self-leaning mechanism has been incorporated [35].

CHAPTER 5 SIMULATION RESULTS

5.1 SYSTEM INTRODUCTION AND GROUPING RESULTS

The previous chapters have proposed a self-healing scheme for large disturbances. As introduced before, slow coherency theory is employed to obtain the groups of generators with slow coherency. Then the automatic islanding program is run to get the optimum cut sets considering certain criteria. A three-layer islanding switching mechanism has been proposed, which integrate the fast local measuring, tripping and the wide area phasor measuring and remote tripping. Finally, in the load rich area, a new two-level load shedding scheme has been designed to stabilize the islanded system. Though the restoration scheme is not designed, it has been taken into account in designing the self-healing scheme.

The self-healing scheme has been tested on a 179-bus, 29-generator sample system, which is a representation of WSCC system shown as Fig. 5.1.1. The system has a total generation of 61410MW and 12325Mvar. It has a total load of 60785MW and 15351Mvar. Detailed information of the system is provided in the Table 5.1.1.

Table 5.1.1 Test system's profile.

Buses	Generators	Loads No. (CI, CMVA)	Lines	Transformers	Generations (MW, MVAR)	Loads (MW, MVAR)
179	29	104 (67,24)	203	60	61410, 12325	60785,15351
Northern part	Southern part	Generator Model	Governor	PSS		Exciter
Generation rich	Load rich	Detailed	Not Available	Modeled		Modeled

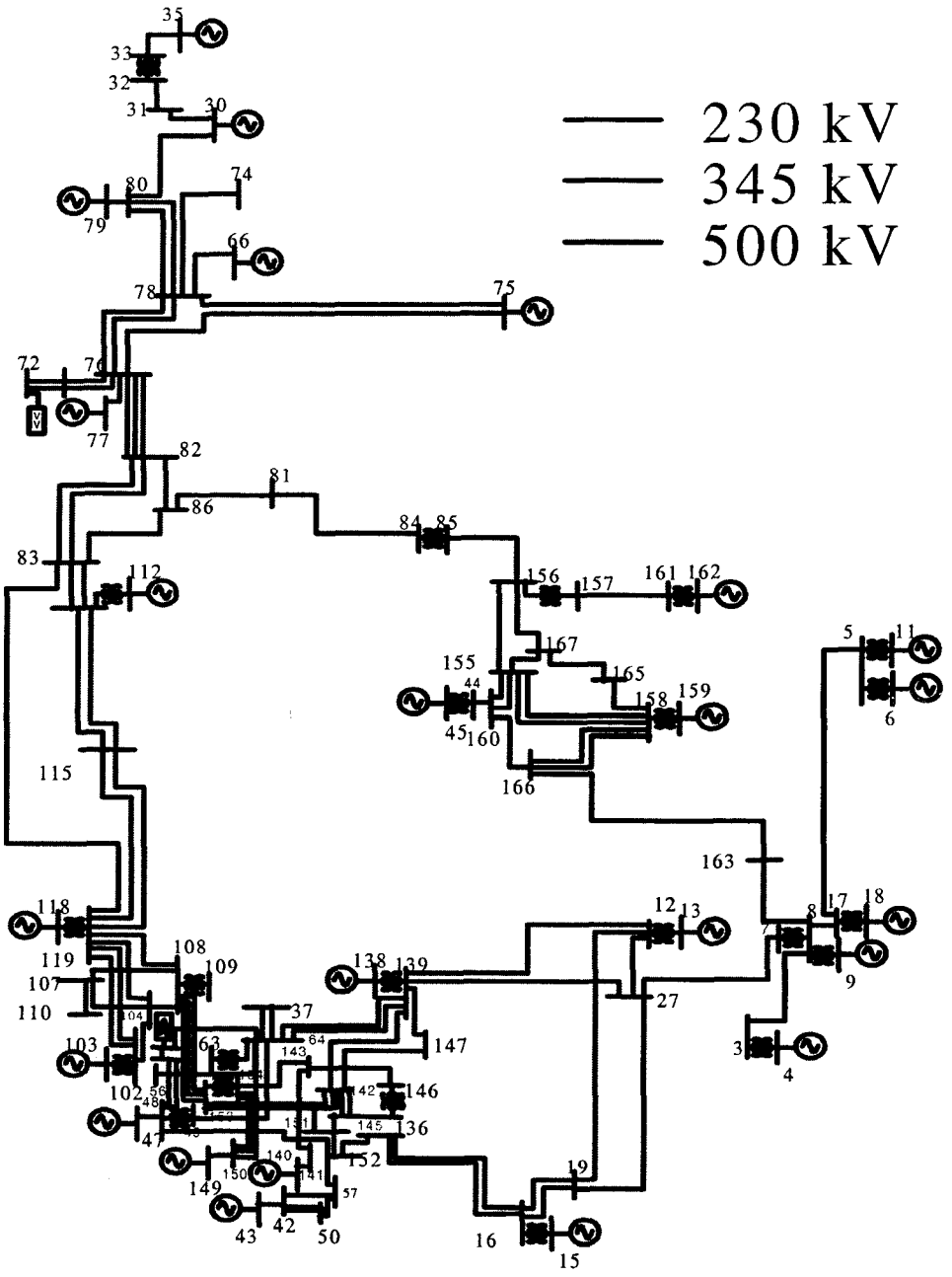

Fig. 5.1.1 The 179-bus, 29-generator test system

In the table, CI represents constant impedance and CMVA means constant power. The simulation is made using a detailed generator model with governors, exciters and power system stabilizers (PSS). Three different cases and several types of tests are made and the scheme shows very good performance.

The power flow and dynamic data files for the system are obtained from Advanced Power Technologies Consortium (APT). It should be noted that the original dynamic data file doesn't include the governor's model, which is very important in the simulation of the transient time scale. As a result, we add a governor model and compare the simulation results using three sets of data. Then we choose one of them for all the simulations. The issue regarding the governor model will be discussed in section 5.2.

The DYNRED program in the PSAPAC software package [8] was chosen to form groups of generators based on slow coherency. With the help of the automatic islanding program, we determine the cut sets of the island taking into account the least generation-load imbalance and topology requirements. The DYNRED program was employed to find groups of generators with slow coherency on the 179-bus, 29-generator system on a base case initially. The 29 generators are divided into 4 groups by the slow coherency program as shown by the dotted lines in Fig. 5.1.2. The four groups of generators can be characterized as the north island, the middle west island, the middle east island and the south island. The exact boundary between the generator groups has not been determined at this point.

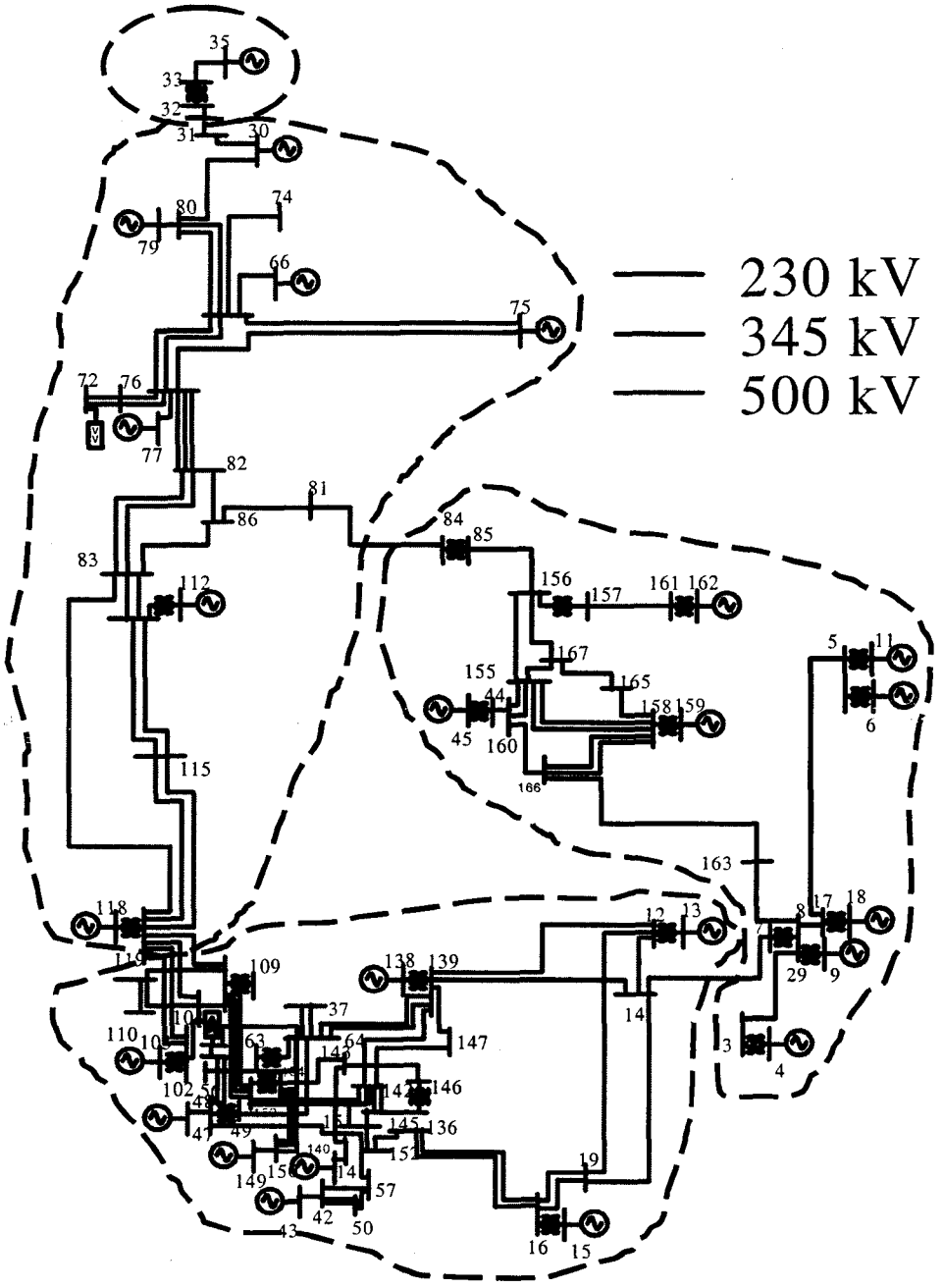

Fig. 5.1.2 Grouping results of the 179-bus ,29-generator test system.

In this case, the automatic islanding program is employed to find all the possible cut sets in the south island and select the optimal one. For the west part of the south island in Fig. 5.1.2, a sub-network of 29 lines is found to form the interface network. With the limit of 4 lines to be tripped, the program altogether searches: $C_{29}^{1}+C_{29}^{2}+C_{29}^{3}+C_{29}^{4}=27{,}840$ different

combinations of the 29 lines of the sub network. 18 islanding strategies with load generation profiles are output as a file. For the east part of the south island in Fig. 5.1.2, a sub-network of 17 lines is found to form the interface network. The program searches: $C_{17}^{1}+C_{17}^{2}+C_{17}^{3}+C_{17}^{4}=3{,}213$ different combinations of the 17 lines of the sub network. 58 islanding strategies with load generation profiles are output. The optimum tripping lines are from 14 (MOENKOPI 500) to 29 (FOURCOR2 500) in the east part, and 133 (TEVATR2 500) to 132 (TEVATR1 500), 134 (TEVATR3 500) to 104 (GATES 500) in the west. This strategy considers the topology and provides a cut set with the least generation load imbalance in the southern island.

It has been shown in the previous chapters that fast dynamics are propagated through the weak connections determined by the boundary between groups of generators. Since this is a network characteristic, the boundary will not change much with the variation of the power flow base case. In order to verify this, we set up a scenario with the load changing as a percentage of the base case and the change of the load is distributed to the generators according to the inertia of each generator. The increment or decrement of the load is distributed proportional to the inertia of each generator. For each case, the grouping is recalculated using the DYNRED program. The results are shown in Table 5.1.2. The power flow does not converge when the system load increases more than 6% or is reduced by 30%. During the other ranges, it shows grouping will be mostly the same if the load doesn't vary very much except at some specific amount of load change. For example, during the range of -30% to -17% of load change, with precision of 1% load change, the same grouping result is obtained except at -25% load change. Minor generator grouping difference is found in the north part of the test system at the point of -25% of load change. But that doesn't affect the result of forming the islands in all of our simulation cases.

Table 5.1.2 Grouping changed as the load change

Load Change Percentage	<-30%	-30% to -17% (except at -25%)	-16% to 0%	1% to 6% (except at 1% and 5%)	>6%
System Condition	Unstable	Obtain Same Grouping	Obtain Same Grouping	Obtain Same Grouping	Unstable

5.2 GOVERNOR ISSUE

As mentioned before, the governor modeling is very important in transient stability analysis. IEEE governor model type 8 is a commonly accepted type. Therefore, we select this type in our nonlinear simulations. The governor model chosen is shown in Fig. 5.2.1 [40].

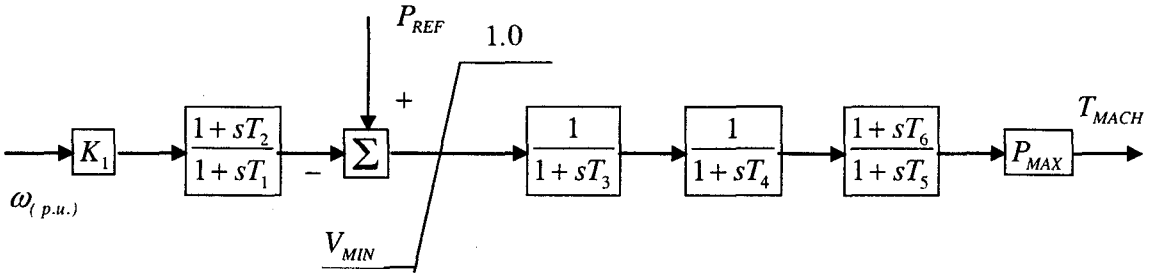

Fig. 5.2.1 Diagram of IEEE governor's model No. 8.

Then three sets of data are generated. Data 1 doesn't contain any governor representation, which is the original case. In data 2, the governors are represented by the IEEE model No. 8 and the data are created by experience. In data 3, the governors are represented by the IEEE model No. 8 and the data are created with values normally used in industry studies. In order to show the effect of the three sets of data and for the reason of future analysis, three scenarios of disturbances and control actions are set up, which are referred to as case 1, 2 and 3. The three cases will be explained in detail in section 5.3, 5.4 and 5.5.

In case 1, the following three lines in the system are tripped simultaneously. This corresponds to a catastrophic transmission failure where an incident takes out all the three transmission lines simultaneously. The lines are connected between buses:

- Bus 83 - Bus 168
- Bus 83 - Bus 170
- Bus 83 - Bus 172

Simulations have shown that the disturbance will result in system being unstable. To save the system from an impending blackout, the system is split into two islands 0.2 seconds after the contingency. In the first case, **the islands are formed by experience**. The following lines are tripped:

- Bus 139-Bus 12
- Bus 139-Bus 27
- Bus 136-Bus 16(1 and 2)

After islanding, the system is divided into two areas shown as Fig. 5.2.2. Load shedding is performed in the south island after the system is islanded.

In case 2, the same disturbance mentioned above is applied with three transmission lines disconnected simultaneously. Then we split the system into three islands 0.2 seconds after the contingency. **The islands are determined by slow coherency**. In order to create the islands, the following lines are tripped:

- Bus 133-Bus 108
- Bus 134-Bus 104
- Bus 29-Bus 14

After islanding, the system is divided into three areas shown as Fig. 5.2.3. Load shedding is performed in both the central island and the south island after the system is islanded.

In case 3, an incident takes out all four transmission lines located in the southeast portion of the system. The four lines are connected between buses:

- Bus 12 - Bus 139
- Bus 27 - Bus 139
- Bus 16 - Bus 136(1and 2)

To save the system from an impending blackout, we split the system into three islands 0.2 seconds after the contingency. **The islands are determined by slow coherency**. In order to create the island, the following lines are tripped:

- Bus 133 - Bus 108
- Bus 134 - Bus 104

The two islands are shown as Fig. 5.2.4.

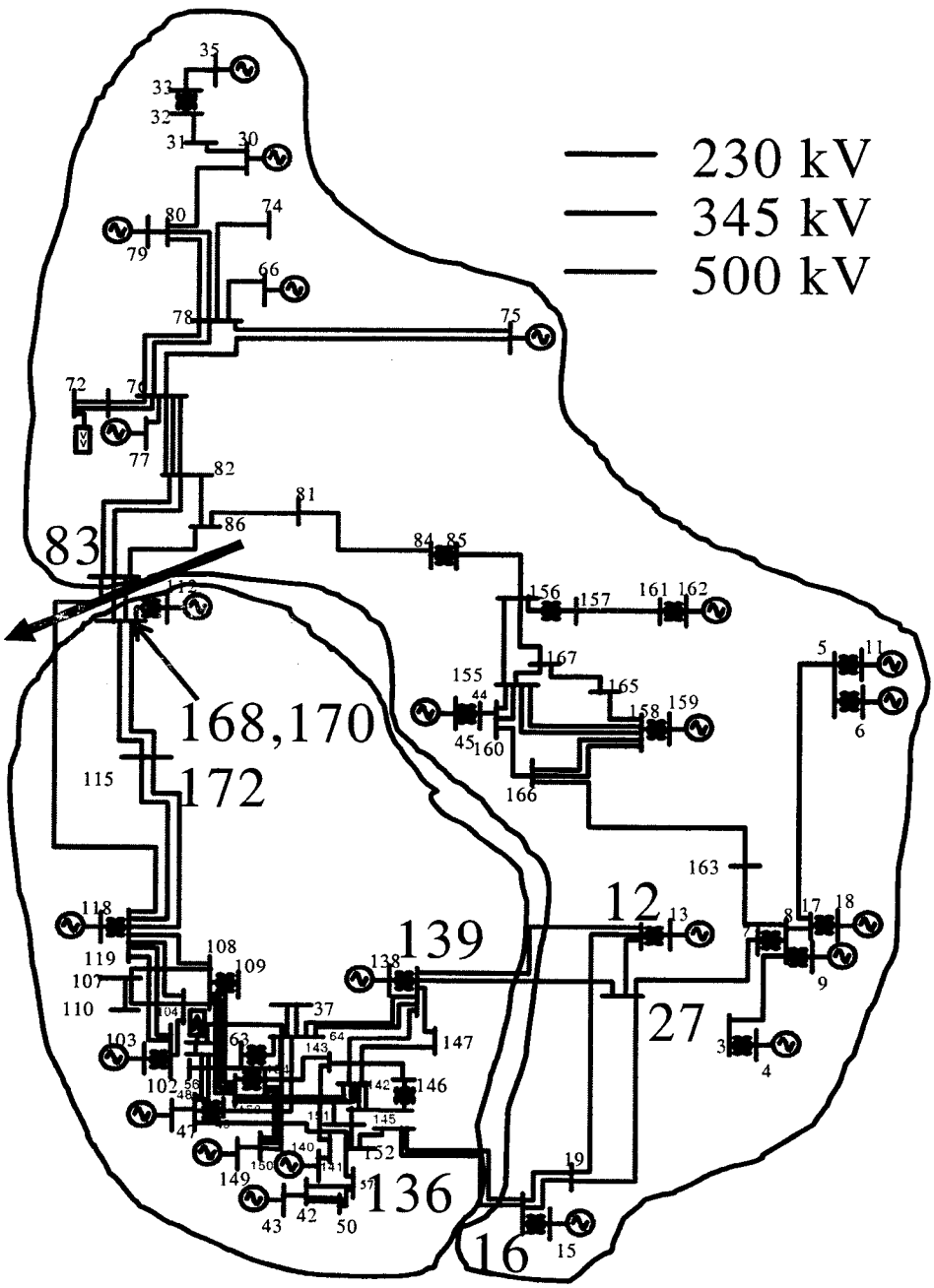

Fig. 5.2.2 Case 1-Two islands of the test system

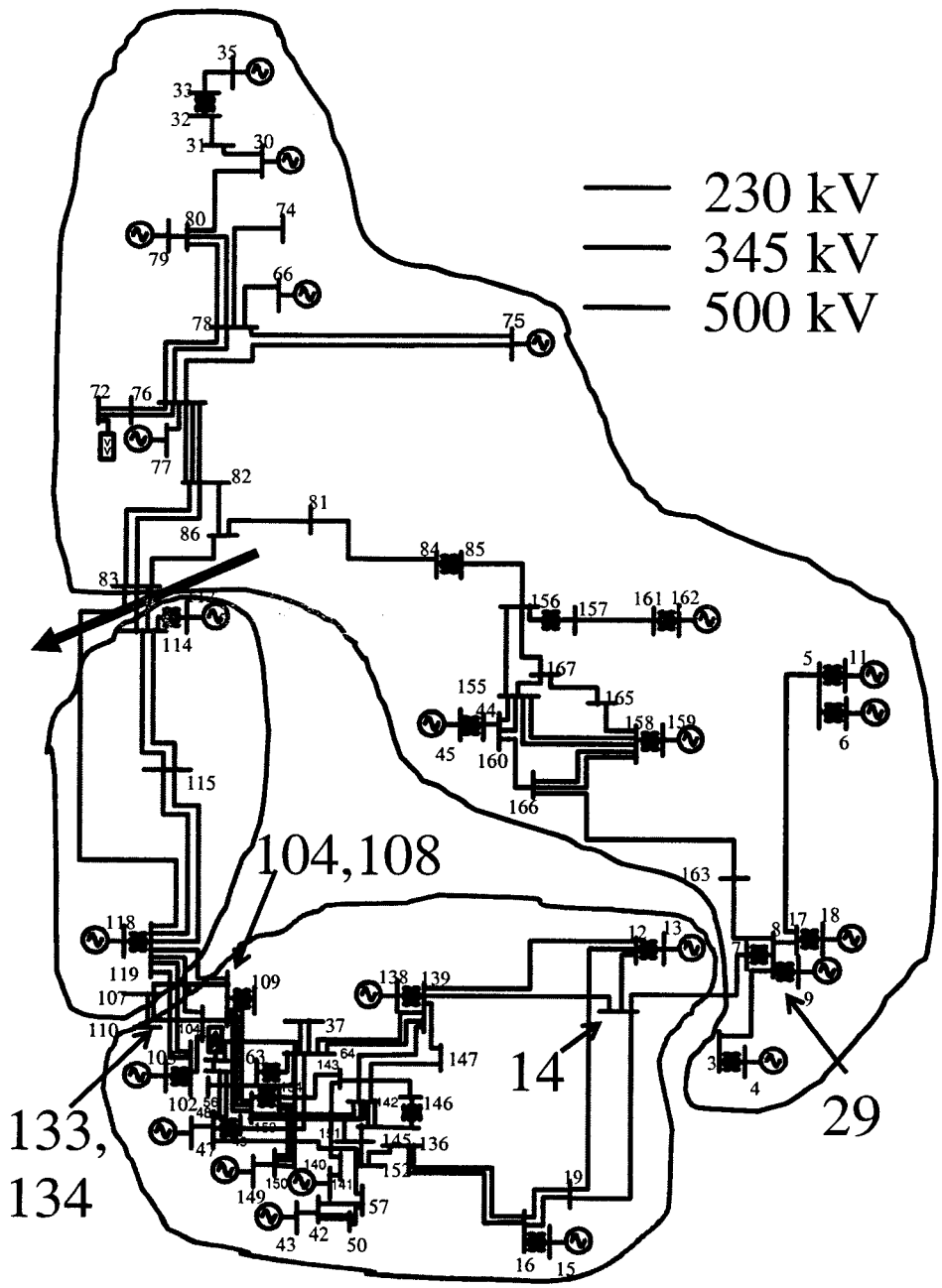

Fig. 5.2.3 Case 2-Three islands of the test system.

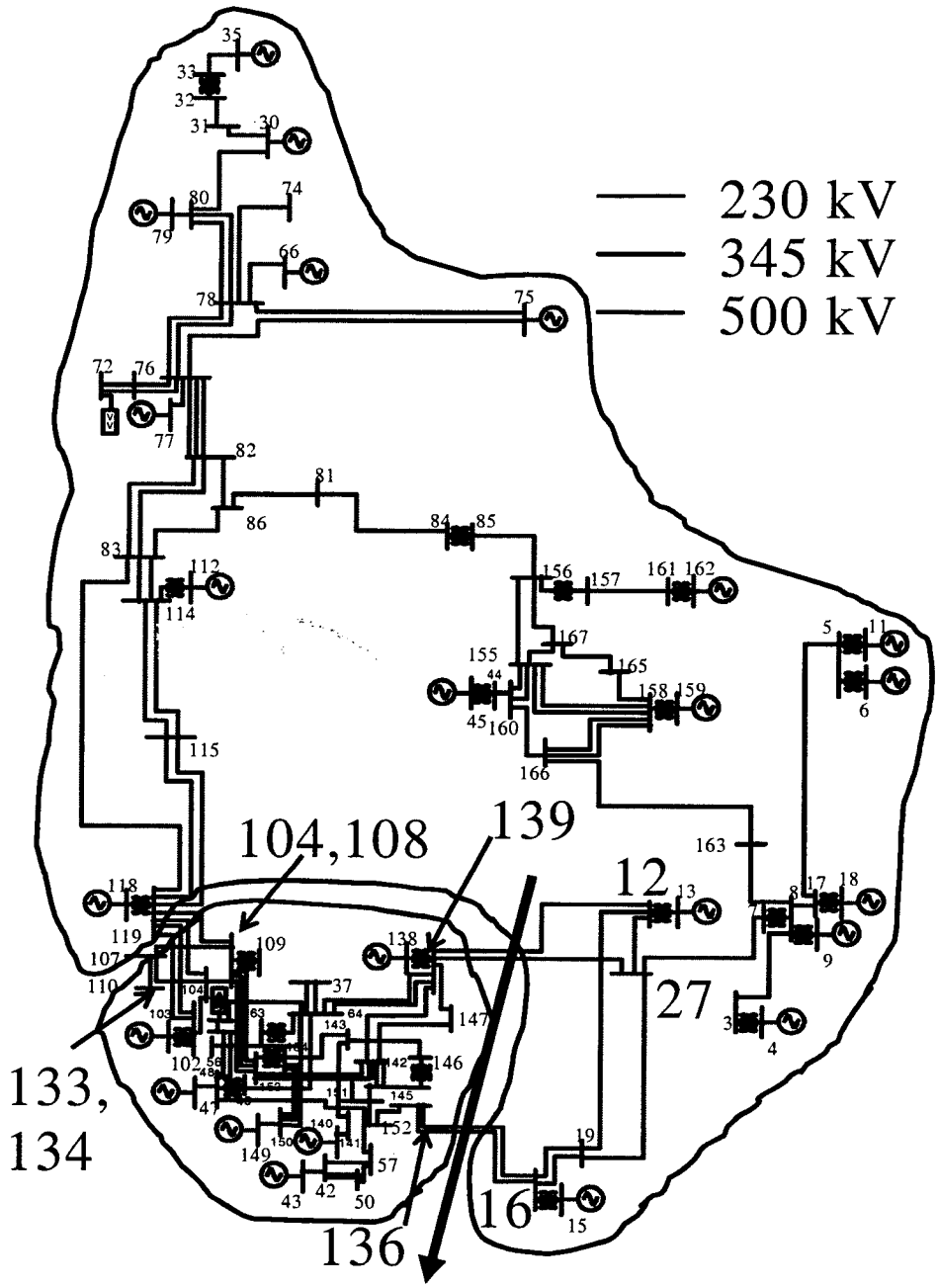

Fig. 5.2.4 Case 3-Two islands of the test sytem.

For each of the above scenario and each set of data above, one typical generator's relative angle curve is plotted in three different situations: no control actions after the disturbance; only islanding after the disturbance; islanding with load shedding after the disturbance. The nine groups of plots are shown as Fig. 5.2.5-Fig. 5.2.13.

The following can be observed from these figures:

- With either one of the three sets of governor data, the system loses the stability after the disturbance.
- With either one of the three sets of governor data, the system is still unstable if only islanding action is applied after the disturbance.
- With either one of the three sets of governor data, the system can be stabilized if both the islanding and the load shedding actions are applied after the disturbance.
- With governors modeled, the system's frequency recovers faster after the disturbance than it does without governors modeled.
- With governors modeled, the system's frequency recovers faster if the system is islanded after the disturbance than it does without governors modeled.
- With governors modeled, the system's frequency recovers faster if both the islanding and the load shedding actions are applied after the disturbance than it does without governors modeled.
- Comparing the curves of Fig. 5.2.6 and Fig. 5.2.7; Fig. 5.2.9 and Fig. 5.2.10; Fig 5.2.12 and 5.2.13, under three various situations the system with governor data 3 will experience less oscillations than with governor data 2, which means the governor data 3 are more tuned with the system.

From the above analysis, it is necessary to add the governor model in the system. Furthermore, we use data 3 for the governor model in all the simulations henceforth.

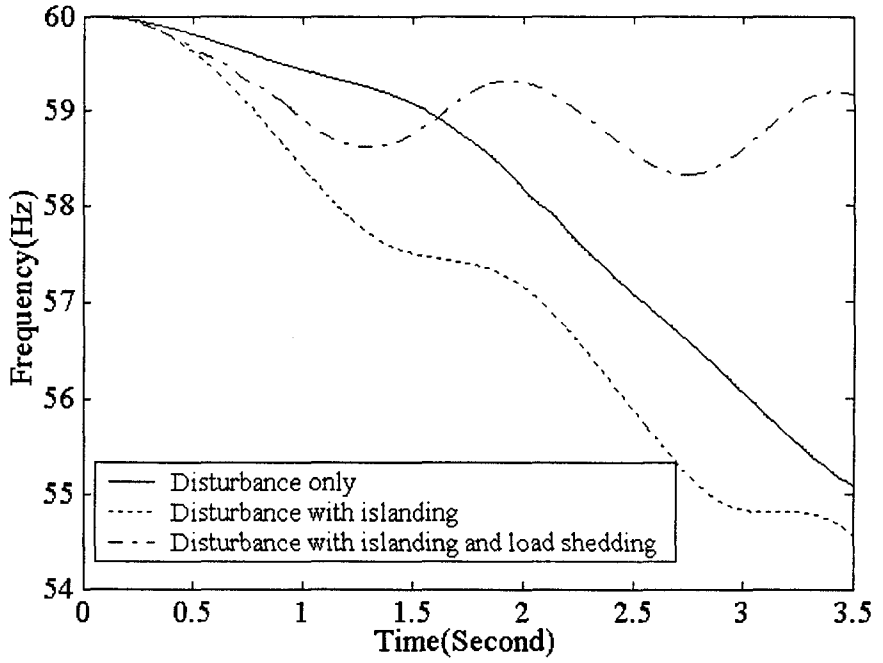

Fig. 5.2.5 Case 1: Frequency responses of generator 140 with governor data 1.

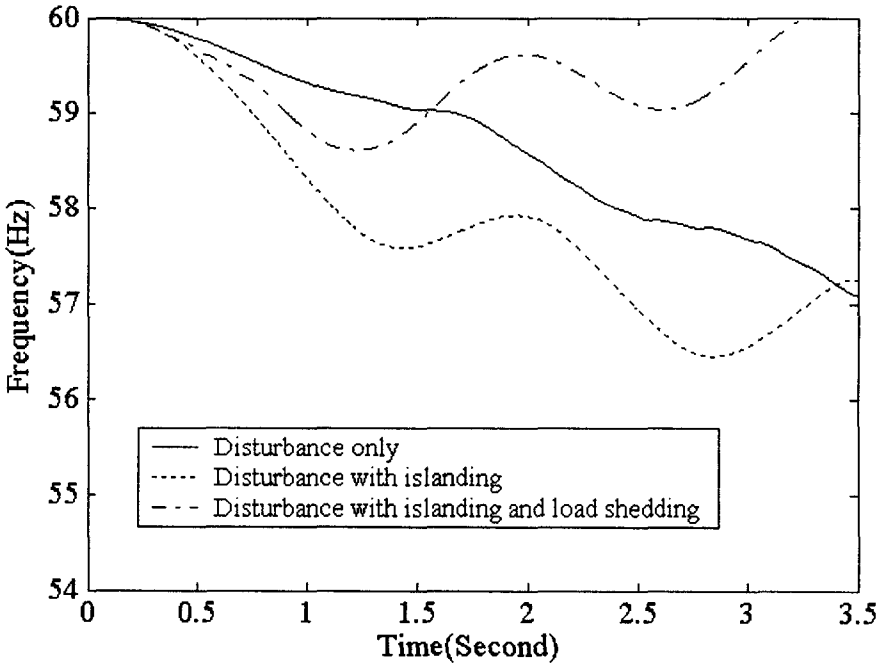

Fig. 5.2.6 Case 1: Frequency responses of generator 140 with governor data 2.

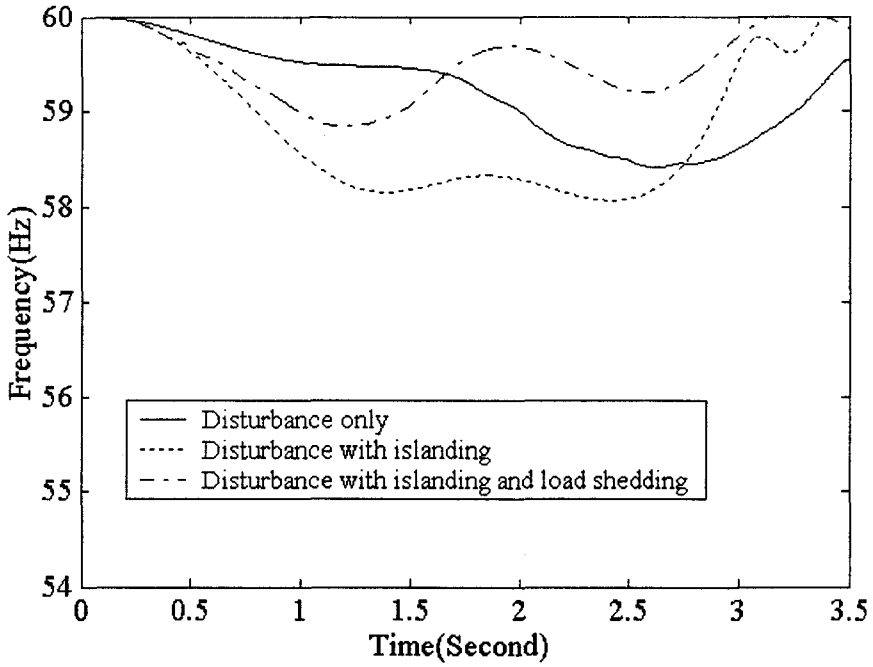

Fig. 5.2.7 Case 1: Frequency responses of generator 140 with governor data 3.

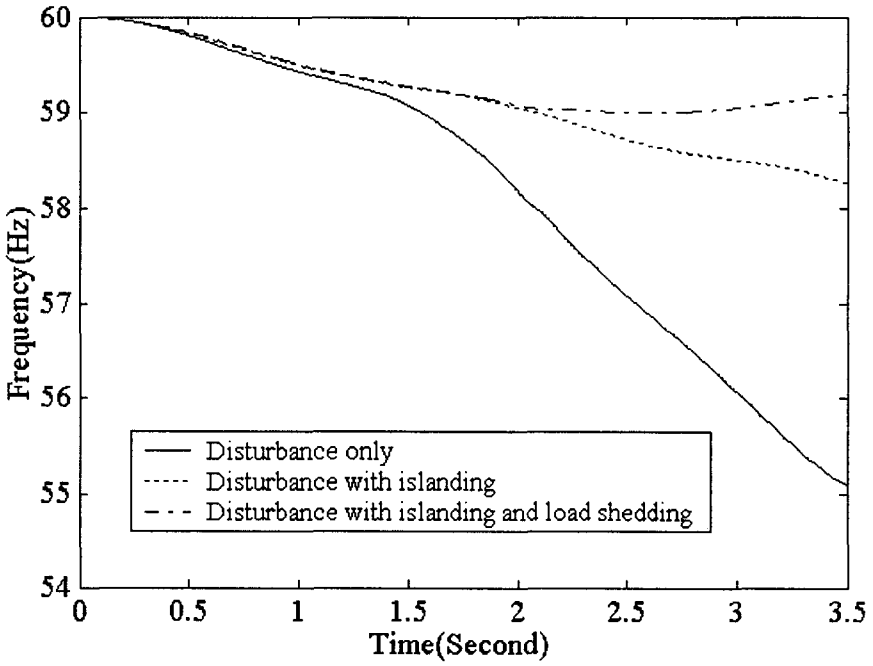

Fig. 5.2.8 Case 2: Frequency responses of generator 140 with governor data 1.

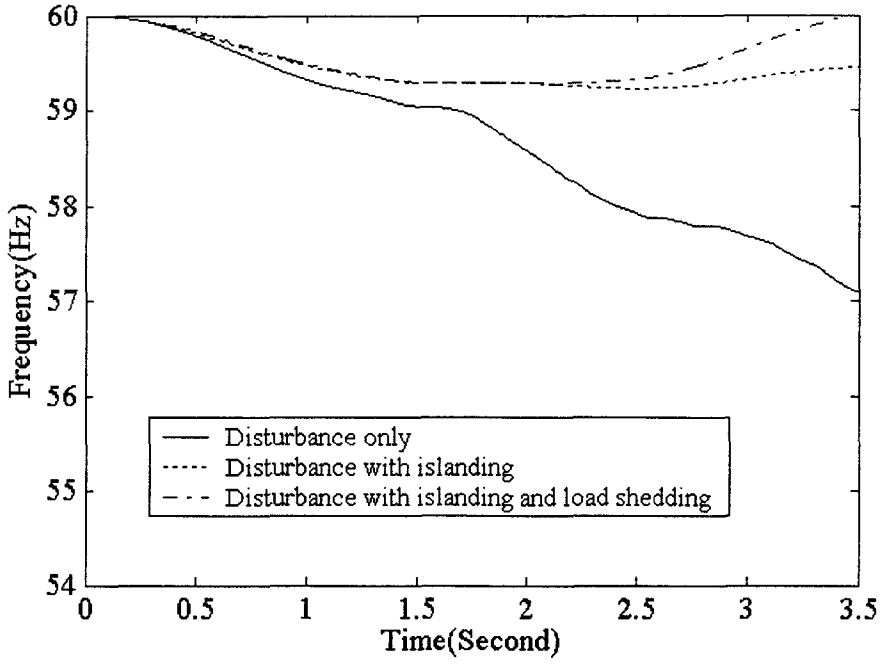

Fig. 5.2.9 Case 2: Frequency responses of generator 140 with governor data 2.

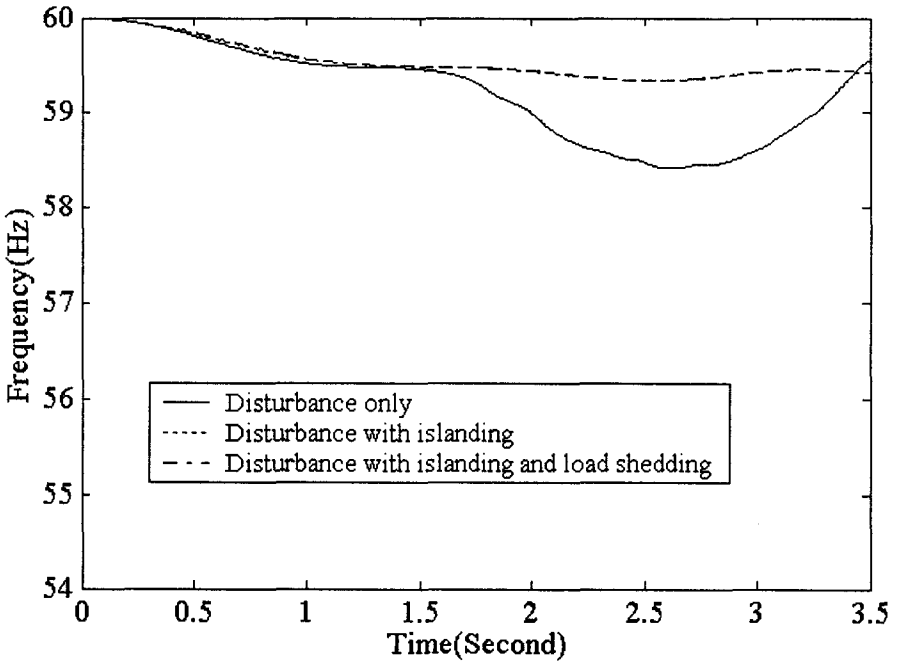

Fig. 5.2.10 Case 2: Frequency responses of generator 140 with governor data 3.

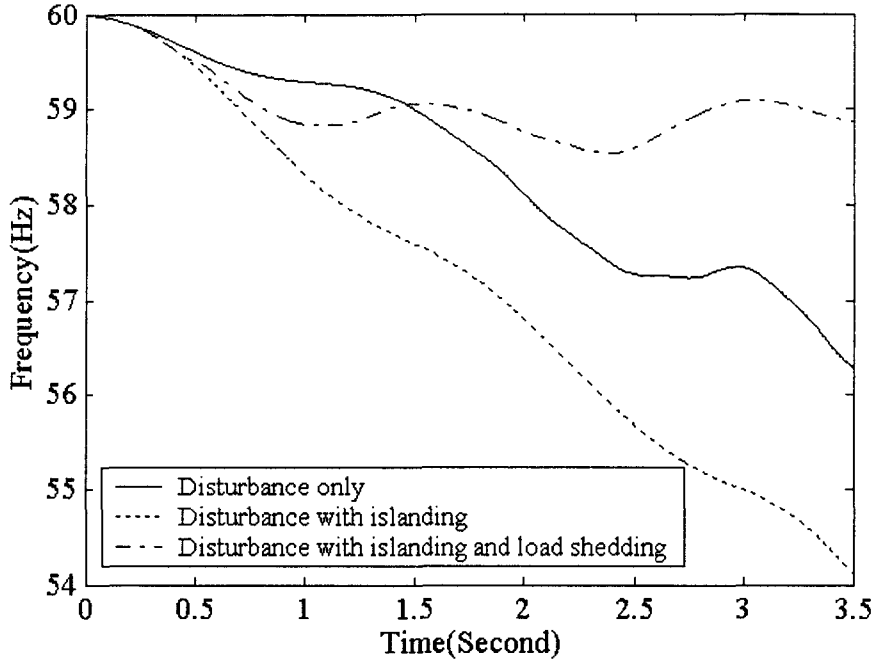

Fig. 5.2.11 Case 3: Frequency responses of generator 140 with governor data 1.

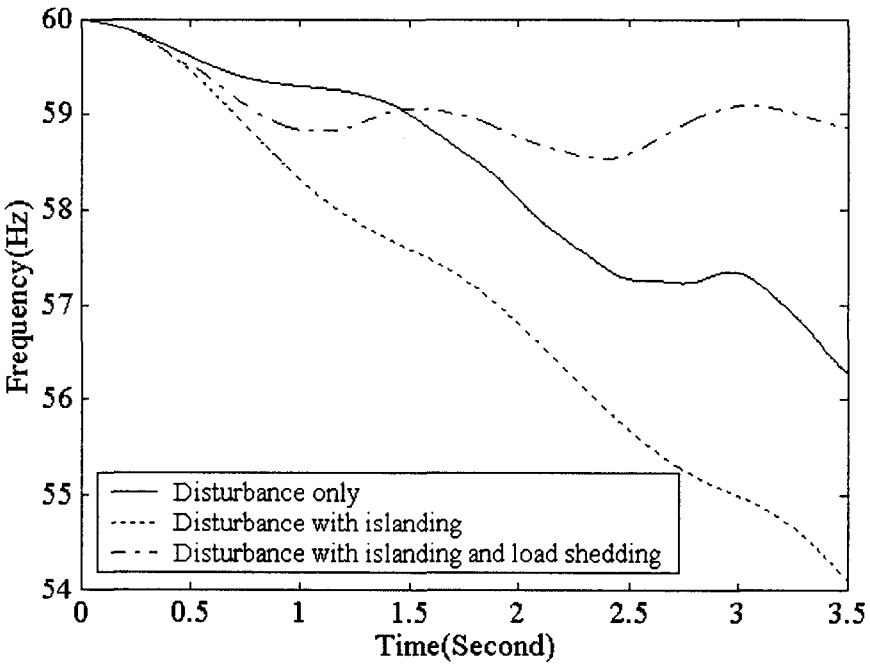

Fig. 5.2.12 Case 3: Frequency responses of generator 140 with governor data 2.

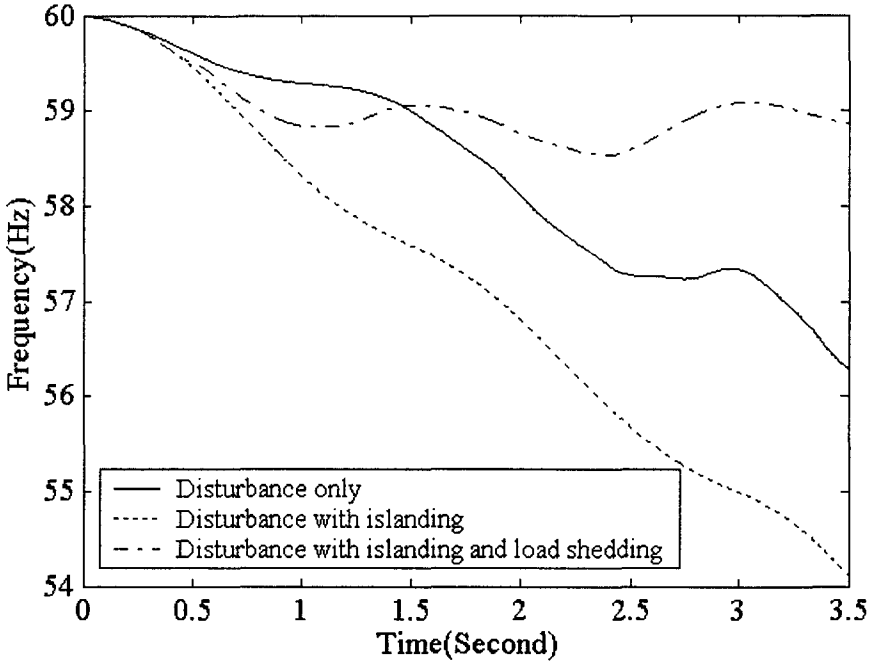

Fig. 5.2.13 Case 3: Frequency responses of generator 140 with governor data 3.

5.3 ISLANDING OF DIFFERENT DISTURBANCES

In order to test the system response to a severe contingency, two large disturbances are set up [41].

In case 2, three 500kV transmission lines in the system are tripped simultaneously, which corresponds to a catastrophic transmission failure where an incident takes out all the three transmission lines simultaneously. If no protection settings are considered, previous simulations in the section 5.2 show that the system will be unstable. Then the automatic islanding program determines that three islands should be formed 0.2 seconds after the disturbance. Three tie lines are tripped to form the islands:

- Bus 133-Bus 108
- Bus 134-Bus 104
- Bus 29-Bus 14

The disturbance and the three islands have been shown in Fig. 5.2.3. The biggest arrow shows the location where the disturbance happens, which has caused a disconnection of the

loop to the west of the test system. The three islands can be characterized as the north island, the central island and the south island. There are 11 generators in the south island, 3 generators in the central island and 15 generators in the north island. In order to form the islands, the R-Rdot out of step relay should be able to detect the large disturbances and trip the three tie lines of the south island. This is confirmed by the simulation on the system with the disturbance but without forming the islands and load shedding. The apparent resistance is monitored on the three tie lines, which is shown as Fig. 5.3.1.

In the three tie lines tripped, the first two lines are in the west and the third one is in the east. It is observed that around 0.2 seconds after the disturbance, the apparent resistances have abrupt changes on the two west tie lines shown in the Fig.5.3.1. It can be captured by the R-Rdot out of step relay. But the resistance doesn't change very much on the east tie line until about 1.8 seconds after the fault. So the remote tripping signal needs to be sent to the east tie line to form the appropriate island. This indicates that the islands determined by the automatic islanding program can be formed utilizing the R-Rdot relays.

In case 3, an incident takes out all four 500kV transmission lines located in the southeast portion of the system. To save the system from an impending blackout, we split the system into two islands 0.2 seconds after the contingency. Then the automatic islanding program is deployed to find the optimal cut sets. In order to create the island, the following lines are tripped:

- Bus 133 - Bus 108
- Bus 134 - Bus 104

The two islands have been shown as Fig. 5.2.4. They are characterized as the north island and the south island. There are 9 generators in the south island, all of which belong to the south island for the first case. All the other 20 generators belong to the north island in this case. The biggest arrow shows where the disturbance takes place. As a result, the connection to the southwest of the system is lost. For this case, the apparent resistances on the three tie lines of case 1 have been monitored and plotted again shown as Fig. 5.3.2. It is observed that around 0.2 seconds after the disturbance, the apparent resistance has abrupt changes on the east tie line. It can be captured by the R-Rdot out step relay. Since the changes on the west tie lines are not obvious until 1.7 seconds after the disturbance, the remote tripping signal needs to be sent to the west tie lines in order to from the south island quickly.

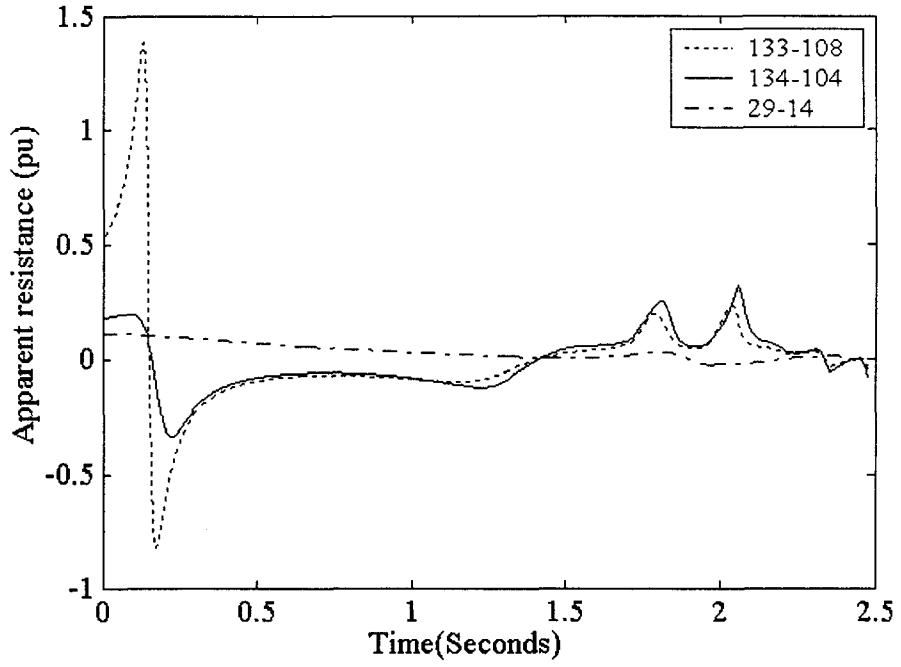

Fig. 5.3.1 Case 2: Apparent resistance plot on tie lines of south island.

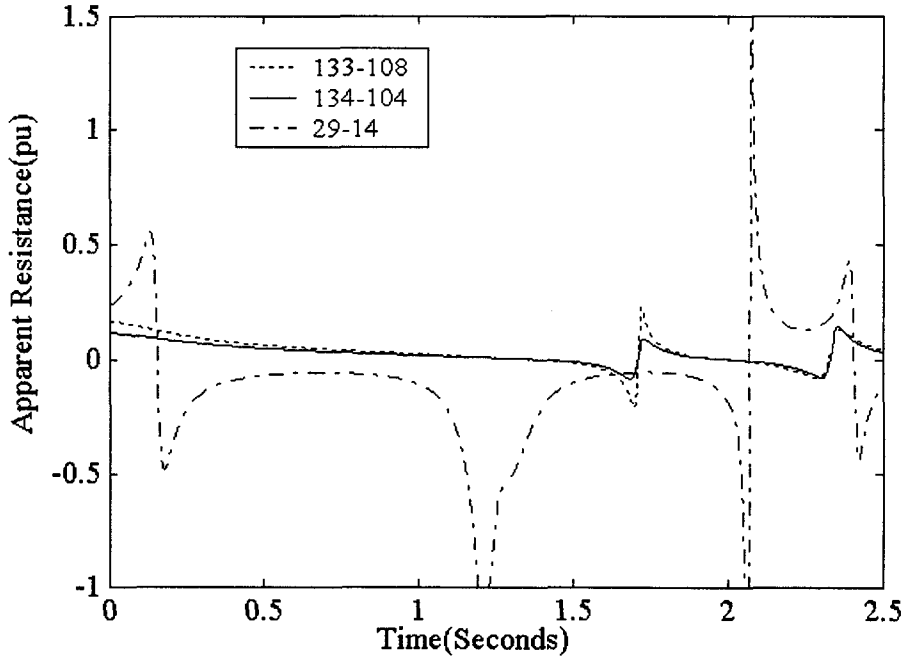

Fig. 5.3.2 Case 3: Apparent resistance plot on tie lines of south island

As a summary of this section, the following conclusions can be reached:

- Two large disturbances are set up with one of them simultaneously tripping off three 500kV transmission lines and the other tripping off four 500kV transmission lines. Both of them are large enough to cause the system lose stability in a very short period if no protection settings are taken into account.
- Three and two islands are formed respectively in each case with the generator grouping decided by the slow coherency theory and the boundary determined by automatic islanding program. Tie lines of the south island need to be tripped off in both disturbances. By monitoring the apparent resistance of the tie lines in both disturbances, it is observed that the R-Rdot out of step relays installed at the tie lines close to the location of the disturbance are able to detect the large disturbances at around 0.2 seconds, while the relays on the other tie lines will operate around 1.7 seconds. So local tripping will happen very shortly after the disturbance, while remote tripping signal needs to be sent to the other tie lines to make appropriate tripping.

5.4 NONLINEAR SIMULATIONS

In case 2 and case 3 in the previous section, the islands are determined by slow coherency. In order to verify the correctness of the islanding schemes for the two large disturbances, nonlinear simulations have been conducted on different operating conditions for both cases. In the simulations, no islanding actions or load shedding actions are taken after the fault. Generator rotor relative angles are observed. The simulations last 0.25 seconds since the islands are formed 0.2 seconds after the fault. The generators' relative angle curves are plotted to show the coherency within the groups. The different operating conditions are compared with the base condition's total load. Four different load conditions are considered. They are: 30% load decrease, 16% load decrease, base condition and 6% load increase. They are selected based on the grouping result in Table 5.1.2. For each disturbance, the generators' relative angle curve in the load rich island and the generation island, are plotted on each load condition. Altogether 10 figures are plotted shown from Fig. 5.4.1 to Fig. 5.4.10. They are:

- Fig. 5.4.1 through Fig. 5.4.8 are plotted for case 2. In Fig. 5.4.1, Fig 5.4.3, Fig. 5.4.5 and Fig. 5.4.7, the relative angle curves of 11 generators from the south island and 3 generators from the central island are plotted. They correspond to 30% load decrease, 16% load decrease, base case

and 6% load increase. In Fig. 5.4.2, Fig. 5.4.4, Fig. 5.4.6, Fig. 5.4.8, the relative angle curves of 15 generators from the north island are plotted. They correspond to 30% load decrease, 16% load decrease, base case and 6% load increase.

- Fig. 5.4.9 through Fig. 5.4.16 are plotted for case 3. In Fig. 5.4.9, Fig. 5.4.11, Fig. 5.4.13, Fig. 5.4.15, the relative angle curves of 9 generators from the south island are plotted. The relative angle curves of the 3 generators from the central island in case 2 are also plotted for comparison. They correspond to 30% load decrease, 16% load decrease, base case and 6% load increase. In Fig. 5.4.10, Fig. 5.4.12, Fig. 5.4.14 and Fig. 5.4.16, the relative angle curves of 20 generators from the north island are plotted, which include the 3 generators from the central island in case 2. They correspond to 30% load decrease, 16% load decrease, base case and 6% load increase.

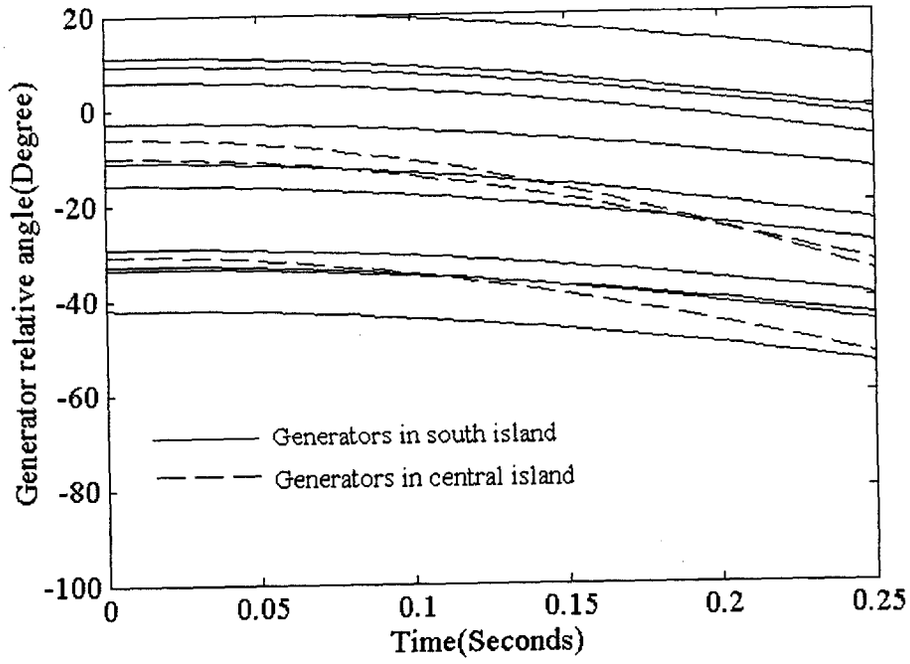

Fig. 5.4.1 Case 2-Generator relative angle curves with 30% load decrease in load rich islands.

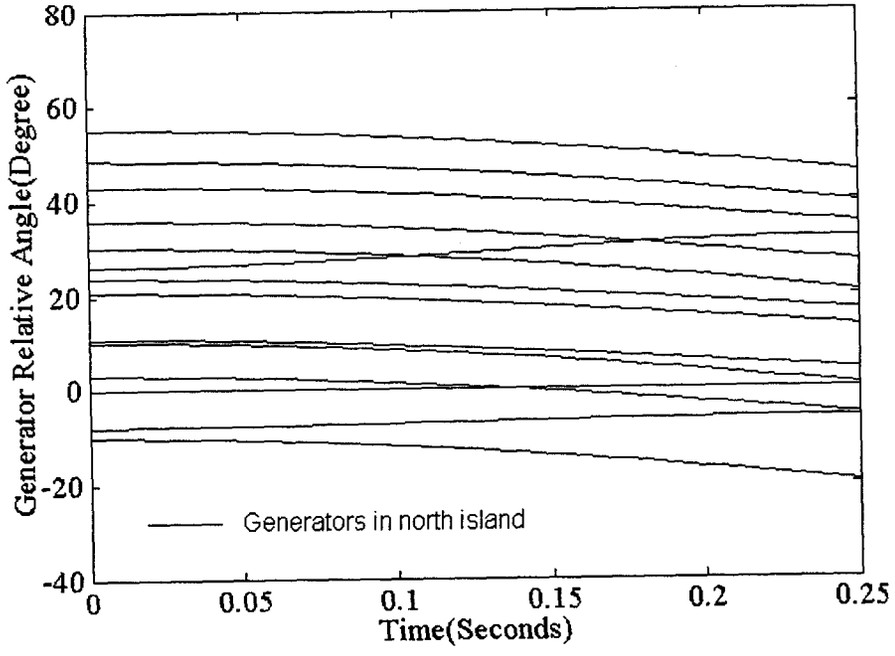

Fig. 5.4.2 Case 2-Generator relative angle curves with 30% load decrease in generation rich island.

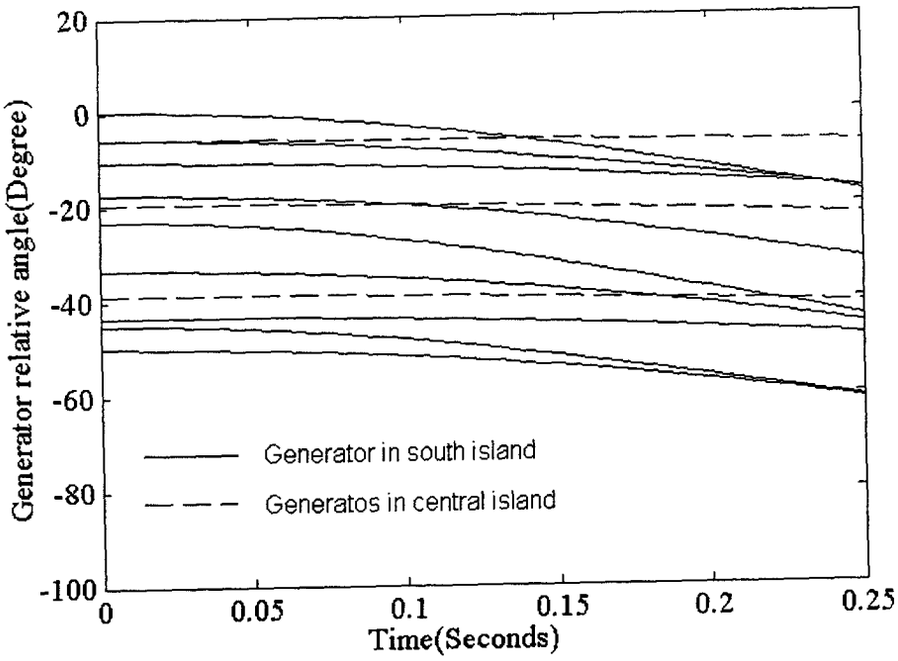

Fig. 5.4.3 Case 2-Generator relative angle curves with 16% load decrease in load rich islands.

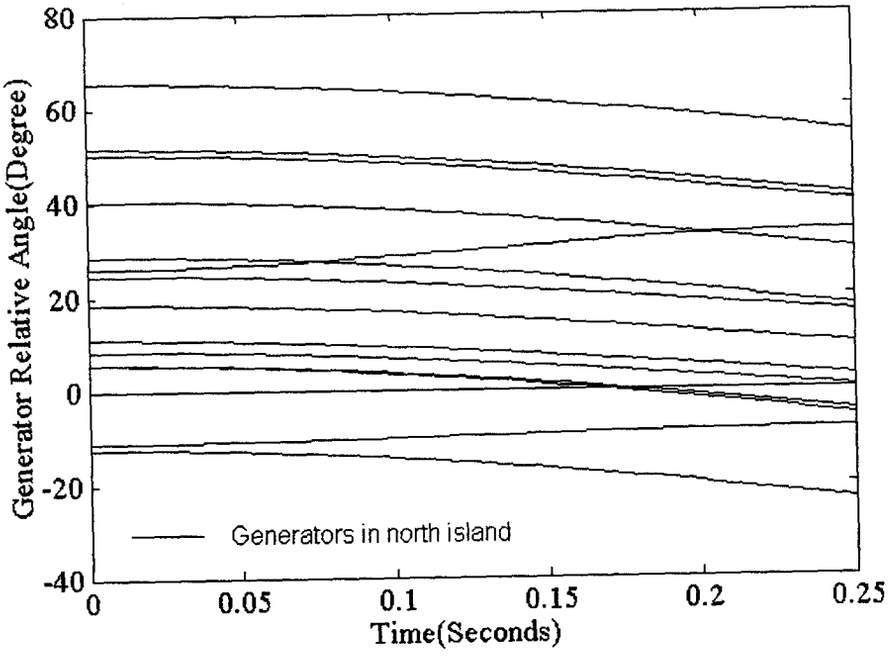

Fig. 5.4.4 Case 2-Generator relative angle curves with 16% load decrease in generation rich island.

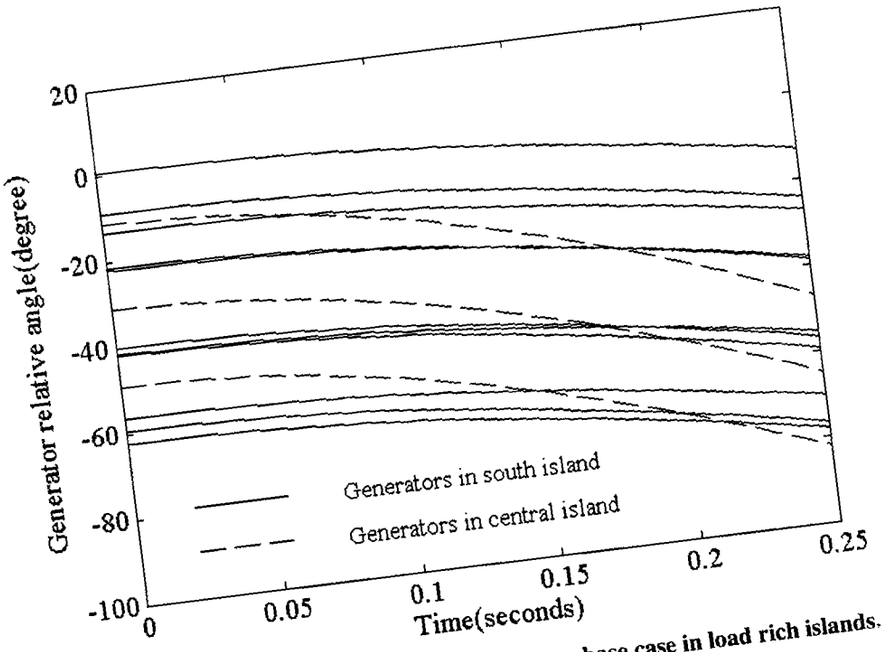

Fig. 5.4.5 Case 2-Generator relative angle curves base case in load rich islands.

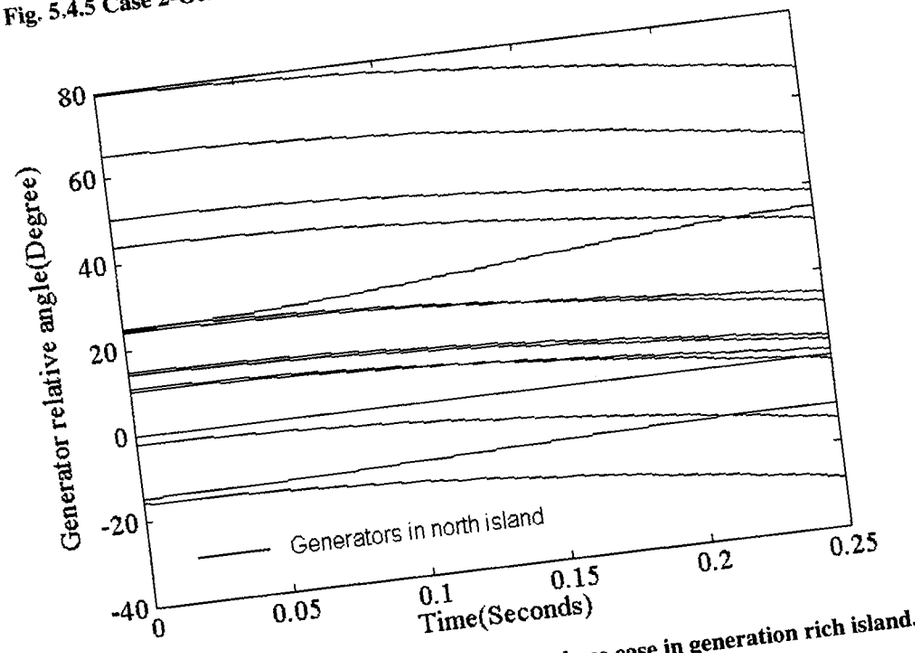

Fig. 5.4.6 Case 2-Generator relative angle curves base case in generation rich island.

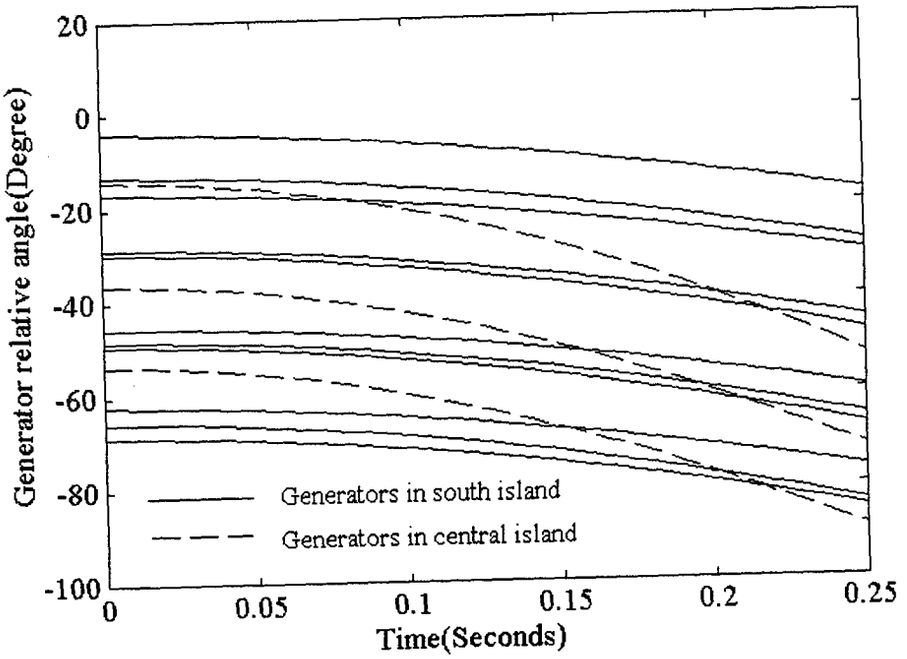

Fig. 5.4.7 Case 2-Generator relative angle curves with 6% load increase in load rich islands.

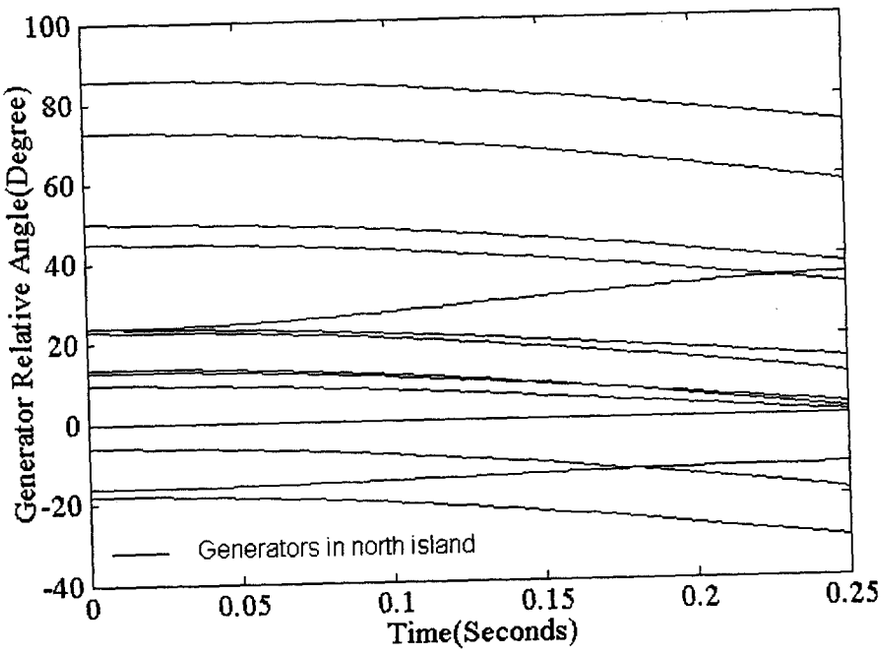

Fig. 5.4.8 Case 2-Generator relative angle curves with 6% load increase in generation rich islands

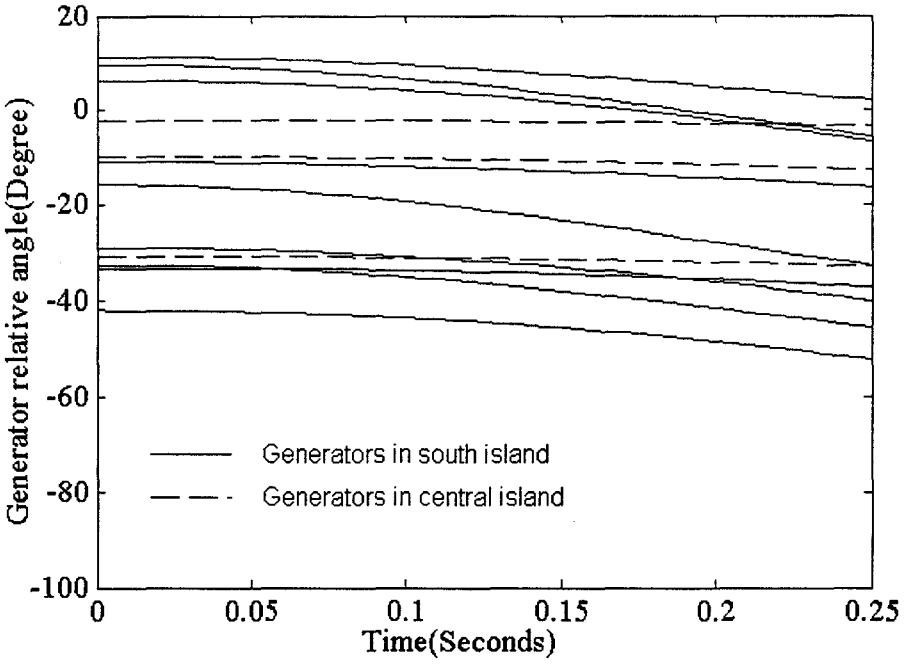

Fig. 5.4.9 Case 3-Generator relative angle curves with 30% load decrease in load rich island.

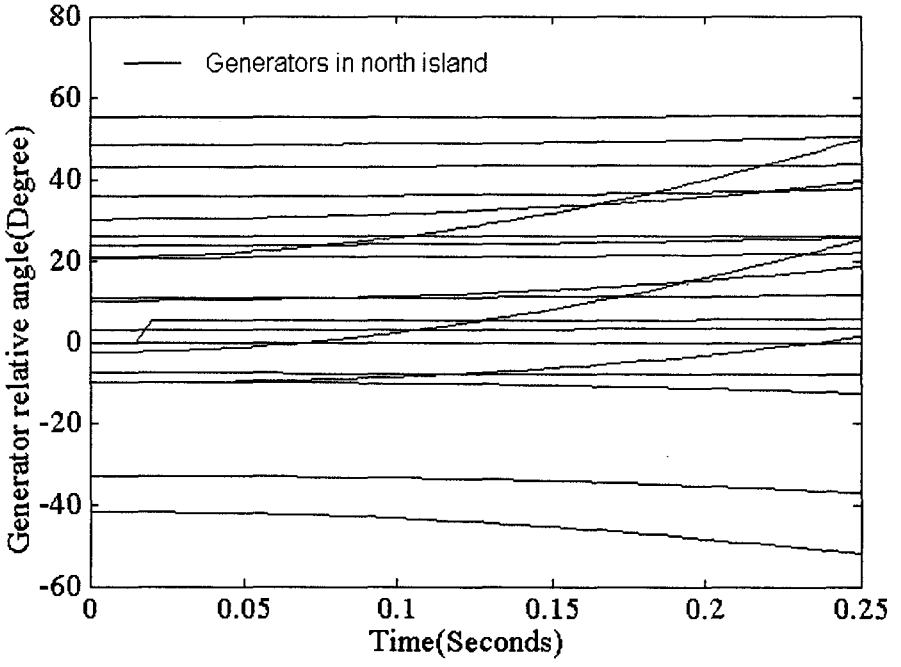

Fig. 5.4.10 Case 3-Generator relative angle curves with 30% load decrease in generation rich island

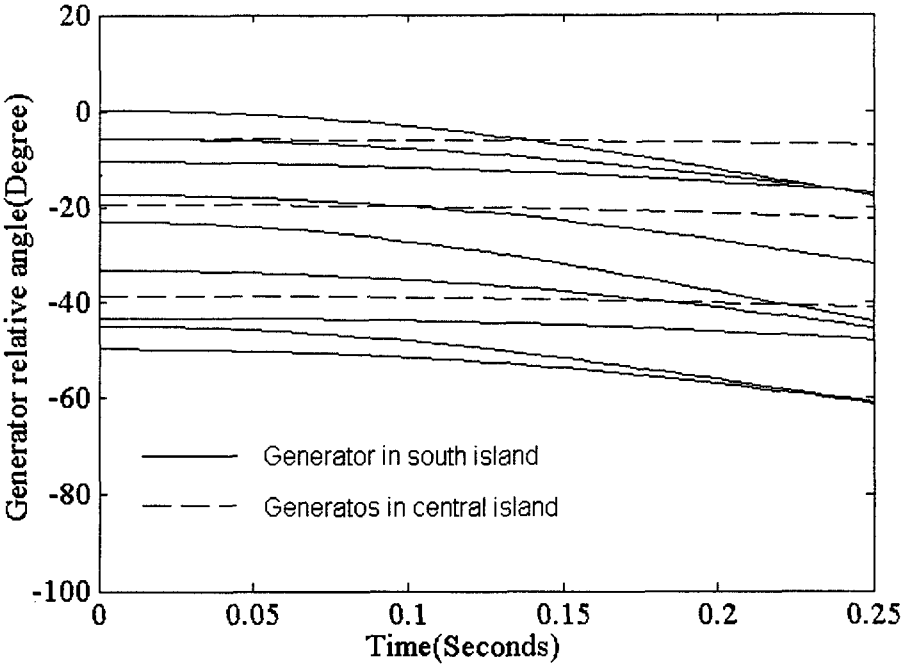

Fig. 5.4.11 Case 3-Generator relative angle curves with 16% load decrease in load rich island.

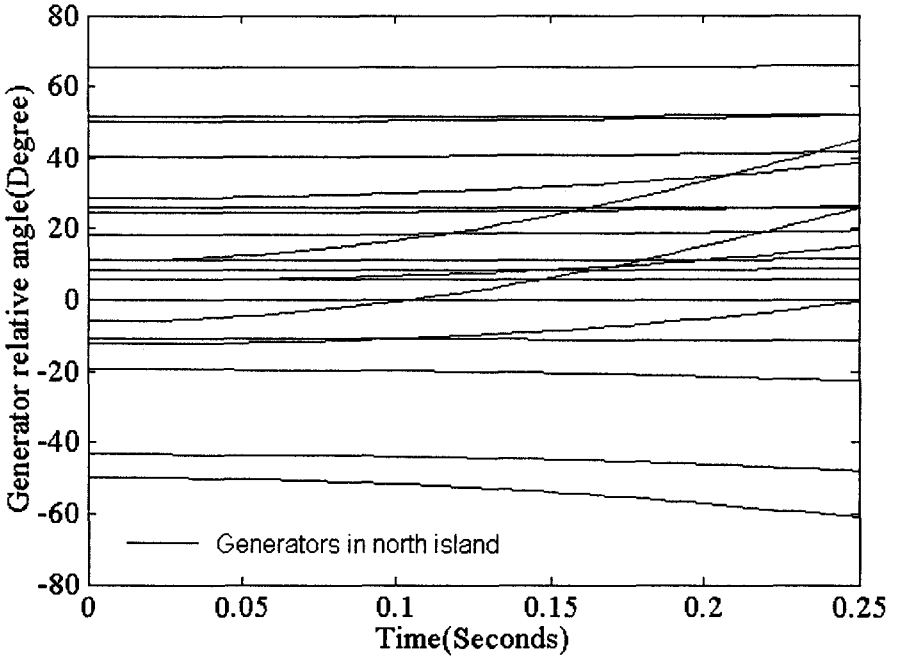

Fig. 5.4.12 Case 3-Generator relative angle curves with 16% load decrease in generation rich island.

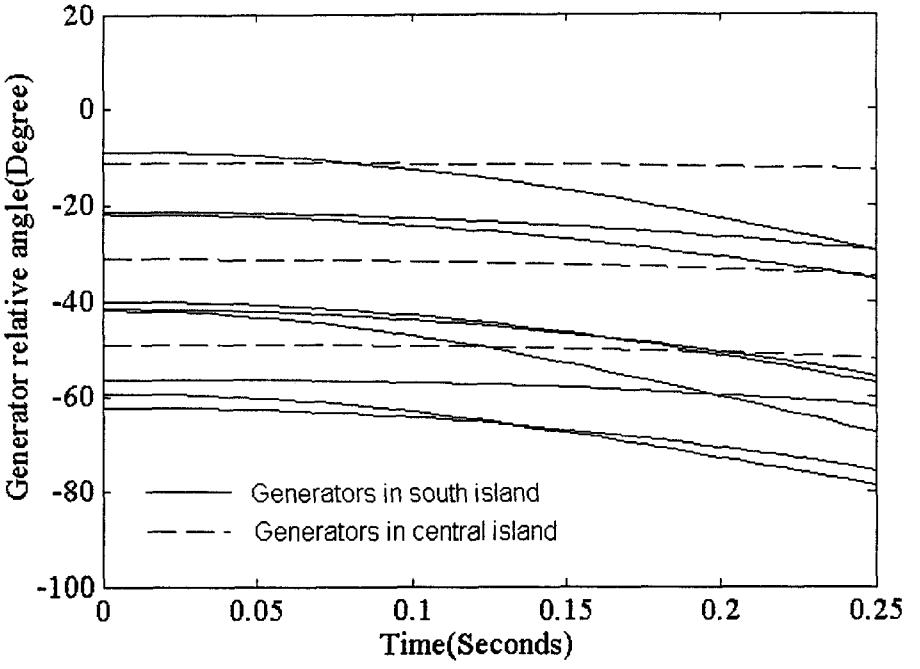

Fig. 5.4.13 Case 3-Generator relative angle curves base case in load rich island.

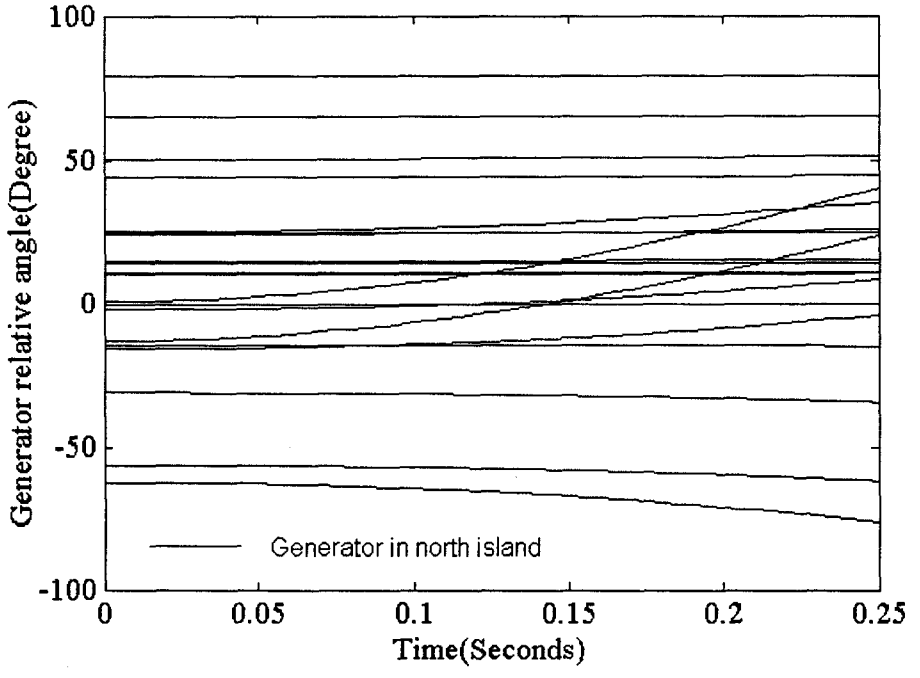

Fig. 5.4.14 Case 3-Generator relative angle curves base case in generation rich island.

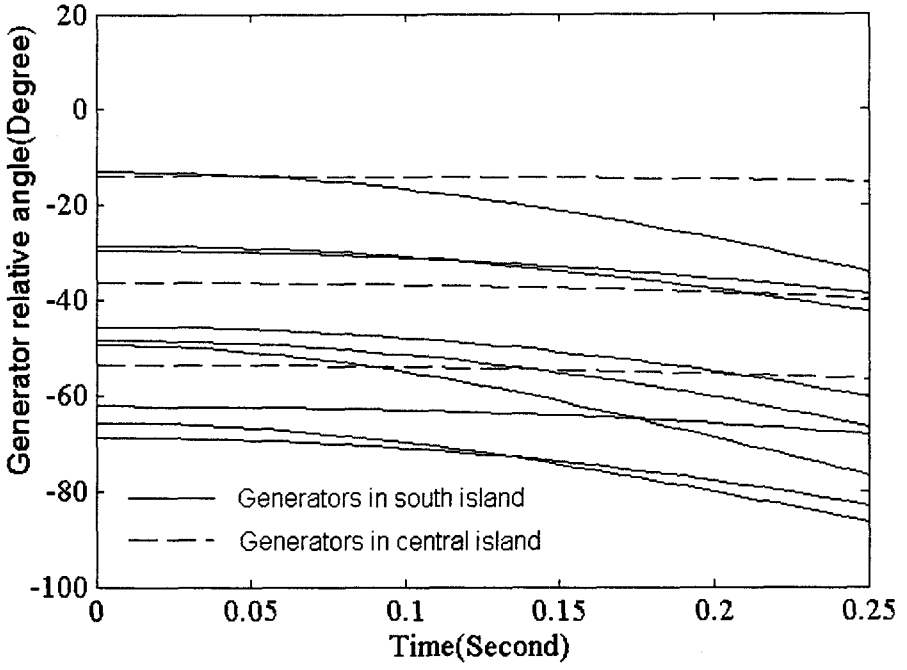

Fig. 5.4.15 Case 3-Generator relative angle curves with 6% load increase in load rich island.

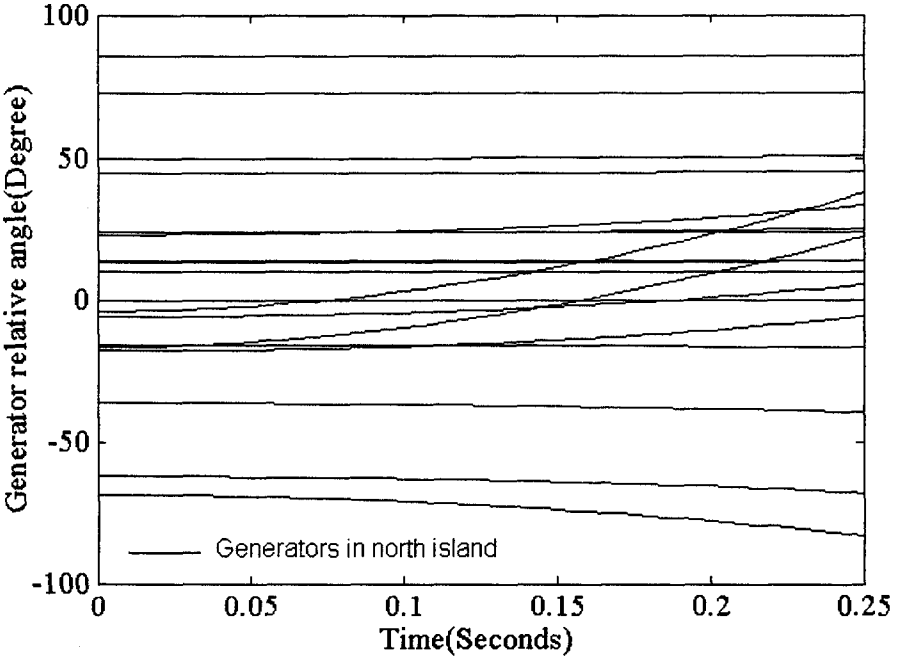

Fig. 5.4.16 Case 3-Generator relative angle curves with 6% load increase in generation rich island.

The following conclusions can be reached from the figures:

- For case 2, the generators in each island have almost constant angle difference with each other during the period or they are coherent with each other. This conclusion holds for various load conditions including 30% load less, 16% load less, base case and 6% load more, which means the islanding scheme works for various power initial conditions.
- For case 2, the generators in the north island are mostly coherent with each other, but the angle patterns of the generators near the location of the disturbance are much different because of impact of the disturbance.
- Near coherency also holds for case 3. Similar plots have been obtained with 6% load increase, 16% load decrease and 30% load decrease.

The two sets of nonlinear simulations show that the grouping results obtained from the slow coherency theory are not significantly related with the disturbance and the power flow initial condition. The same grouping result will hold for a relatively large range of working conditions from the existing tests made. More tests are made showing a slightly different result, which will be shown in section 5.6. In the next section, the new two-layer load shedding scheme is applied on the load buses of the load rich islands. The result shows very good performance of the self-healing scheme of controlled islanding followed by load shedding based on the rate of frequency decline.

5.5 LOAD SHEDDING RESULT

The self-healing scheme is composed of an islanding scheme based on slow coherency theory and a two-layer load shedding scheme based on rate of frequency decline. In order to show the performance of the self-healing scheme, especially the effect of the new two-layer load shedding scheme, three different cases with the two large disturbances discussed before are set up for comparison. For each case, one typical generator is selected from each island to plot the frequency response curve in four different situations. The result shows the self-healing scheme has very good performance.

As mentioned before, in case 1 the disturbance is applied on the west tie lines of the test system, which is a simultaneous tripping of three transmission lines. Simulations have shown that the disturbance will result in system being unstable. To save the system from an

impending blackout, the system is split into two islands 0.2 seconds after the contingency. In the first case, **the islands are formed by experience**.

After islanding, the system is divided into two islands shown in Fig. 5.2.2. The biggest arrow shows the location of the disturbance. The disturbance disconnects the portion to the central west of the system. The two islands can be characterized as the northeast island, which is generation rich, and the southwest island, which is load rich. Load shedding is applied in the load rich island. Various load shedding schemes are applied for comparison. For the application of the new two-layer load shedding scheme, the layer of the scheme to select depends on the rate of the frequency decline, which indicates the impact of the disturbance on the bus. In the southwest island, some of the buses have m_i smaller than m_0. So the conventional load shedding scheme is deployed at these buses. For the other buses at which m_i is larger than m_0, the load shedding scheme based on the rate of frequency decline is deployed. Simulations are conducted using EPRI's Extended Transient-Midterm Stability Program (ETMSP). Fig. 5.5.1 shows the frequency responses of a typical generator 118 in the southwest island in four situations. They are:

- Curve 1: Disturbance only.
- Curve 2: Islanding with no load shedding after the disturbance.
- Curve 3: Islanding followed by load shedding based on frequency difference.
- Curve 4: Islanding followed by load shedding based on the rate of frequency decline.

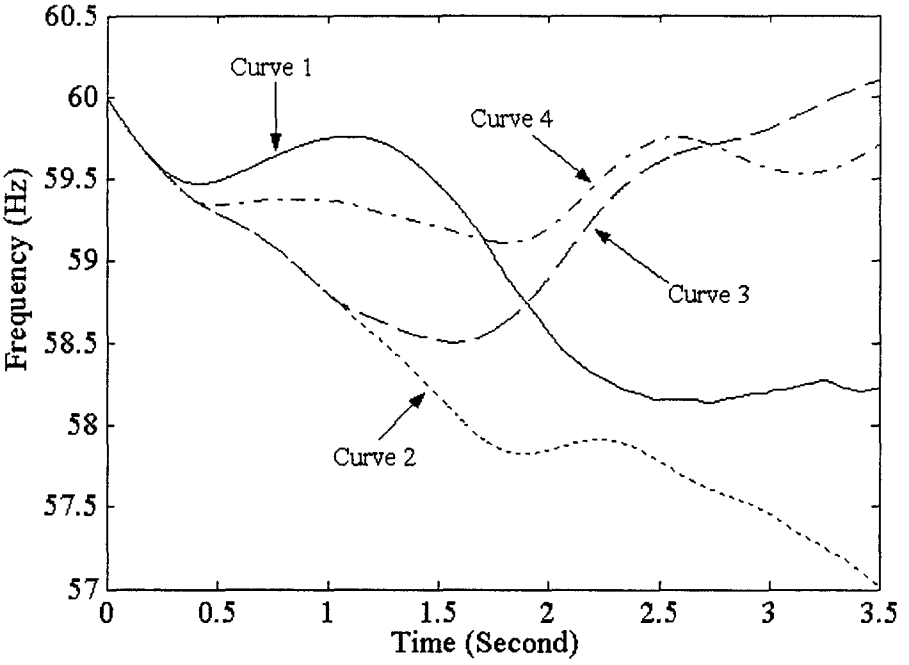

Fig. 5.5.1 Frequency response of generator 118 after the disturbance of the 179-bus test system-Case 1.

Curve 1 and curve 2 show that, following the disturbance, the system will lose stability without any self-healing strategy or only with islanding. Curve 3 and curve 4 give a comparison between the two load shedding schemes. They are the load shedding scheme based on frequency difference and the two-layer load shedding scheme based on the rate of frequency decline. It is observed that to maintain the stability of the system, less load needs to be shed with the new load shedding scheme than the old scheme. At the same time, the system experiences smaller frequency excursions under the new scheme than the old scheme.

In case 2, the same disturbance in case 1 is applied with the connection to the central west of the test system is lost. Then the automatic islanding program is employed to split the system into three islands according to slow coherency theory. The three islands have been shown in Fig. 5.2.3. The biggest arrow shows the location of the disturbance. The three islands can be characterized as the north island, the central island and the south island. Load shedding is applied in the two load rich islands, which are the central island and the south island. Various load shedding schemes are applied for comparison. In the application of the new load shedding scheme, the load shedding scheme based on the rate of frequency decline is deployed on all the load buses of the central island since all of them have m_i larger than m_0.

While the conventional underfrequency load shedding scheme is deployed on all the load buses of the south island since all of them have m_i smaller than m_0. The same four frequency responses as the ones in case 1 are plotted. Generator 118 is again chosen as the typical generator in the central island. Similar results can be obtained from the four curves in the Fig. 5.5.3 except the amount of load shed, which will be shown later. That is, to maintain the stability of the system, less load needs to be shed with the new load shedding scheme than the old scheme. At the same time, the system experiences smaller frequency excursions under the new scheme than the old scheme. Generator 43 is chosen as the typical generator in the south island. It is observed that curve 2, 3 and 4 coincide. The system is stabilized only with islanding action from curve 2. Curve 3 shows no load needs to be shed under the conventional underfrequency load shedding scheme. Although after 1.2 seconds the frequency at generator 43 drops below 59.5 Hz, which is a threshold of the second layer of the new scheme according to Table 4.2.1, no load has been shed. The second layer is not activated because all of the buses in the south island have m_i smaller than m_0. This is the reason why curve 4 coincides with curve 3.

Similar results have been confirmed by case 3. In this case, a different disturbance is applied and two islands are formed by the automatic islanding program based on slow coherency. The two islands have been shown in Fig. 5.2.4, which are characterized as the north island and the south island. The south island is load rich. Various load shedding schemes are applied for this case, too. The same four curves are plotted for the frequency response of one typical generator 43 after the disturbance. Previous results hold for this case, too.

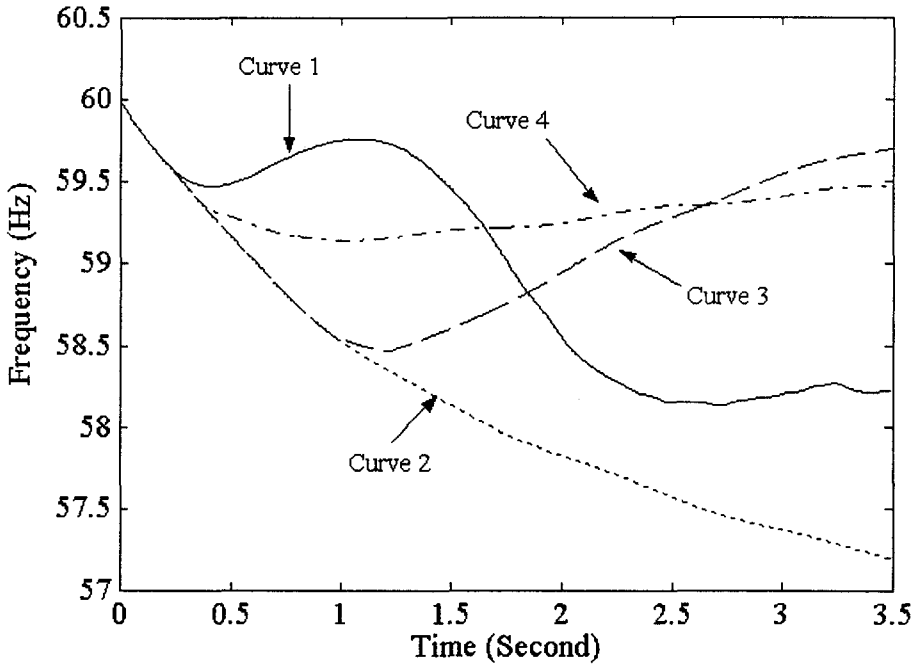

Fig. 5.5.2 Frequency response of generator 118 after the disturbance of the 179-bus test system-Case 2.

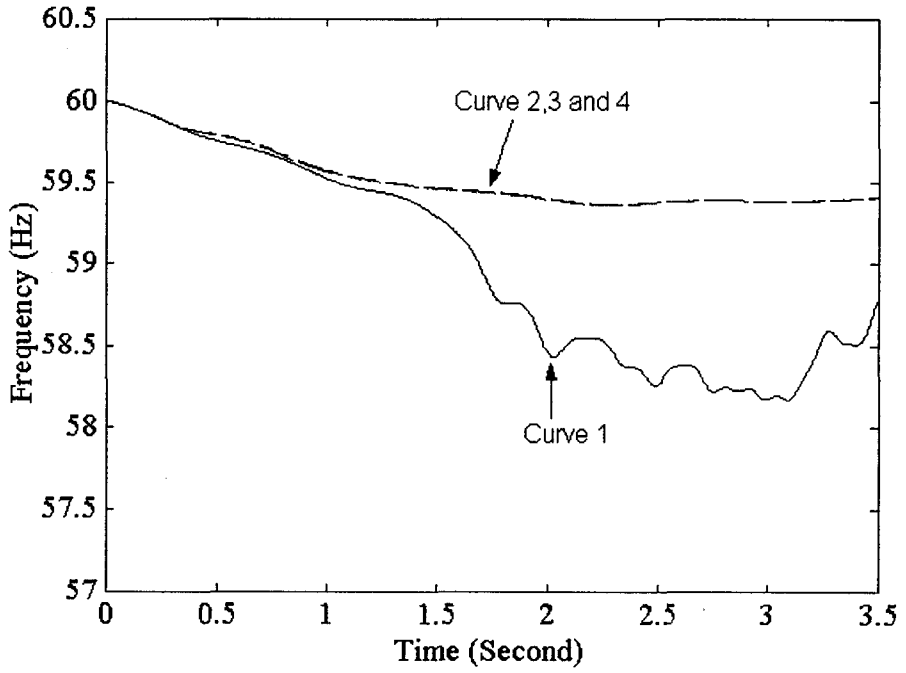

Fig. 5.5.3 Frequency response of generator 43 after the disturbance of the 179-bus test system-Case 2.

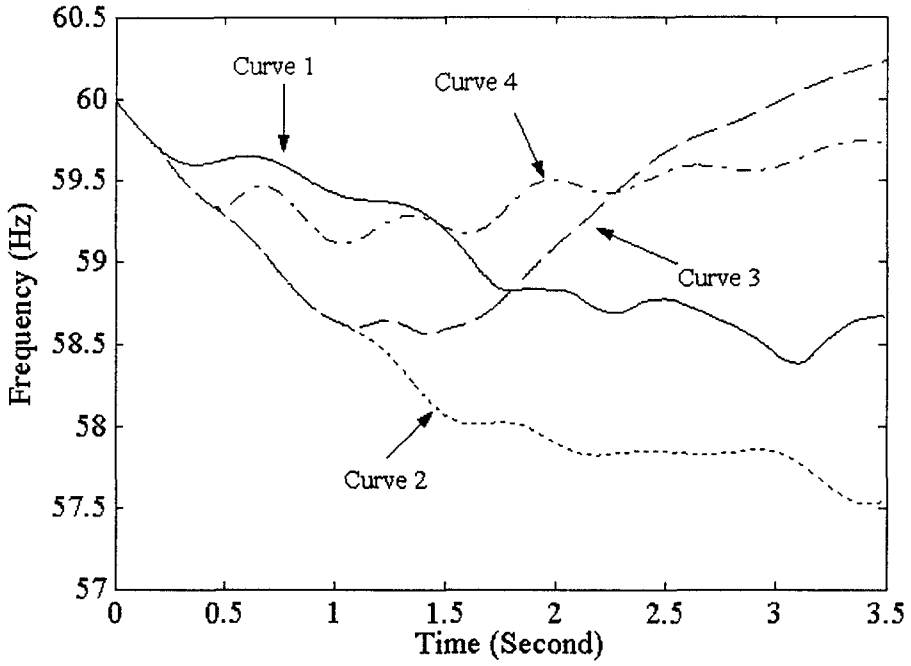

Fig. 5.5.4 Frequency response of generator 43 after the disturbance of the 179-bus test system-Case 3.

Although in all three cases, the system can be stabilized with the new two-layer load shedding scheme, the amounts of the load that has been shed are much different. Table 5.5.1 provides a comparison of the two load shedding schemes in three cases. In the cell that shows the amount of load shed, the first percentage is the ratio of the load shed compared to the total system load. The second percentage is the ratio of the load shed compared to the island load. It is observed that the load shedding scheme based on the rate of frequency decline sheds much less load than the conventional load shedding scheme in all three cases. On the other hand, between case 1 and case 2, though they have the same disturbance, the self-healing scheme with islanding based on slow coherency will finally shed much less load to stabilize the system than the scheme with island based on experience. Only 26% of the load shed in the first case need to be shed in the second case to stabilize the system, while the same two-layer load shedding scheme is applied. The curves and the table not only show the advantage of the new load shedding scheme over the conventional one, but also the advantage of the islanding scheme based on slow coherency than the one based on experience.

Table 5.5.1 Comparison of the two load shedding schemes in three cases.

Cases	Generation Load Imbalance (MW)	Load Shed with Conventional Scheme (MW)	Load Shed with New Scheme (MW)
No. 1	Generation 16,265 Load 22,679	6,937 (11.4% 30.6%)	5,698 (9.4% 25.1%)
No. 2	Central Island: Generation 5,118 Load 7,006 South Island: Generation 15,477 Load 17,373	1,810/0 (3.0%/0% 25.8%/0%)	1,450/0 (2.4%/0% 20.7%/0%)
No. 3	Generation 11,148 Load 15,674	5,127 (8.4% 32.7%)	3,672 (6.0% 23.4%)

Another observation demonstrates the advantage of the islanding scheme based on slow coherency. In the case 2 above, simulations indicate that no load needs to be shed in the south island according to our load shedding scheme from Table 5.5.1. The frequency in the island can be recovered through coordination of the generators' governors, and voltage regulators. Since no load is shed in this case, it is reasonable to ask why not form only one central island instead of two islands. But simulations show the necessity to form the south island. Fig. 5.5.6 shows the frequency response curve of one representative generator 43 when only the central island is formed, which was in the south island. The curves are obtained with exactly the same disturbance and the load shedding scheme except now at 0.2 seconds, only two islands are created, which are the central island and the rest of the system. The system will experience large oscillations without forming the south island. As mentioned before, the fault-on trajectory shows out of step condition can be captured by the R-Rdot relay around 0.2 seconds after the disturbance on the west tie lines of the south island, but not so soon on the east tie line. So it is necessary to isolate the area before the fast dynamics propagate beyond the south island.

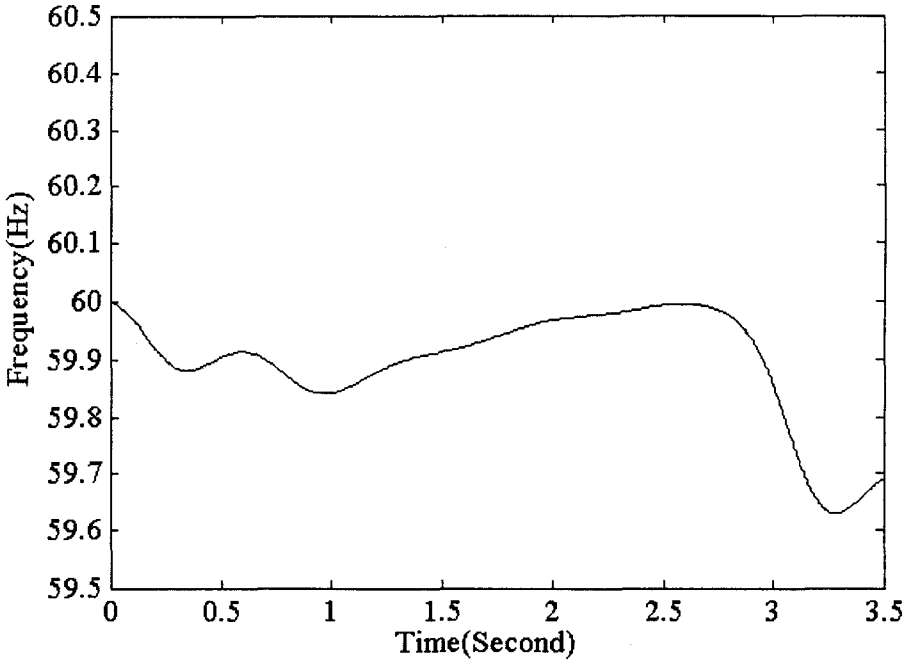

Fig. 5.5.5 Frequency response of generator 43 after the disturbance if not forming the south island-Case 2.

5.6 SOME NEW TEST RESULT AND DISCUSSIONS

Some new tests were made to support the material presented in [41]. These new tests are designed to verify in a further step the group results are generally unchanged with small load changes. These results also verify the R-Rdot measurements on the tie lines of the tripping sets identified by the software have the correct indication of the fault condition. Both non severe and severe faults have been set up instead of only severe faults to observe the response on the tie lines. Tests are now more comprehensive and more simulation results are obtained. New case numbers and new scenarios different from those discussed earlier are presented. All the following discussions in section 5.6 refer to the new cases and new scenarios if not mentioned otherwise.

In the new tests, we still consider the two faults, one with 3 transmission lines open and the other with 4 lines open. But we have the lines open sequentially one by one. Also we monitor more lines and draw the R-Rdot plots. The two test sets are shown in Table 5.6.1.

Table 5.6.1 New cases analyzed

Set 1		
New Case #	**Lines Removed**	**Lines Monitored**
1	Bus 83- 168	Bus 133 – 108
2	Bus 83- 168, Bus 83- 170	Bus 134 – 104
3	Bus 83- 168, Bus 83- 170 Bus 83 –172	Bus 29 – 14 Bus 139 – 27 Bus 136 – 16 Bus 49-- 48
Set 2		
New Case #	**Lines Removed**	**Lines Monitored**
1	Bus 12 - 139	Bus 133 – 108
2	Bus 12-139, Bus 27-139	Bus 134 -- 104
3	Bus 12-139, Bus 27-139 Bus 16 -136 (Ckt1)	Bus 29 – 14 Bus 37 – 64
4	Bus 12-139, Bus 27-139 Bus 16 -136 (Ckt1, Ckt2)	Bus 104 – 135 Bus 154 – 143 Bus 49 -- 48

For test set 1, from the fault-on nonlinear simulation, there is not much change of system frequency on each bus for both case 1 and case 2. So islanding for these two cases are not needed. Simulations considering no conventional protection settings indicate in case 3 the disturbance will result in the system being unstable. A six line apparent resistance plot is shown in Fig. 5.6.1.

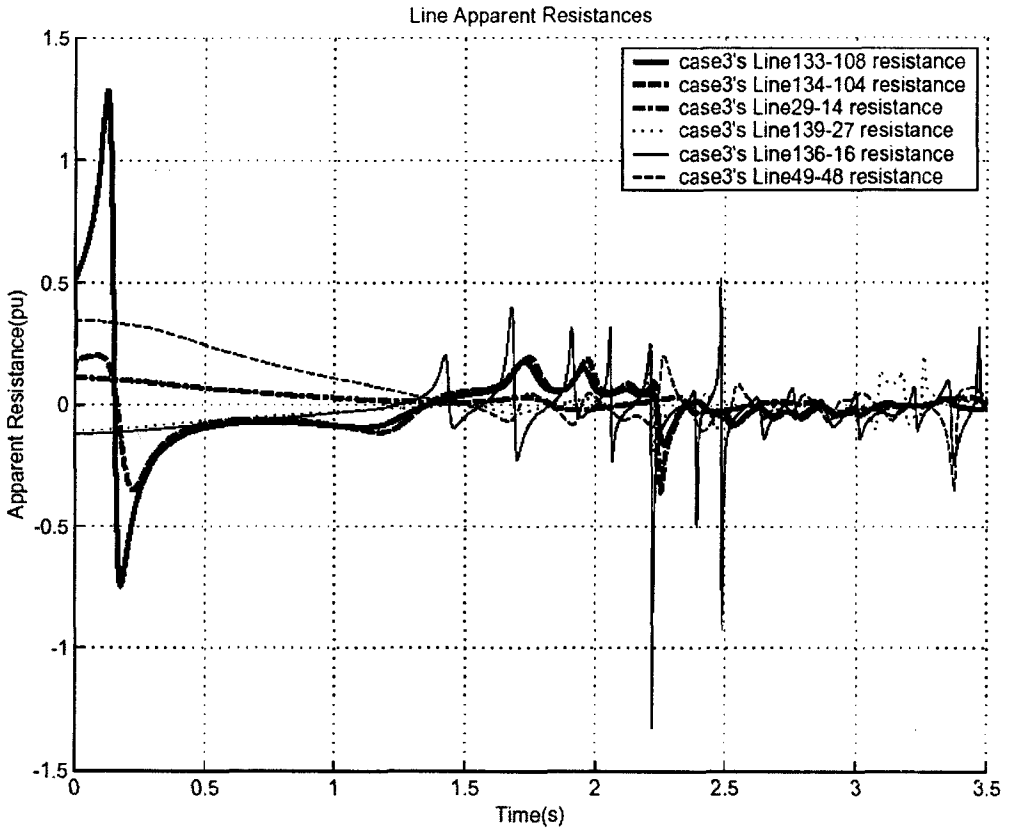

Fig. 5.6.1 Line apparent resistance plots-Set 1, Case 2.

The plots for lines 133-108, 134-104 and 29-14 are the same as in Fig. 5.3.1, where 133-108, 134-104 are the most west lines and 29-14 is the most east lines. The other lines in Fig. 5.6.1 are located between them. Since the large oscillations represent the fault passing, we can watch clearly from the figure that the disturbance is propagating from the west to the east.

As mentioned before, in order to control the disturbance, a central and a south island are formed by tripping tie lines 133-134, 104-134 and 14-29. They are obtained by the automatic islanding program under the grouping of slow coherency. Detailed information about how to determine the tie lines is given below.

For the western part of the south island, a sub-network of 30 lines is formed as the interface network. For the eastern part of the south island, a sub-network of 17 lines is formed to be the interface network. The possible cut sets along with stored in a file. Several typical samples of the candidate cut sets for this case are shown in the Table 5.6.2

Table 5.6.2 Candidate cut sets for case 3.

Cutset	Load-Generation Imbalance
133 – 134 104 – 134 14 – 29	North: Gen=40814.63 Load=36405.90 South: Gen=15477.70 Load=17373.60 Central: Gen=5118.00 Load=7005.91
133 – 132 104 – 107 104 – 135 104 – 102 14 – 29	North: Gen=40814.63 Load=36405.90 South: Gen=15477.70 Load=17068.60 Central: Gen=5118.00 Load=7310.91
133 – 132 104 – 135 104 – 102 108 – 135 14 – 29	North: Gen=40814.63 Load=36405.90 South: Gen=15477.70 Load=16763.60 Central: Gen=5118.00 Load=7615.91
132 – 119 104 – 102 107 – 108 108 – 135 14 – 29	North: Gen=40814.63 Load=36405.90 South: Gen=15477.70 Load=16763.60 Central: Gen=5118.00 Load=7615.91

Among these, we observe that the first cut set has a slightly large imbalance for the south island, which has an inertia of 966.66 sec, but a smaller mismatch for the central island, which has an inertia of 343.39 sec, in comparison to the other candidate cut sets. Consequently, the first cut set will result in islands that have significantly lower frequency oscillations than the other cut sets. Hence, this cut set is chosen as the optimal islanding strategy.

In the second sets of cases, the fault on four transmission lines was placed in the southeast portion of the system. Four cases are analyzed. Case 1 doesn't require islanding. Case 2 results in rapid changes of line apparent resistance shown in Fig. 5.6.2. The change

first occurs on line 29-14 around 0.4 seconds after the disturbance because it is near the disturbance. Then at about 1.8 seconds the line 154-143 experiences a large oscillation. Lines 133-108 and 134-104 detect big changes on apparent resistances at about 2.4 seconds after the fault.

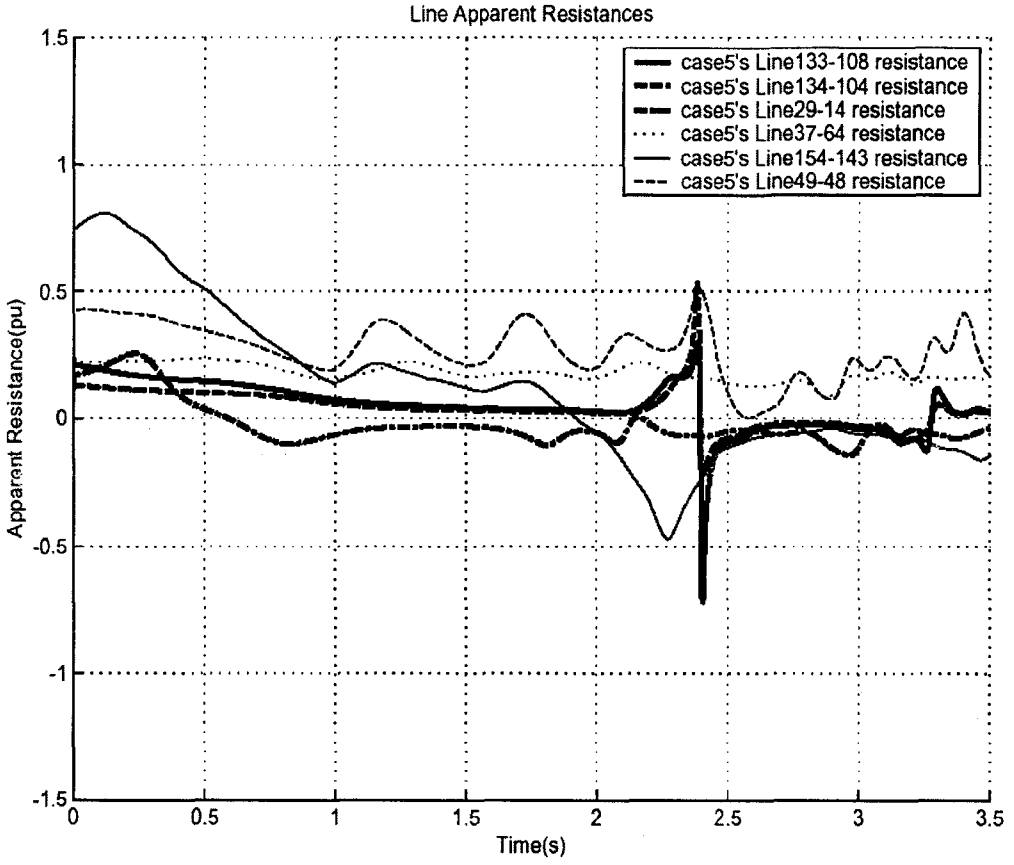

Fig. 5.6.2 Line apparent resistance plots-Set 2, Case 2.

To save the system from an impending blackout, we split the system into two islands. The cut set identified by the automatic islanding program results in the following lines being tripped:

- Bus 133-Bus 108
- Bus 134-Bus 104
- Bus 29-Bus 14

The two islands are shown in Fig. 5.6.3. There are 11 generators in the south island. The biggest arrow shows where the disturbance takes place. Compared with Fig. 5.2.4, in this case, the connection on the south-east is not lost due to the fault. So the south island is formed as determined by the slow coherency grouping and automatic islanding program.

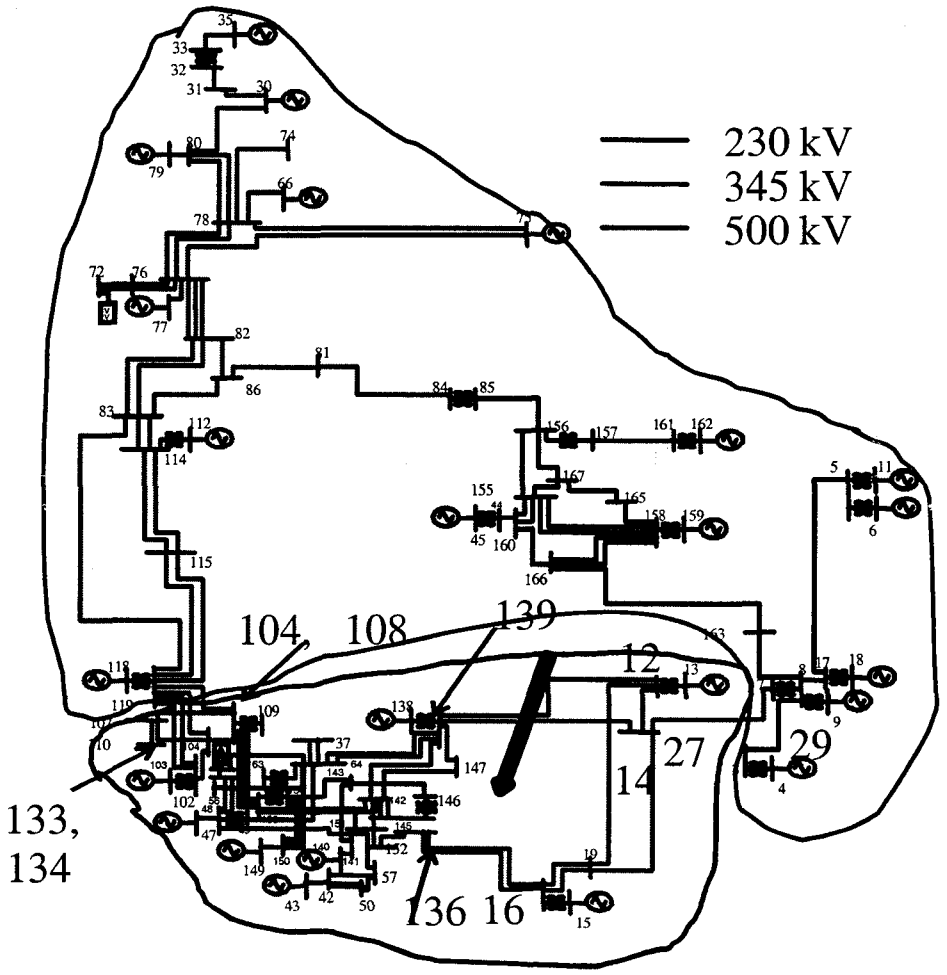

Fig. 5.6.3 Slow coherency Set 2-Case 2: Disturbance and islands formed.

Case 3 is also a severe disturbance. Rapid changes on line apparent resistance are observed. The islands determined are the same as in Case 2. As mentioned before, case 4 is the most severe one among case 1 to case 4. Fig. 5.6.4 provides the line apparent resistance plots in this case. Fig. 5.2.4 provides the illustration for the islands formed. In these set of cases, the apparent impedance first undergoes a significant change on the line 29-14 that is close to the disturbance. As the disturbance progresses, we observe that the apparent

impedances on the lines in the central portion and the western portion of the south island change at later times as the disturbance propagates towards the western portion of the system.

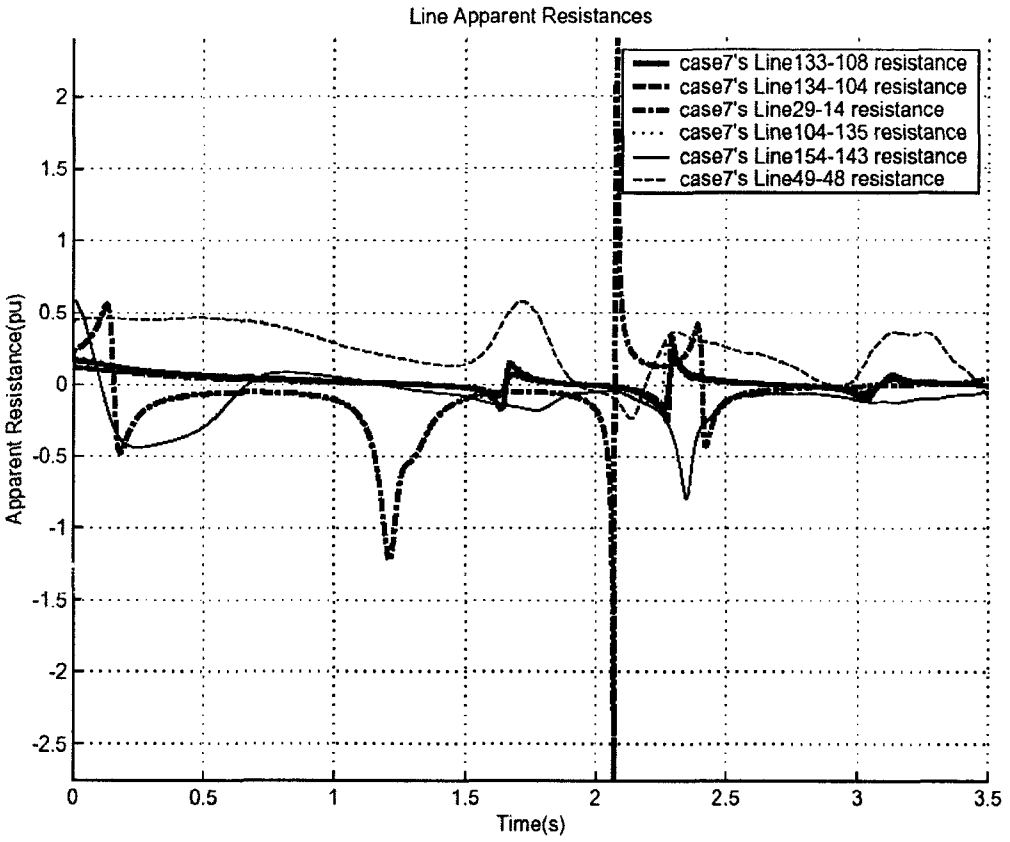

Fig. 5.6.4 Line apparent resistance plots for Set 2, Case 4.

Generally the slow coherency base grouping is independent of the power flow initial condition. More tests have been designed to verify this point based on set 1-case 3. Since the southern area is basically load rich and affected most by stability problem, different loading conditions are set up by randomly picking some load buses and changing the loads by a certain amount.

In the following tables displaying the various load scenarios, scenario I and scenario II have the same generator groupings as indicated by DYNRED. The same islands should be formed under these two scenarios. In the other two scenarios III and IV, the generator grouping is slightly different. Fig. 5.6.5 and Fig. 5.6.6 denote the islands formed by the islanding program for these two load scenarios.

Table 5.6.3 Scenario I: Load change at buses in southern area.

Load Bus	Base Load	New Load	Change(%)
136	856.00	898.80	-5
141	3191.00	3350.55	+6
142	204.20	214.41	-7
143	377.40	396.27	+8

Table 5.6.4 Scenario II: Load change at buses in southern area.

Load Bus	Base Load	New Load	Change(%)
136	856.00	898.80	+5
137	175.00	183.75	+5
139	902.30	947.42	+5
141	3191.00	3350.55	+5
142	204.20	214.41	+5
143	377.40	396.27	+5
145	3098.00	3252.90	+5

Table 5.6.5 Scenario III: Load change at buses in southern area.

Load Bus	Base Load	New Load	Change(%)
136	856.00	813.20	-5
137	175.00	166.25	-5
139	902.30	857.19	-5
141	3191.00	3031.45	-5
142	204.20	193.99	-5
143	377.40	358.53	-5
145	3098.00	2943.10	-5

Table 5.6.6 Scenario IV: Load change at buses in southern area.

Load Bus	Base Load	New Load	Change(%)
5	2350.00	2232.50	-5
31	4400.00	4180.00	-5
44	2053.00	1950.35	-5
80	5000.00	4750.00	-5
119	5661.00	5377.95	-5
141	3191.00	3031.45	-5
150	3118.00	2962.10	-5

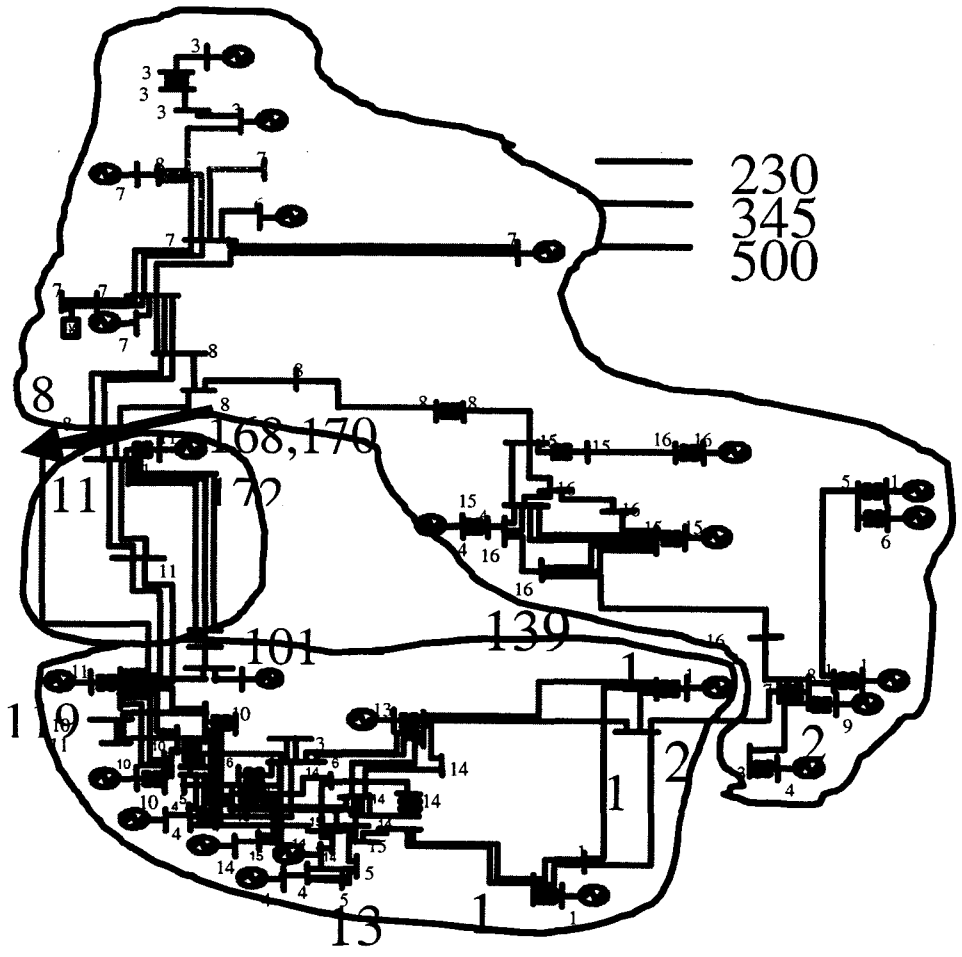

Fig. 5.6.5 Islands formed by islanding program (Scenario III).

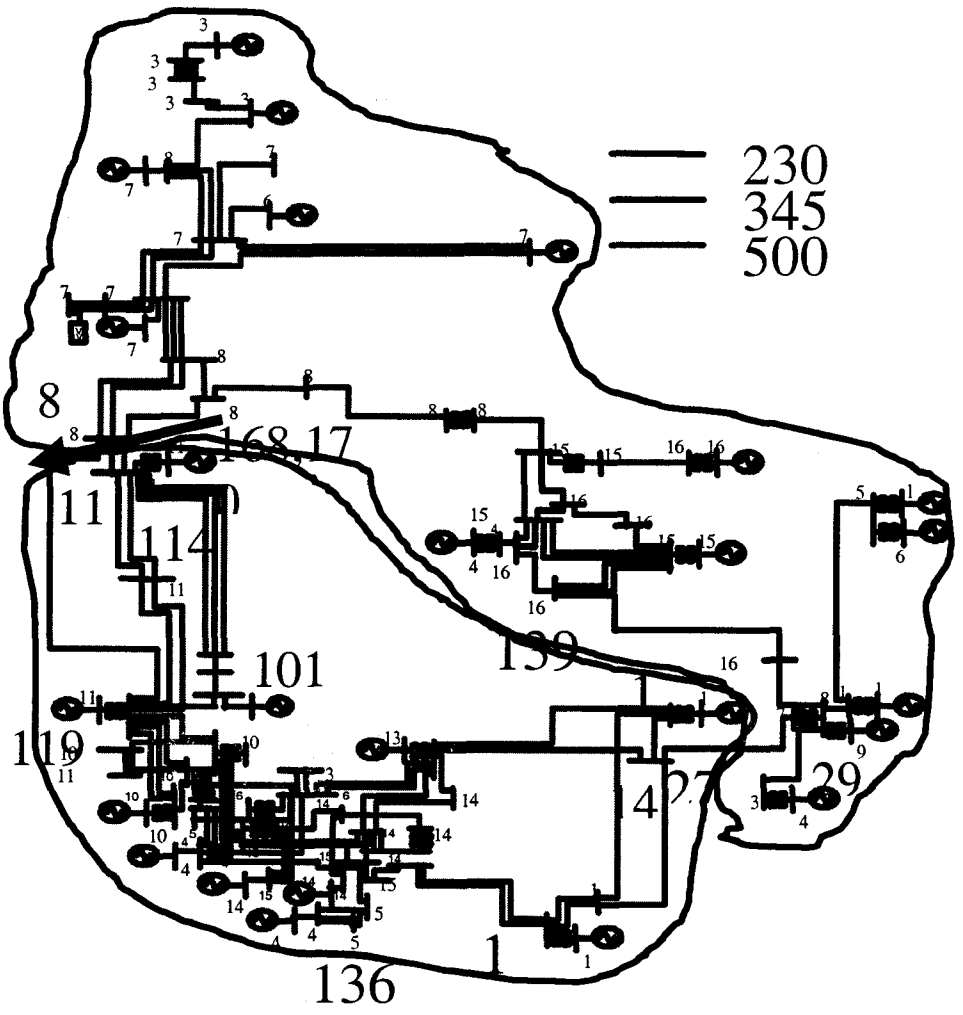

Fig. 5.6.6 Islands formed by islanding program (Scenario IV).

Fig. 5.6.5 and Fig. 5.6.6 show the islanding scheme for the two cases is slightly different from each other. With the different loading conditions, the slow coherency grouping program returns different results. This is because generator buses (112, 116 and 118) in the central island are loosely coherent with other generators. With slight change in load, these generators can jump from coherent group to another. The optimal cut sets and generation-load imbalance for the two scenarios are shown in Table 5.6.7.

Table 5.6.7 Optimal cut set and generation-load imbalance.

Scenario	Cutset	Load-Generation Imbalance
III	119 - 123 119 - 129 119 - 131 101 - 113 29 - 14	North: Gen=40814.63 Load=36405.90 South: Gen=19538.70 Load=23881.02 Central: Gen=1057.00 Load=247.30
IV	83 - 89 83 - 94 83 - 98 29 - 14	North: Gen=40814.63 Load=36744.90 South: Gen=20595.70 Load=23939.32

This set of cases essentially shows that the grouping can possibly change with change in loading conditions. The difference lies in the grouping among the loosely connected generators. The automatic islanding program determines the appropriate optimal cut sets and created islands that have an optimal imbalance of generation and load. The islands are not significantly different, and we observe that the system is broken up into either two or three islands, and in scenario IV the central island is merged with the south island.

Then the verification of the principal basis for the islanding scheme is done by conducting nonlinear simulations for different operating conditions. The generator rotor angle curves without any islanding action and any load shedding action during the fault-on period for the designed scenarios are plotted. These plots include complete nonlinear model of the system and provide a verification of the ability of the slow coherency approach in picking up the weak connections in the system independent of the loading disturbance. These plots are similar to the results in section 5.4. The generators in each island have almost constant angle difference with each other during the simulated period and the groups maintain coherency well beyond the time at which a significant rate of change of impedance occurs on tie lines separating these groups. Our premise of utilizing the slow coherency approach to identify the weakest links are well justified.

It needs to be noted that in the 179-Bus 29-Generator simulation case, DYNRED program calculated and obtained a predefined number of groups of generators, four in this case. Thus, the automatic islanding program decided the exact boundary between the islands based on the four groups of generators. When the number of groups, four here, is decided, it can be proven with the linear model that the groups of generators decided by the slow coherency have the weakest connections than the other types of grouping. The proof has been demonstrated in section 2.5.2. But there is no guarantee four groups instead of three groups will be the optimal strategy to deal with the large disturbance. Furthermore, from the test results, one group will be divided into more groups when the number of groups becomes larger. However, it is not the case when the number of groups is small. Therefore, it is necessary to design a strategy to find the optimal strategy. The optimal strategy here means it has the minimum number of islands formed, which has the minimum impact to the system. At the same time, it is able to shed the minimum amount of loads and successfully prevent the disturbance from extending to a cascading event thus save the system from an impending blackout. Thus, we design the following procedure to obtain the optimal grouping database for individual contingency.

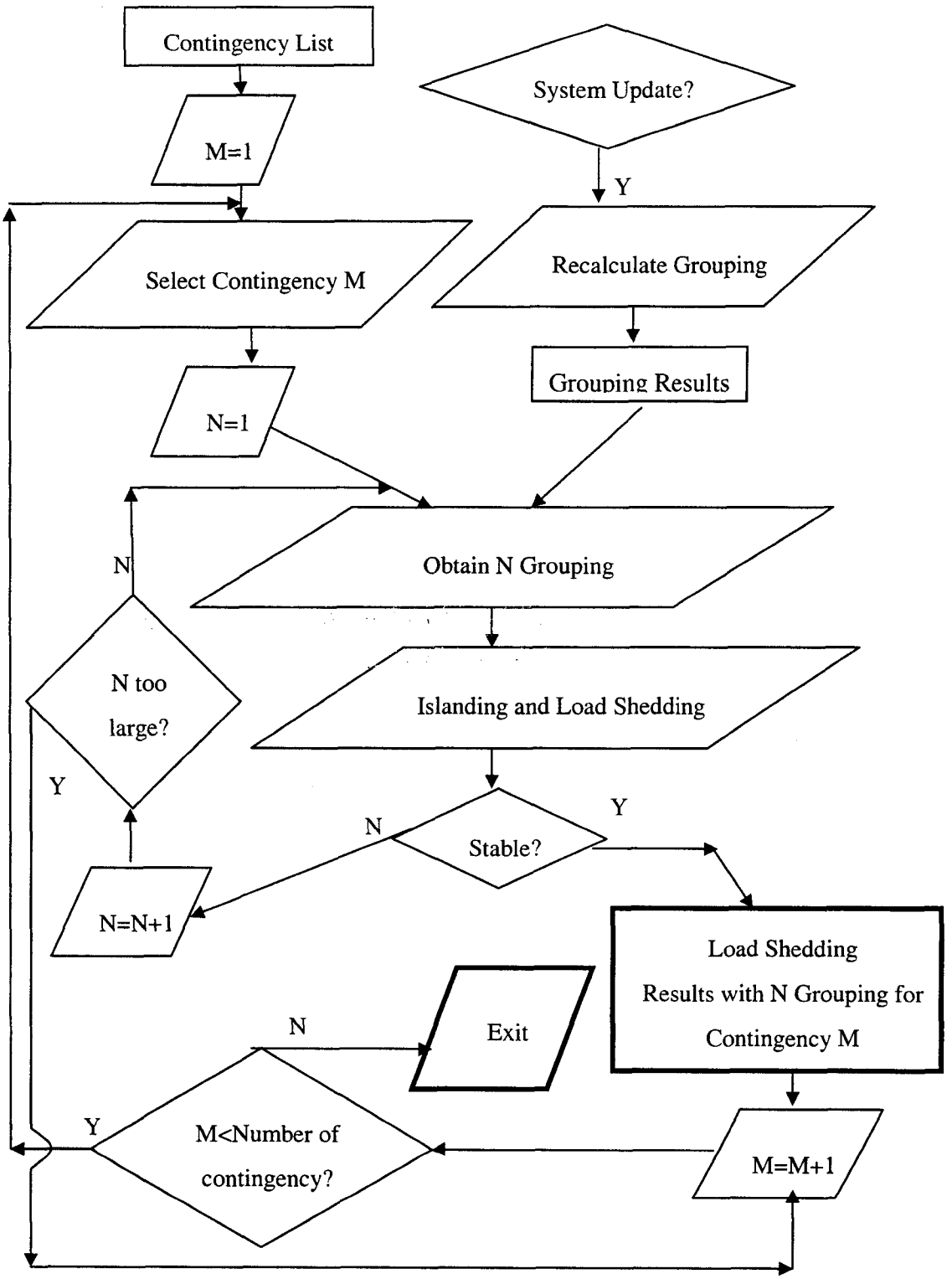

Fig. 5.6.7 Diagram to obtain the optimal grouping strategy

CHAPTER 6 CONCLUSIONS, CONTRIBUTIONS AND FUTURE WORK

6.1 CONCLUSIONS

In this dissertation, a slow coherency based islanding strategy is developed for large disturbances. A two-level load shedding scheme, which consists of a layer of conventional underfrequency load shedding scheme and a layer of load shedding scheme based on the rate of frequency decline, is applied in the load rich island after the tripping action. An automatic islanding program is developed to identify the optimal cut sets based on several criteria given the grouping results. Switching action of islanding is based on the R-Rdot out of step relay. A three-level switching mechanism is developed which is an integration of the local measurement, local action and phasor measurement, centralized decision. A framework of the overall self-healing strategy is provided. The analytical basis for the slow coherency based islanding scheme is presented. This includes the development of the procedure for grouping. The identification of the weakest link in the network based on the slow coherency grouping is presented on the linearized power system electromechanical model. A discussion of how this approach can be extended to the nonlinear model is also presented. Since the slow coherency grouping is based on a linearized model, the issues of its applicability to highly nonlinear power systems and the efficacy of the procedure in determining the grouping are raised. To verify the applicability and validity of the procedure, the scheme is tested on a 179-bus, 29-generator test system.

Two kinds of tests are conducted to verify the slow coherency based grouping. In the first set of tests, the validity and the efficacy of the procedure is tested for varying operating conditions. The results of this analysis clearly indicate that the grouping obtained remains fixed for a fairly wide range of operating conditions when the loads are changed conformingly with a certain percentage. With more rigorous load change test, the result also indicates the grouping obtained is not very sensitive to the disturbance location. The inherent

structural characteristic of the system determines the slow coherency behavior and other important parameters related to topological ability to form islands, and load-generation imbalance results in the formation of either two or three islands. The basic configuration of the islands does not change with different lines removed. The location of the islands does depend on the existing system conditions prior to the disturbance. The out-of-step operation following the disturbance splits the system into islands one location at a time as the disturbance propagates through the system. This has been clearly established using the R-Rdot relay plots.

In the second set of tests, the grouping is verified for two different disturbances to verify the disturbance independent feature of the slow coherency approach. In this case once the grouping is determined, the automatic islanding program determines the cut sets to form the appropriate islands. The results indicate that the change in operating condition will affect the grouping of generators. We do observe a change in the configuration of the islands formed. However, it should be noted that the islands formed are quite similar, and the method accurately captures the weak connections.

An added issue of great significance is that even though the grouping in the slow coherency approach is done using a linearized model of only the electromechanical model of the system, it accurately captures the gross dynamic behavior of the detailed nonlinear model as shown by the rotor angle curves obtained from nonlinear time domain simulation using detailed models. These curves clearly indicated that the machines that are grouped based on slow coherency are coherent even in the nonlinear simulations.

Plots of the rate of change of impedance also verify that the islands determined by the automatic islanding program can be formed using the proposed R-Rdot out of step relays. The signal corresponding to a large disturbance is sent to the load shedding relays, which will in turn make selections of the load shedding scheme.

Then the overall self-healing scheme including the load shedding scheme is tested on three cases, which include one case with islanding based on experience and two cases with islanding based on slow coherency but having different disturbances. First of all, the islanding scheme based on slow coherency works more effectively than the one based on experience, which is shown from the savings in the Table 5.5.1 of the amount of the load shed. Then the new two-layer load shedding scheme is proven with its capability of reducing

the oscillation and saving in the amount of load shedding. The two layers successfully identify the difference between a large disturbance and a small disturbance by the different settings in terms of the step size, time delay and threshold.

6.2 CONTRIBUTIONS

Contributions have been made in the following aspects:

- This is the first known attempt to apply slow coherency theory to the problem of power system islanding. This work has presented all the applicable features of slow coherency theory in solving the islanding problem. It provides the industry with a completely new strategy for corrective action following large disturbances in the power grids. This should attract attention particularly after recent blackouts in the North Eastern U.S and the other countries.
- An automatic islanding program has been developed to assist the grouping program to locate the optimal boundary sets based on certain criteria. The criteria have been designed with restoration consideration and some other practical considerations. The software acts as one of the basis for the whole self-healing strategy and its inheritance from the C++ language style makes it expandable to more practical applications.
- A two-layer load shedding scheme based on rate of frequency decline developed in [26] has been applied to prevent frequency decline in the load rich islands. The load shedding scheme benefits from the islanding by having the knowledge of the generation load imbalance and information of the generators in the island. The flexibility of the load shedding scheme lies in the dependence on the locally measured rate of change of frequency instead of a system average frequency. Its effectiveness is displayed clearly in the Table 5.5.1.
- A self-healing strategy to deal with large disturbances has been designed, which includes the slow coherency based islanding and load shedding based on rate of frequency decline. An overall scheme of the islanding decision, tripping action and load shedding action has been set up and described in Chapter 3. The strategy provides a practical solution to the problem of when and where to island the disturbed power system and provide proper corrective actions for restoration.
- Detailed simulation tests have clearly verified from various aspects the efficacy of the self-healing scheme and demonstrated that the concept is sound and effectively enhances the ability to

restore the system quickly because of the nature of the load generation balance in the islands formed by the controlled separation.

6.3 FUTURE WORK

The formal principles underlying the self-healing procedure developed in this task can be applied to other systems and applications. A specific analogy with control of natural disasters [42] is presented below. When natural disasters occur, their severity is assessed based on the following criteria:

- Degree of damage
- Degree of danger
- Expansion speed of a hazard

The same guiding principles form the basis of the self-healing approach in power systems. Using the techniques developed in [26] we assess the severity of any given contingency. This provides an indication of the impact the disturbance will have on the system. This is akin for examples to determining the damage area following a natural disaster. The questions typically asked are, does the damage involve part of a city or an entire city, or are several cities affected? In our case the power system model together with the existing operating conditions are used to determine whether the disturbance will affect only a portion of the system or a wide area in the system. Another important aspect of this analysis following natural disasters is to determine if the disaster will affect a large portion of the population, if it is life threatening, or of it will cause wide spread damage to infrastructure. This is analogous to determining the severity of the disturbance in power systems. We determine if the disturbance is large, whether it will damage equipment, and result in a wide spread blackout.

Having specified the degree of damage, the next step following a natural disaster is to determine whether the effects of a natural disaster are progressing, or whether the immediate threat has ended. If the effects of the disaster are progressing (for example the spreading of a large forest fire), how quickly is the affected area expanding and what can be done to stop the progress? In other words the expansion speed of the hazard is evaluated and the degree of danger is determined. This is identical to the procedure we have developed for power

systems. Once we determine that the disturbance will affect a wide spread area of the system, we invoke self-healing to contain the damage. This is done by breaking up the system into smaller parts and isolating the effect of the disturbance. The smaller parts are designed to operate at a slightly degraded level, and the entire system can be restored very fast.

These fundamental principles adopted in our approach can be extended to other networked systems like natural gas pipelines, communication networks, and information networks.

Limiting the scope of the application of the self-healing strategy in power system, several suggestions are provided hereby in the development of future work:

- More simulations need to be done to verify the scheme with various contingencies and different systems. The islanding scheme needs to consider different numbers of groups to form the islands after a large disturbance. Criteria should be developed to choose the optimal number of groups to form the islands. The number should be as small as possible to reduce the impact to the system brought by islanding. But the objective of self-healing should still be fulfilled.
- More work can be developed around the switching action. Currently, a hierarchy of three-level switching mechanism is identified. But detail works on the scheme need to be developed. Especially, a vulnerability index based on the slow coherency theory is in need for the reason of adding self-learning function into the R-Rdot out of step relay. The index aims to value the correctness of operation of the relay and feeds back to the part of parameter settings of the relay. Proper decision can thus be made after field training. The index should utilize the two-time-scale feature of power system. That is, a correct islanding decision should have the generators slow coherent with each other in an island. The amount of the load shedding needed to save the system from losing stability is also an important index for a correct islanding decision.
- Application of the modified grouping algorithm into a large power system is necessary. Especially, achieve the objective of the design of a corrective control strategy with voltage stability consideration.
- Incorporation of the current self-healing strategy into a multi-agent architecture. Islanding agent and load shedding agent with their respective functions should be designed appropriately.

BIBLIOGRAPHY

[1] C. C. Liu, G. T. Heydt, A. Phadke, V. Vittal, "Conceptual Design of a Strategic Power Infrastructure Defense (SPID) System," EPRI, Palo Alto, CA, and Department of Defense: Nov. 1999. TR-000000.

[2] R. Brooks. Web site on Subsumption Architecture. Date retrieved: 2001, March. Available: http://www.mit.edu/people/brooks.

[3] P. Crossley, F. Ilar, D. Karlsson, "System protection schemes in power networks: existing installations and ideas for future development", in *Developments in Power System Protection, 2001, Seventh International Conference on (IEE), 2001*, pp. 450-453.

[4] G. Trudel, S. Bernard, G. Scott, "Hydro-Quebec's defence plan against extreme contingencies," *IEEE Transactions on Power Systems*, vol. 14, Aug. 1999. pp. 958-965.

[5] J. Jyrinsalo and E. Lakervi, "Planning the islanding scheme of a regional power producer", in *Electricity Distribution, 1993. CIRED. 12th International Conference on*, 1993. pp. 4.21/1-5 vol. 4.

[6] V. Vittal, W. Kliemann, Y.-X. Ni, D. G. Chapman, A. D. Silk, D. J. Sobajic, "Determination of generator groupings for an islanding scheme in the Manitoba Hydro System using the method of normal forms", *IEEE Transactions on Power Systems*, vol. 13, pp. 1345-1351, Nov. 1998.

[7] M. Begovic, D. Novosel and M. Milisavljevic, "Trends in power system protection and control", in *Systems Sciences, 1999. HICSS-32. Proceedings of the 32nd Annual Hawaii International Conference on, 1999.*

[8] Ontario Hydro, "Dynamic Reduction," Version 1.1, vol. 2: User's Manual (Revision 1) EPRI TR-102234-V2R1, May 1994.

[9] R. Podmore, A. Germond, "Development of dynamic equivalents for transient stability studies", System Control, Inc., EPRI EL-456, Final Report, April 1977.

[10] C.D.Vournas, P.W.Sauer, M.A.Pai, "Time-scale Decomposition in Voltage Stability Analysis of Power", *Proceddings of the 34th Conference on Decision & Control*, New Orleans, LA – December 1995.

[11] P.M.Anderson, A.A.Fouad., "Power system control and stability", 1994, the Institute of Electrical and Electronics Engineers, Inc.

[12] P. Kundur, "Power System Stability and Control", McGraw-Hill, Inc. 1993.

[13] J. H. Chow, "Time-Scale Modeling of Dynamic Networks with Applications to Power Systems". Lectures notes in Control and Information Sciences. 46. Springer-Verlag Berlin. Heidelberg. New York. 1982

[14] Nonlinear System, Hassan Khalil, Second Edition, Prentice Hall.

[15] Adibi, M.M., "Power System Restoration: Methodologies & Implementation Strategies". IEEE Press, 2000.

[16] M. S. Tsai, "Development of islanding early warning mechanism for power systems", in *Power Engineering Society Summer Meeting, 2000. IEEE, Vol. 1*, pp. 22-26.

[17] M. Klein, G. J. Rogers, and P. Kundur, "A fundamental study of inter-area oscillations," *IEEE Transactions on Power Systems,* Vol. PWRS-6, No. 3, pp. 914-921, August, 1991.

[18] D. K. Mugwanya and J. E. Van Ness, "Mode coupling in power systems," *IEEE Transactions on Power Systems,* Vol. PWRS-2, pp. 264-270, May 1987.

[19] H. You, V. Vittal, "A slow coherency identification algorithm considering load dynamics," 34th Annual North American Power Symposium, Tempe, Arizona, U. S. A, Oct 14-15, 2002.

[20] Ontario Hydro, "Extended transient-midterm stability program (ETMSP)," Version 3.1, vol. 1: Final Report (Revision 1) EPRI TR-102004-V1R1, May 1994.

[21] Ontario Hydro, "Extended transient-midterm stability program (ETMSP)," Version 3.1, vol. 3: Application Guide (Revision 1) EPRI TR-102004-V3R1, May 1994.

[22] J.M. Haner, T. D. Laughlin, C. W. Taylor, "Experience with the R-Rdot Out-of-step Relay," *IEEE Transactions on Power Systems*, Vol. PWRD-1, No. 2, April 1986.

[23] C.W.Taylor, J.M.Haner, L.A.Hill,W.A.Mittelstadt, R.L.Cresap. "A new out-of-step relay with rate of change of apparent resistance augmentation," *IEEE Transactions on Power Apparatus and Systems*, Vol. PAS-102, No. 3, March 1983.

[24] V.Centeno, A.G.Phadke, A.Edris, J.Benton, M.Gaudi, G.Michel. "An Adaptive Out-of-step Relay," *IEEE Transactions on Power Delivery*, Vol. 12, No.1, January 1997.

[25] S. Rovnyak, Y. Sheng, "Using Measurements and Decision Tree Processing for Response-based Discrete-event Control," *IEEE Power Engineering Society Summer Meeting*, 1999. Vol. 1, 10-15.

[26] Z. Yang, "A new automatic under-frequency load shedding scheme," Master of Science thesis, Dept. of Electrical and Computer Engineering, Iowa State University thesis, 2001.

[27] D. W. Smaha, C. R. Rowland, J. W. Pope, "Coordination of load conservation with turbine-generator underfrequency protection," in *IEEE Transactions on Power System Apparatus and System*. Vol. PAS-99, No. 3, pp1137-1145, May/June 1980.

[28] G. S. Grewal, J. W. Konowalec, M. Hakim, "Optimization of a load shedding scheme", in *IEEE Industry Application Magazine*, pp25-30, July/Augest 1998.

[29] C. J. Drukin, Jr. E. R. Eberle and P. Zarakas, "An Underfrequency Relay with Frequency Decay Compensation", *IEEE Transactions on Power Apparatus and Systems*, Vol. PAS-88, No. 6, June 1969, pp.812-819.

[30] A. A. Girgis and F. M. Ham, "A New FFT-based Digital Frequency Relay for Load Shedding", *IEEE Transactions on Power Apparatus and Systems*, Vol. PAS-101, No. 2, February 1982, pp. 433-439.

[31] M. M. Elkateb and M. F. Dias, "New Technique for Adaptive-Frequency Load Shedding Suitable for Industry with Private Generation", *Generation, Transmission and Distribution, IEE Proceedings C*, Volume: 140 Issue: 5, September 1993.

[32] M. M. Elkateb and M. F. Dias, "New Proposed Adaptive Frequency Load Shedding Scheme for Cogeneration Plants", *Developments in Power System Protection, 1993, Fifth International Conference on.*

[33] J. G. Thompson, B. Fox, "Adaptive Load Shedding for Isolated Power Systems", *Generation, Transmission and Distribution, IEE Proceedings*, Volume: 141 Issue: 5, September 1994.

[34] V. N. Chuvychin, N. S. Gurov, S. S. Venkata, R. E. Brown, "An Adaptive Approach to Load Shedding and Spinning Reserve Control During Underfrequency Conditions", in *IEEE Transaction on Power Systems*, Vol. 11,No. 4, pp.1805-1809, November 1996.

[35] H. You, V. Vittal, J. Jung, C-C. Liu, M. Amin, R. Adapa, "An Intelligent Adaptive Load Shedding Scheme," Proceedings of the 14th Power System Computation Conference, Paper 6, Session PS17 Wide-Area Control, Seville, Spain, June, 2002.

[36] P. M. Anderson, M. Mirheydar, "An Adaptive Method for Setting Underfrequency Load shedding Relays", in *IEEE Transaction on Power Systems*, Vol. 7,No. 2, pp.720-729, May 1992

[37] *American National Standard Requirements for Synchronous Machines*, ANSI C50.10-1977, New York, 1977.

[38] *IEEE Guide for Abnormal Frequency Protection of Power Generating Plants*, IEEE Standard C37.106-1988, New York, 1988.

[39] H. You, V. Vittal, and Z. Yang, "Self-healing in power systems: an approach using islanding and rate of frequency decline based load shedding," *IEEE Trans. Power Systems*, Vol. 18, no. 1, pp.174-181, February 2003.

[40] Ontario Hydro, "Extended transient-midterm stability program (ETMSP)," Version 3.1, vol. 2: User's Mannual (Revision 1) EPRI TR-102004-V2R1, May 1994.

[41] H. You. V. Vittal, X. Wang "Slow coherency based islanding," To appear in the *IEEE Transactions on Power Systems.*

[42] R. Ishii, "Control In Natural Disasters," *IEEE Control Systems Magazine*, Vol. 20, No. 1, pp. 9-12, February 2000.